

**A Thesis Submitted for the Degree of PhD at the University of Warwick**

**Permanent WRAP URL:**

<http://wrap.warwick.ac.uk/110545/>

**Copyright and reuse:**

This thesis is made available online and is protected by original copyright.

Please scroll down to view the document itself.

Please refer to the repository record for this item for information to help you to cite it.

Our policy information is available from the repository home page.


For more information, please contact the WRAP Team at: [wrap@warwick.ac.uk](mailto:wrap@warwick.ac.uk)

PERFORMANCE EVALUATION AND DEVELOPMENT OF  
A SYNCHRO-DRIVE MOBILE ROBOT

By

CHARLES NNONYELUM J. NWUFOH, M.Sc

A thesis submitted in fulfillment of the requirements for the degree of Doctor of Philosophy in  
Engineering



Department of Engineering  
University of Warwick  
Coventry, ENGLAND

May, 1992.

#### ABSTRACT

The work described in this thesis is concerned with the performance of the mechanical system of a mobile robot that is capable of omnidirectional motion. The main attribute of such mobile robots is that their direction of motion is independent of chassis orientation. This attribute endows them with exceptional manoeuvrability, but it is also found to pose substantial problems by changing the level of accuracy and stability of the robot as its direction of travel changes.

The main objective of the research is to conduct a detailed evaluation of the performance of a mobile robot which is capable of omnidirectional movement achieved by means of a synchronized all-wheel steering and all-wheel drive (Synchro-drive) technique. The objective is met by comparing the synchro-drive method with other configurations used for mobile robots, by comparing different designs of the synchro-drive method and by analyzing synchro-drive mechanical behaviour in response to drive and steering inputs. A kinematic model of the synchro-drive arrangement is formulated and this is used to analyze different designs and to assess the limits of the control variables beyond which a Synchro-Drive Mobile Robot (SDMR) operation will become unstable. A new version of the synchro-drive arrangement was developed and was used to perform extensive practical testing in order to determine factors affecting positional accuracy and the trajectory actually executed by the mobile robot.

The analysis of the boundaries of the control space revealed the limits on acceleration which may be allowed by the robot's control system for it to remain stable. It also showed that the acceleration limits depend on the angle between the wheel heading and the chassis orientation, which is defined as the robot's posture. Practical experimentation identified the major influences on robot accuracy and also related the form, magnitude and direction of these errors to the robot's posture. The experiments revealed that the errors were due partly to aspects of the design itself and partly due to inevitable errors in the complete mechanical system. A continuous position error correction method is proposed which uses experimental data as the basis for correction. Correction quantities vary with posture, and the method uses a modification to the steering rate to minimize trajectory error.

Overall the study reveals the factors which must be considered to enable the potential of the synchro-drive mobile robot to be fully realized.

#### ACKNOWLEDGEMENT

I wish to express my deep felt gratitude to my supervisor Dr. T.C. Goodhead for his motivation, enthusiasm and encouragement. He is also thanked for his advice and support in every aspect that made this research possible. My special thanks go to Dr. S.A.G Chandler and Dr. E.L. Mines both of whom provided substantial advice and support.

Acknowledgment is given to Prof. S.K. Bhattacharyya for his support, which made it possible for this project to be completed.

My thanks go to Mr. G.J. Robinson whose experience and patience was very valuable in the construction of the mobile robot. And also to Mr. D.G. Thompson for his interest and attention he gave to the project, and all other members of engineering workshop staff who contributed to the construction of the mobile robots. Finally I would like to thank Mr. M. Stevens who assisted in the development of the control system for the mobile robot.

I am grateful to Drs. J.C. & M. Nduaguba, Mr. & Mrs. V.C. Nwufoh, and other members of my family and friends for their advice, moral and financial support throughout the period of this project. May God bless you all.

I do accept the responsibility for any error in presentation and typing of this thesis.

Charles N.J. Nwufoh  
(Author)

Dedication

*This work is dedicated to Mr. & Mrs. I.J.C. Nwufoh and family.*

## CONTENTS

ABSTRACT	
ACKNOWLEDGEMENT	
DEDICATION	
CHAPTER 1	1
INTRODUCTION	1
1.1 DESCRIPTION OF A WHEELED MOBILE ROBOT.	1
1.2 RESEARCH MOTIVATION.	2
1.3 RESEARCH SPECIFICATION.	3
1.4 RESEARCH OBJECTIVES.	5
CHAPTER 2	8
LITERATURE SURVEY	8
2.1 LOCOMOTION SYSTEMS.	8
2.1.1 LEG LOCOMOTION SYSTEMS.	8
2.1.2 TRACK LOCOMOTION SYSTEMS.	11
2.1.3 WHEEL LOCOMOTION SYSTEMS.	12
2.1.3.1 BASIS OF DISTINCTION BETWEEN WHEEL MOBILE ROBOTS.	13
2.1.3.2 DIFFERENT WHEELED MOBILE ROBOT'S KINEMATIC CONFIGURATION.	16
2.2 OMNIDIRECTIONAL MOTION.	27
2.2.1 COMPOUND WHEEL BASED DESIGNS.	29
2.2.1.1 ILONATOR OR MECANUM WHEEL.	29
2.2.1.2 WHEEL COMPRISING OF ROLLER DRUMS.	33
2.2.1.3 ADVANTAGES AND DISADVANTAGES OF COMPOUND WHEEL.	34
2.2.2 CONVENTIONAL WHEEL SYNCHRO-DRIVE (ALL- WHEEL DRIVE/ STEERING) CONFIGURATION.	35

2.2.3	DESIGNS OF SYNCHRO-DRIVE MOBILE ROBOT (SDMR).	39
2.2.3.1	WHEEL ASSEMBLY, WITH WHEEL-OFFSET FROM THE STEERING AXIS (TYPE-1).	44
2.2.3.2	WHEEL ASSEMBLY, WITH DIFFERENTIAL GEAR COUPLED WHEEL SET (TYPE-2).	45
2.2.3.3	WHEEL ASSEMBLY, WITH WHEEL-SET ON STEERING AXIS (TYPE-3).	46
2.3	TRANSMISSION SYSTEM.	47
CHAPTER 3		52
ANALYSIS OF FACTORS THAT INFLUENCE PERFORMANCE		52
3.1	WHEEL FORCE/TORQUE ANALYSIS.	52
3.1.1	COMPONENT FORCES, MOMENTS AND ANGLE OF A WHEEL.	52
3.1.2	SDMR WHEEL.	57
3.2	ERRORS THAT AFFECTS THE SDMR PERFORMANCE.	61
3.2.1	TYPES OF ERROR.	61
3.2.1.1	PREDICTABLE ERRORS.	61
3.2.1.2	NON-PREDICTABLE ERRORS.	64
3.2.2	SOURCES OF ERROR.	66
3.2.2.1	POWER TRANSMISSION MECHANISM.	66
3.2.2.2	TYRE.	68
3.2.2.3	WHEEL ALIGNMENT.	69
3.2.2.4	NATURE OF FLOOR SURFACE (ROUGHNESS).	69
3.2.2.5	SENSORS AND COMPUTATION.	69

3.3	SDMR BEHAVIOUR.	70
3.3.1	BEHAVIOUR UNDER DRIVE INPUT ONLY.	70
3.3.1.1	EQUATIONS OF MOTION AND TRAJECTORY ANALYSIS.	71
3.3.2	BEHAVIOUR UNDER A STEERING INPUT.	79
3.3.2.1	STEADY-STATE BEHAVIOUR.	80
3.3.2.2	TRANSIENT STATE BEHAVIOUR.	83
3.3.2.3	DIRECTIONAL STABILITY.	88
CHAPTER 4		94
KINEMATIC MODELING AND BOUNDARIES OF CONTROL SPACE		94
4.1	SYNCHRO-DRIVE MOBILE ROBOT'S (SDMR'S) KINEMATICS.	95
4.1.1	COORDINATE SYSTEM ASSIGNMENT.	98
4.1.2	SDMR KINEMATIC VELOCITIES AND ACCELERATIONS.	99
4.1.2.1	WHEEL-OFFSET FROM WHEEL ASSEMBLY STEERING AXIS (TYPE-1).	101
4.1.2.2	WHEEL-SET ON WHEEL ASSEMBLY STEERING AXIS (TYPE-3:A).	103
4.1.2.3	WHEEL-SET ON WHEEL ASSEMBLY STEERING AXIS WITH MECHANICAL COMPENSATOR UNIT (TYPE-3:B).	104
4.2	BOUNDARIES OF THE CONTROL SPACE.	108
4.2.1	NO SLIPPING CONDITION.	110
4.2.2	NO OVERTURNING CONDITION.	121
CHAPTER 5		128
PROTOTYPE DEVELOPMENT AND FURTHER ANALYSIS OF DIFFERENT WHEEL ASSEMBLY DESIGNS		128



5.1	PROTOTYPE DEVELOPMENT.	128
5.1.1	STRUCTURE AND LAYOUT OF THE PROTOTYPE SDMR.	128
5.1.2	METHODS TO COMPENSATE WHEEL ASSEMBLY DESIGN-ERROR.	135
5.1.2.1	SOFTWARE COMPENSATION.	137
5.1.2.2	HARDWARE COMPENSATION.	137
5.2	THE IMPACT OF WHEEL FORCES/TORQUE AND STEERING INPUT ON SDMR PERFORMANCE.	140
CHAPTER 6		149
	EXPERIMENTAL TECHNIQUE TO DETERMINE SDMR ERRORS AND BEHAVIOUR	149
6.1	EXPERIMENTAL OBJECTIVES.	149
6.2	EXPERIMENTAL PROCEDURE.	150
6.2.1	TESTS CONDUCTED.	151
6.2.2	METHODS USED TO RECORD PATHS AND SET THE SDMR STATES.	157
6.2.3	MEASUREMENTS TAKEN AND EQUIPMENT USED.	160
CHAPTER 7		166
	EXPERIMENTAL RESULTS	166
7.1	TEST RESULTS WITH VERSION 1 SDMR.	170
7.1.1	DETERMINATION OF LATERAL ERROR ( $\delta y$ ), LONGITUDINAL ERROR ( $\delta x$ ), AND ARC RADIUS (R).	178
7.1.2	STATISTICAL ANALYSIS.	181
7.2	TEST RESULTS WITH VERSION 2 SDMR.	185
7.2.1	TEST RESULTS WITH THE SDMR OPERATING IN THE NORMAL STATE (CATEGORY A).	186
7.2.1.1	STATISTICAL ANALYSIS.	193

7.2.2	TEST RESULTS IN WHICH THE SDMR WHEELS BARES UNEVEN LOAD (CATEGORY B).	196
7.2.3	TEST RESULTS WITH WHEEL NUMBERED 1 MISALIGNED (CATEGORY C).	204
7.2.4	TEST RESULTS WITH TWO WHEELS MISALIGNED INWARDLY TOWARDS THE CENTRE OF MASS (CATEGORY D).	209
7.2.5	TEST RESULTS WITH TWO WHEELS MISALIGNED OUTWARDLY FROM THE CENTRE OF MASS (CATEGORY E).	214
7.2.6	TEST RESULTS WITH ONE WHEEL HAVING A SMALLER RADIUS (CATEGORY F).	218
7.2.7	COMBINED RESULTS.	222
7.2.8	RESULTS SUMMARY.	231
CHAPTER 8		235
DISCUSSION OF RESULTS		235
8.1	RESULTS DISCUSSIONS.	237
8.2	MAIN DIFFERENCES BETWEEN SDMR CONFIGURATION AND CONVENTIONAL MOBILE ROBOT CONFIGURATION WHEN OPERATING IN AN ERROR STATE.	248
8.3	FORMULATION OF POSITION ERROR CORRECTION METHOD.	252
CHAPTER 9		263
CONCLUSIONS AND RECOMMENDATIONS FOR FURTHER WORK		263
9.1	CONCLUSIONS.	263
9.2	RECOMMENDATIONS FOR FURTHER WORK.	272
APPENDIX A		275
RESEARCH PUBLICATIONS		275
A.1	DEVELOPMENT OF AN OMNIDIRECTIONAL MOBILE ROBOT.	276

A.2	AGV CONTROL USING AN INTELLIGENT ENVIRONMENT	
	APPROACH (IEA).	287
APPENDIX B		298
B.1	STEERING SYSTEM ACCELERATION REQUIREMENT.	298
B.1.1	FOR A DIFFERENTIAL DESIGN.	301
B.1.2	FOR A TRICYCLE DESIGN.	302
B.1.3	FOR A SDMR DESIGN.	302
B.2	EFFECT OF MECHANICAL ERRORS.	303
APPENDIX C		306
SYNCHRO-DRIVE MOBILE ROBOT (SDMR) SPECIFICATIONS		306
C.1	FIRST PROTOTYPE.	306
C.2	SECOND PROTOTYPE.	308
REFERENCES.		310

## CHAPTER 1

### INTRODUCTION

This chapter considers the area within the robotics field on which the research is centred, the factors that motivated the study, the specification of the research, and the overall objectives.

#### 1.1 DESCRIPTION OF A WHEELED MOBILE ROBOT.

This research is centred on the mobility aspects of mobile robots. A mobile robot is considered to be a machine that is capable of being programmed to move around within its environment and does not necessarily carry a manipulator. In particular this work deals with robots that achieve their mobility through the use of wheels and it is not concerned with mobility achieved using other methods such as legs or tracks. For the purpose of focusing the study, the following operational definition of a 'wheeled mobile robot' is adopted;

'A wheeled mobile robot is a reprogrammable machine capable of locomotion by means of the forces created at the contact between the wheels and the ground'.

Mobility is provided by means of drive and steering power inputs to the wheels. The transmission of power to enable movement is achieved through a series of links and joints. These links and joints are classified as, higher-pair, closed-chain joints [Muir'86].

## 1.2 RESEARCH MOTIVATION.

The motivation for this research is to identify and evaluate wheeled mobile robot mechanical designs which provides the minimum constraint to robot mobility and provides improved performance over existing designs. Much of the mobile robot research investigation documented concentrates on the application of the mobile 'platform' as a testbed to study artificial intelligence [Moravec'83], [Nilsson'84], [Giralt'85]. The investigation of the capabilities of the mobile platform mechanisms in order to assess the limits that it can impose on the overall task have mostly been neglected. The concentration of efforts into investigation of intelligence stems from the widely held opinion that accuracy and manoeuvrability of the platform itself do not contribute greatly to the overall performance of the mobile robot. Such schools of thought believe that software can compensate for any deficiency in the platform. Assumptions of this sort have proved very costly in many projects [Holland'86].

Improved mechanical system designs affecting mobility, and better understanding of the control requirements will enable the rethinking of some of the present approaches to intelligent system development. For example, if a mobile robot senses that it has encountered an obstacle, even if it knows how to avoid it, it may not be possible to avoid the obstacle if it does not have the desired manoeuvrability and accuracy, irrespective of the knowledge of the situation.

In this thesis the foundation for the design and development of a high performance mechanism for wheeled mobile robots is laid. This is achieved through kinematic modeling, performance analysis and feasibility study.

### 1.3 RESEARCH SPECIFICATION.

It was considered necessary at the outset to define the type of mobile robot for which the mechanical system was to be the basis of study. Despite the fact that robots are generally defined as multi-functional machines and therefore able to perform a variety of tasks, it has to be accepted that mechanical hardware always imposes limitations on the potential application areas. For a mobile robot the major factor influencing the design is the type of terrain over which the robot must travel.

It was decided that the research would consider terrains of the type found in man-made environments such as industrial and commercial buildings and their immediate surroundings. The main type of surface encountered in man-made environments is relatively hard, smooth and quite flat. Mobility occurs mostly in a horizontal two-dimensional (2D) plane, although steps and stairs are common place. It was decided at this stage to restrict movement to the 2D plane as the addition of a step climbing capability adds considerable complexity to any mechanical design [Knasel'86] and there are many applications where a robot capable of moving only in 2D can use ramps and auxiliary devices such as lifts to change level.

Within most man-made environments there are space limitations. There are also a huge range of possible paths that the mobile robot may be required to execute. Ideally the robot should be able to execute any path that is required of it and should be able to access any space that is physically large enough to accept it.

The particular class of wheeled mobile robot that are of major interest in this research are those capable of omnidirectional motion. Omnidirectional motion allows a mobile robot to move from rest along a vector at any angle to its current heading. Consideration is given to other arrangements such as the differentially steered type and tricycle type. In the omnidirectional motion class a variety of designs exist, but the study will concentrate on a design which uses all-wheel steering and all-wheel drive. In this design the wheels are always driven and steered in synchronization, and the mobile robots constructed using this design are referred to in this thesis as Synchro-Drive Mobile Robots (SDMRs).

The concept of synchro-drive for mobile robots is not new and has been implemented in a number of cases, the most notable being the Cybernation K2 [Holland'86] which is a commercially available product. However no detailed analysis of the design of SDMR's and no evaluation of the design features which affect their performance could be found. In particular it was considered that one feature associated with the design of the wheel assemblies

could substantially improve the robots' performance capabilities.

In order to evaluate the performance of a new design of wheel assembly two SDMR's were built (Fig. 1.1 shows the first SDMR at the initial stage of this study) and experiments were conducted to establish the factors influencing performance of such design and the behaviour of SDMRs in general. In addition to the influence of the mechanical system, the relationship between the control system and the mechanical system was studied and the means of finding the limits of the control input variables to ensure stable operation was established.

#### 1.4 RESEARCH OBJECTIVES.

This research study has five main objectives, which comprises of;

- ▷ Investigating ways of achieving omnidirectional motion.
- ▷ Analysis of Synchro-Drive Mobile Robot (SDMR) mechanical system behaviour,
- ▷ Kinematic modeling of the SDMR,
- ▷ Establishing the control boundaries for stable operation.
- ▷ Experimental testing, qualitative and quantitative analysis of test results to create better understanding of the factors that influence performance.

Performance criteria of SDMRs are considered in the light of; position error comprising of lateral and longitudinal error, chassis precession, systems stability and nature of the trajectory actually executed by a SDMR with mechanical errors.



In view of the research motives, specification and objectives, a detailed review of mobile robots was conducted, with particular reference to those capable of omnidirectional motion (chapter 2).

In analyzing SDMR behaviour, factors that influence performance are highlighted and considered (chapter 3). Such factors as the interaction between the SDMR and its environment, sources of mechanical system errors, and the way the SDMR responds to drive and steering inputs.

Kinematic modeling considerations (chapter 4) have created a new method of modeling SDMR's based on the constraints which they experience. Through kinematic modeling detailed theoretical comparisons of different SDMR designs have been achieved. The modeling of SDMR's and the need to determine the basic control system requirements have provided the means to establish the SDMR control space (chapter 4). This is the space within which the SDMR operation is stable (i.e. no slipping or overturning).

Practical experimental testing and statistical analysis are used to assess performance and feasibility of two functional prototype SDMRs. Tests conducted with the two prototypes gave a detailed insight into the physical operation of SDMR's and the characteristics which they possess. It created the understanding for the formulation of a new method of position error correction. This method uses the experimental results to determine parameters that will form part of the control system and also the nature of

path specification that will facilitate the correction process.

The entire study has revealed the shortcomings of SDRM's, such as the changing level of performance due to changing wheel heading. This arises from the fact the SDRM chassis orientation and wheel heading are independent. It is anticipated that the information, approaches and solutions which this study provides will be very useful to designers of wheeled mobile robots, particularly those with interest in high manoeuvrability and high performance who contemplates the use of the Synchro-drive mechanism.



Fig. 1.1 Mobile robot chassis and initial drive mechanism.

## CHAPTER 2

### LITERATURE SURVEY

In this chapter, means of achieving locomotion is briefly discussed. The different configurations of wheeled mobile robots are reviewed on the basis of their operations, benefits and limitations. Methods of achieving omnidirectional motion by wheeled mobile robots which enables them to be highly manoeuvrable are considered in greater detail. Also discussed briefly are methods of power transmission

#### 2.1 LOCOMOTION SYSTEMS.

Mobile robots can achieve mobility using different types of locomotion systems such as legs, tracks and wheels. Within these different locomotion types there are also various designs. Some of the designs and concepts are discussed in this chapter.

##### 2.1.1 LEG LOCOMOTION SYSTEMS.

Mobile robots with legged locomotion are of varying degrees of complexity, the most technically challenging being the two anthropomorphic multi-jointed legs (biped). Well-known research institutes in this area include; MIT in USA, Waseda University, University of Tokyo, and Hitachi all in Japan, Cardiff and Edinburgh Universities in UK. Other leg systems are the four (see Fig. 2.1), six and eight leg types, which are the areas that tend to have received most attention to date, because balancing is much easier and mobility can be achieved with less complex leg

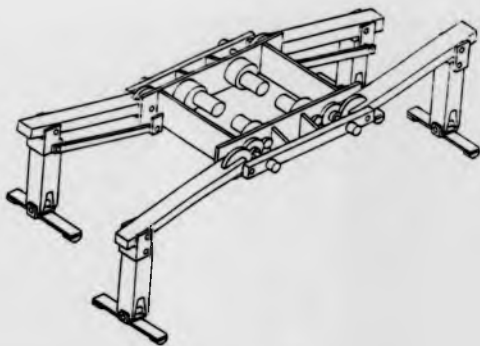


Fig. 2.1 Structure of four-legged robot [Todd'88].

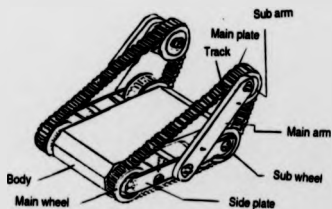


Fig. 2.2 Structure of the transformable track [Fuji'e'85].

structure [Knasel'86]. With more than two legs the mobile robot can easily manoeuvre in difficult terrain.

Mobile robots with legs have high mobility and adaptability. These can be achieved by using coordinated control of its multi-degrees of freedom. For example the biped walking robot developed by Hitachi has a configuration similar to the leg and hip structure of a human being. Each leg has six mechanical joints allowing motion in 12 degrees of freedom. The joints are controlled by hydraulic actuators. The hydraulic unit actuates the joints through the conversion of electrical energy into hydraulic energy [N-Nagy'86].

Walking robots are still at the prototype stages, with the multi-legged ones (those with more than two legs) showing greater potential at present. A parallelogram linked spider-like device is now commercially available through Odette corporation in the USA [Knasel'86]. On the whole mobile robots that use legs to produce locomotion suffer from: low speed even on flat surface, static and dynamic instability, complicated control system, and high energy consumption.

On hard, flat smooth surfaces such as found in most man-made environments, the limitations stated above are serious, particularly the inability to achieve moderate speeds on flat surfaces. They are also limited by their ability to carry a payload. However the result of research in this area will be very useful for applications where the terrain is less hospitable

such as space exploration, agriculture and locations where debris obstructs an otherwise flat floor.

There is one reported instance where attempts are being made to bring legged mobile robots into factories. In this approach it is envisaged that a special path can be made for the mobile robots. The path, which is known as 'born floor' [Knasel'86], is a magnetic platform. The 'born floor' allows attachment of the feet and makes it possible to achieve walking without the need to tackle balancing problems. This approach though novel, lacks both path flexibility and speed. The feasibility of this approach in a manufacturing environment, where there is high demand on flexibility and speed cannot be envisaged.

#### 2.1.2 TRACK LOCOMOTION SYSTEMS.

Mobile robots that use tracks to achieve locomotion have the ability to translate across rough terrain. They have little problem in terms of dynamic stability. With a sophisticated track mechanism and control system, relatively moderate speed can be achieved over most terrains [Fujie'85], [Knasel'86].

For instance in the mobile robot been developed by Fujii, et al [Fujie'85], tracks are mounted on both sides of the robots' body, and each track runs on main, sub and planet wheels (see Fig. 2.2). Rough terrain capability is enhanced by varying the movement of the planet wheels. Another example is the one developed by The Belgium Atomic Energy Agency. This uses three sets of tracks: one main and two auxiliary. Traction is achieved

using the main track, while inclined obstacles are mounted using the auxiliaries [Knasel'86]. It is being developed for use in nuclear reactors.

Research in this area is directed mainly towards outdoor or rough terrain applications, such as in construction sites and nuclear reactors. Tracked locomotion systems suffer from: low speed, high energy consumption caused mainly by the dead load and also poor accuracy because of 'skid steering'. Considering these drawbacks track locomotion system are not seen as an attractive means of achieving mobility for a mobile robot that will be used in the majority of industrial and commercial applications.

#### 2.1.3 WHEEL LOCOMOTION SYSTEMS.

Locomotion systems employing wheels have received the greatest attention among the three forms of locomotion under consideration. The interest was created mainly because of its benefits that easily met man's initial need for long distance transportation of goods. The benefits of wheeled locomotion system are as follows: On flat surfaces, they are highly energy efficient [Bekker'69], they are capable of high speeds, and they can make use of simple control systems.

The above mentioned benefits of wheeled locomotion system notwithstanding, they still suffers some set-backs, such as: limited terrain mobility and wheel slippage problems.

Due to the limitations of the different basic forms of locomotion

systems; research is on-going to try to develop hybrid locomotion mechanisms. The leading researchers in this area are the Japanese [Knasel'86], [N-Nagy'86]. An example is the one developed by Mitsubishi Heavy Industries whose locomotion system makes use of wheels and legs. On a flat surface it tucks in the legs, making use of the wheels to traverse. When climbing stairs the legs are used. For an intermediate obstacle a combination of both are used and in an idle state it puts the wheels at the end of the legs [Knasel'86]. Mitsubishi Electric in a similar interest has extended the work further by developing what they call Multifunctional Robotic Vehicle (MRV-3). It uses four track segments as either legs or tracks depending on the prevailing circumstance. The motivation for the research in this area arises from the construction industry and maintenance work in nuclear reactors (or other unstructured environment).

For environments that are characterized by hard, smooth, flat surfaces with a requirement for load carrying and moderate speed of goods delivery, the wheel locomotion system appears more appropriate. It is therefore selected as the basis for this work.

#### 2.1.3.1 BASIS OF DISTINCTION BETWEEN WHEELED MOBILE ROBOTS.

This review of wheeled locomotion system is performed mainly on the basis of difference in 'steering and drive systems', but not on factors such as number of wheels. The importance and effect of number of wheels on issues such as steering behaviours and stability is recognized, but it is not necessarily fundamental to

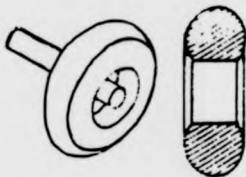


the locomotion method. The majority of existing mobile robots have either three wheels or four wheels, though some have up to six wheels, such as the Terragator [Wallace'85].

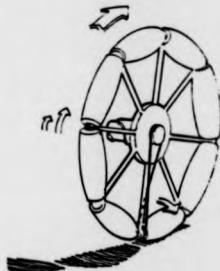
Those based on three wheels tend to benefit from the design of simpler wheel assemblies, and the absence of a spring or spring-damper element to provide suspension. However they suffer from the fact that their wheel's contact with the ground are nearer the centre of mass than other geometries (such as rectangular) for a given mobile robot size, and can run into tipping stability problems.

Those based on four wheels generally have better tipping stability. But they suffer from the need for spring suspension to ensure continuous wheel/floor contact, due to four points of ground contact. More wheels means greater power requirements and also an increase in manufacturing cost. With the four wheel design a tipping stability problem may arise if there is a change of load position that causes excessive change in the centre of mass.

Mobile robots can also be distinguished by the type of wheel used. The choice of wheel is mostly influenced by terrain [Chun'87]. The emphasis in most of the literature is not on wheel types but on the ways in which they may be configured. The existence of different novel types of wheels is noted [Chun'87], [Wright'87]. Some of these wheel types (see Figs. 2.3a - 2.3d) are the conventional wheel, compound or omnidirectional wheel,



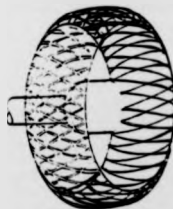
(a) Conventional wheel [Wright'78].



(b) Compound or Omnidirectional wheel [Chun'87].



(c) Ball wheel [Chun'87].



(d) Wire wheel [Chun'87].

Figs. 2.3 Illustration of some of the different wheel types:

ball wheel and wire wheel. Amongst the categories the ball type is highly manoeuvrable without any form of steering or slipping. However it has severe limitations for operation in an autonomous mode because it is very difficult to control. Within the limits of the search conducted, no literature reveals its implementation to date. The approach is at present only a concept [Wright'87]. Consideration of its workability however indicates that it will be extremely difficult to achieve high level of accuracy in both position and directional control.

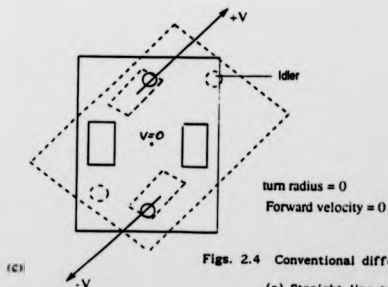
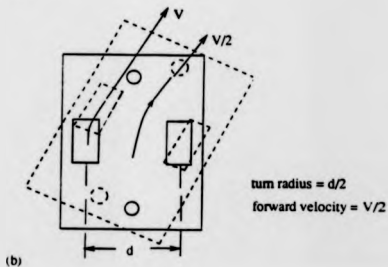
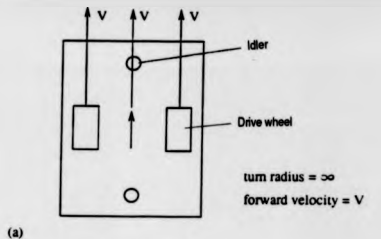
#### 2.1.3.2 DIFFERENT WHEELED MOBILE ROBOT'S KINEMATIC CONFIGURATION

There are several types of mobile robot Kinematic configuration. The most prominent ones are:

- (a) The Differential steering configuration,
- (b) The Tricycle or Swivel bolster configuration,
- (c) Axle pivot or Ackerman steering configuration,
- (d) All-wheel Drive/Steering or Synchro-drive configuration,
- (e) Compound wheel based or Mecanum or Ilonator types.

##### (a) Differential steering configuration.

The differential steering configuration type is the most commonly documented and used type among the above configurations. This stems from its simple geometric and kinematic configuration [Muir'86]. Here two parallel conventional wheels of identical radius are placed on each side of the mobile robot (see Fig. 2.4a to 2.4c). The mobile robot can translate to any destination by driving the wheels at the same speed, resulting in straight line motion, or at different speeds, resulting in motion in a curve



Figs. 2.4 Conventional differential steering:

- (a) Straight line travel.
- (b) Traveling through a curve path.
- (c) Rotation about the centre of gravity.

arc. Most of the mobile robots of this category uses one or two idler (or castor) wheels for static stability. In the differential configuration category the commonly known mobile robots includes; Yamabico [Kanayama'85], Shakey [Nilsson'84], Hilare [Giralt'79].

With the differential configuration one cannot execute a small radius turn without considerable reduction in drive speed. This is because of the way it achieves turning, which involves reduction of the forward speed of one wheel, and in some cases reversal of direction. Hence with this configuration, a slight modification to its path of travel may not be possible without stopping the mobile robot, and this extends journey times, causes expenditure of energy in regaining momentum and hinders smooth motion.

This configuration requires only drive input necessary to control the two motors that drive the wheels. There is no requirement for steering input, and hence mobile robot's theoretical trajectory can be easily determined as a function of the two wheel speeds [Tsumura'81].

#### (b) Tricycle configuration.

The remaining mobile robot configurations are kinematically more complex, in varying degrees, when compared to the differential. The tricycle configuration is the case where the mobile robot has three wheels, with a front wheel that can be steered and driven, while the two rear wheels are undriven and of fixed parallel

orientation (see Fig. 2.5). Such is the case with Neptune [Ponder'84], and Hero-1 [Halmers'83].

Due to the fact that only the speed and heading of the front wheel is controlled, the actual trajectory taken by the mobile robot is not readily predicted, since it is influenced by the two fixed rear wheels. The test conducted by Nelson [Nelson'89]

shows that the accuracy of the path taken by the mobile robot depends on the location of the fixed wheels with respect to the centre of gravity.

#### (c) Ackerman steering configuration.

The Axle pivot or Ackerman steering configuration (see Fig. 2.6) comprises of four wheels, two of which are parallel and opposite one another but coupled together through an Ackerman linkage and they generally serve as the front wheels. The other two are fixed and are parallel to one another. The linkage in the two front wheels is to ensure approximately correct angle turn on both wheels when steering, which avoids wheel slip [Muir'86]. The wheels may or may not be driven. In the Stanford Cart [Moravec'83] type, the wheels are not driven. The wheels can however be independently driven. For example the JPL Rover [Lewis'73] has two sets of ackerman steering wheels, with all the wheels independently driven. However they don't have to be independently driven, because they can use a differential unit to allow for difference in distance travelled by the wheels during a turn.

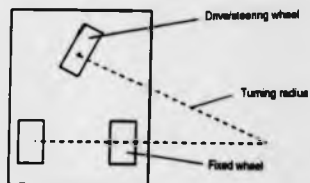


Fig. 2.5 Illustration of Tricycle configuration.

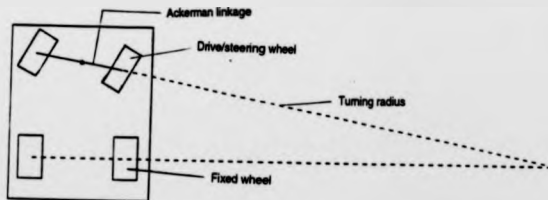


Fig. 2.6 Illustration of Axle pivot steering configuration.

The axle pivot configuration is similar to that used in most motor cars. When compared to the differential and tricycle configuration its mechanism is more complicated.

The tricycle and Ackerman steering wheel configurations both have quite severe turning angle restriction (see Figs. 2.5 and 2.6). And their efficiency in mobility is directionally dependent. That is they do not exhibit the same behaviour in both forward and backward movement.

(d) All-wheel Drive/Steering or Synchro-Drive configuration.

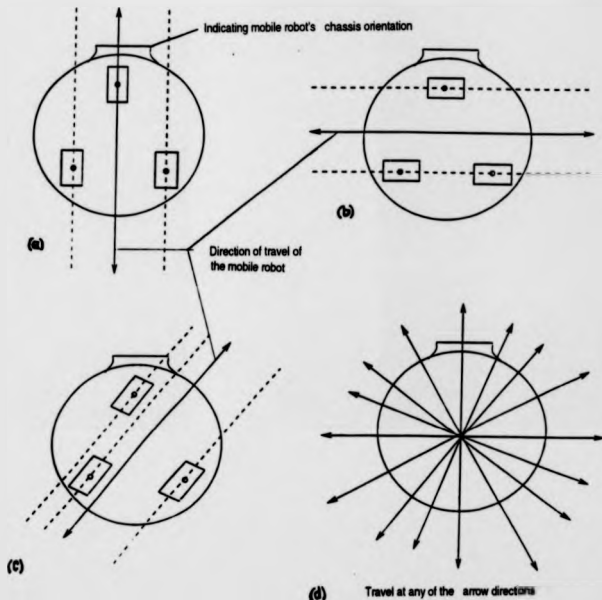
The all-wheel steering configuration as the name implies is a configuration that allows all wheels of a mobile robot to be steered. It can be called a synchro-drive system when it is steered and driven in unison. This configuration achieves motion that gives maximum manoeuvrability on a horizontal plane [Moravec'83]. Such motion is considered 'omnidirectional' [Moravec'83], [Nakano'81].

All-wheel steering only provides omnidirectional motion when all the wheels turn the same direction by the same amount at the same speed, and when steering is possible through a complete  $360^\circ$ . The term all-wheel steering has been applied to cars which have the back wheels steered through very limited angles in opposite direction for better manoeuvrability or in the same direction for better stability at high speed. However they achieve lateral translation through very limited angles and are not capable of omnidirectional motion.



Omnidirectional motion allows a mobile robot to move from rest along a vector at any angle to its current heading (see Figs. 2.5a - 2.5d). With such motion capability a wheeled mobile robot can therefore move between any two points in a plane without restriction. Omnidirectional motion makes a mobile robot's heading independent of its orientation (see Figs. 2.7a - 2.7c) (Appendix A.1); and this can provide substantial benefits as well as several problems.

Mobile robots with an all-wheel drive/steering configuration are not original and have already been built. They include the ODV (Omni-Directional Vehicle) built by MITI in Japan [Arai'81], [Nakano'83], the CMU Rover also known as Pluto [Moravec'83], the Kludge, and its successor Cybermation K2A [Holland'86] and the Denning both of which are now commercial available. Most of the present designs rely on shaft transmission [Holland'86], [Nakano'83]. The Kludge which is an earlier version used chain transmission while the K2A uses twin concentric shafts. There are some based on belt drive like that from Barry [Barry'89] and RWI company that are also commercially available. Further details of different designs of the synchro-drive configuration are given later.



**Figs. 2.7 Basic omnidirectional motion:**

- (a) Longitudinal translation.
- (b) Lateral translation.
- (c) Diagonal (heading) translation.
- (d) Omnidirectional mobile robot's degree of freedom -  
 $0^\circ$  to  $360^\circ$  on X-Y horizontal plane.

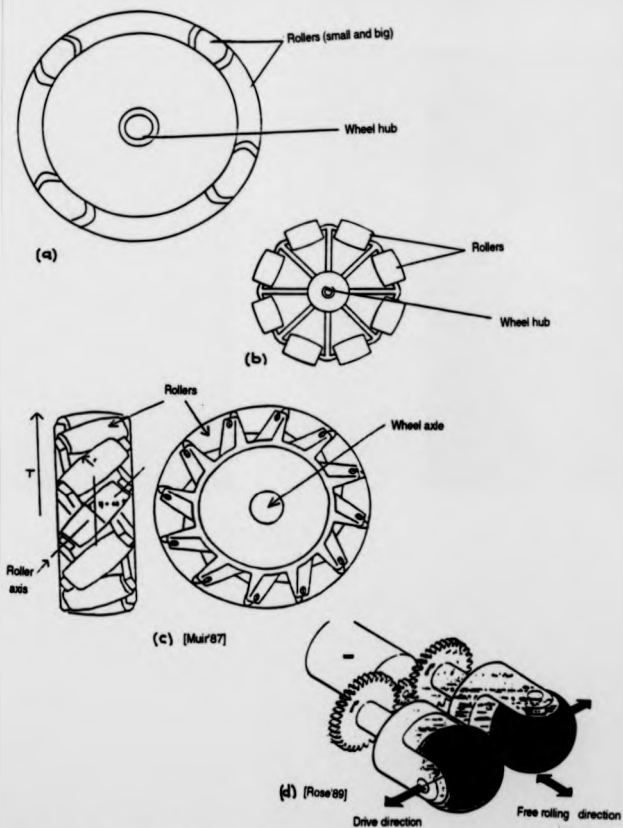


Fig. 2.8 Illustration of some roller arrangements.

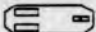



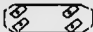
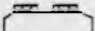
(a) Compound wheel type.

In the compound wheel type, the means to provide steering lies essentially in the wheel. Compound wheels either have a central hub with rollers arranged at the periphery (commonly known as either the Ilonator [Ilon'73] wheel or the Mecanum [Jonsson'85] wheel (see Figs. 2.8a - 2.8c above)); or are without a wheel hub but only made of roller drums [Rose'89] (see Fig. 2.8d).

The compound wheels are held in a fixed relation to one another and they are capable of being independently driven. By driving the wheels in varying combination of speeds and directions, a resultant force is produced which makes it possible to drive the vehicle in any desired direction from 0° to 360° (i.e., Omnidirectionally). Uranus [Muir'87] and others [Carlisle'83], [Jonsson'85], [van der Loos'86] are examples of mobile robots that are based on the compound wheel. Further details of compound wheel mobile robot operation is given later.

In summary, table 2.1 shows different types of steering configuration and the types of motion they can achieve. The mobility limitation of the conventionally steered wheeled mobile robots can be attributed to their inability to move omnidirectionally.

Table 2.1. Steering configuration, motion and turning restrictions.

Steering configuration	Motion Types				Turning Radius Restriction
	Longitudinal		Lateral	Diagonal (any angle)	
	Forward	Reverse			
 Swivel Bolster steering	✓	✓	✗	✗	✗
 Axle Pivot steering	✓	✓	✗	✗	✗
 Dual Swivel Bolster steering	✓	✓	✓	✗	✗
 Differential steering	✓	✓	✗	✗	✓
 All-wheel steering	✓	✓	✓	✓	✓
 Nonsteer wheel	✓	✓	✓	✓	✓

Key

- ✓ Efficient
- ✗ Not Efficient
- ✗ Restriction

## 2.2 OMNIDIRECTIONAL MOTION.

Omnidirectional motion allows a mobile robot to move from rest along a vector at any angle to its current heading (see Fig. 2.7d). It also provides the ability to translate in any direction on a horizontal plane without any associated rotation of the chassis.

The benefits of this type of motion are substantial and are described as follows:

(a) Removal of mobile robot orientation constraints on the path planning algorithms - this results in maximum manoeuvrability which is particularly important to achieve movement in confined spaces.

(b) Elimination of the need to rotate and control mobile robot chassis orientation during motion, in order to travel along a specified path - this results in an ability to respond to a change in direction rapidly.

(c) Elimination of the need to reduce speed during turns except to comply with stability and wheel slip constraints - this results in reduced time to complete a set of moves and allows smooth motion even along complex routes.

(d) There is no path restriction because of zero turning radius - any path can be executed provided that kinematic and dynamic constraints are not violated.

(e) High manoeuvrability allows more scope for the design of larger mobile robots - this is as a result of efficient use of turning space; unlike, for example, the tricycle configuration where an increase in size leads to a decrease in manoeuvrability.

There are however a number of problems associated with the provision of omnidirectional motion. These arise from a fundamental inability to rotate the chassis and they are:

(a) The lack of a constant relationship between the position of the wheels and the direction of travel.

(b) Problem of identifying a specific part of the mobile robot as the 'front' for sensor mounting, etc.

(c) Inability to arrive at a destination in a specified orientation.

(d) Inability to orientate an object or device carried on the mobile robot with respect to its environment.

When implementing a mobile robot capable of omnidirectional motion, items b, c and d can be overcome by the use of an additional platform capable of independent rotation about a vertical axis relative to the chassis.

However, the variability of the wheel positions with respect to the direction of travel cannot be eliminated and this gives rise to different characteristics with regard to stability and accuracy. There is no published work identifying the effect of stability and accuracy characteristics which vary with heading and it was therefore investigated in detail as part of this work.

Two configurations have been identified as capable of producing omnidirectional motion. A further discussion of the configurations now follows.

### 2.2.1 COMPOUND WHEEL BASED DESIGNS.

As mentioned earlier there are two main types of compound wheel, namely;

- (i) Wheel having rollers at the periphery (Ilonator or Mecanum wheel) of the wheel hub.
- (ii) Wheel comprising of roller drums without wheel hub.

#### 2.2.1.1 ILONATOR OR MECANUM WHEEL.

The major difference between mobile robots using the Ilonator wheel are primarily;

- the peripheral roller material, and
- the arrangement of the rollers on the periphery (see Fig. 2.8a - 2.8c).

Attempts have been made to actuate the rollers by using a highly sophisticated driving arrangement [Muir'86], but the complexity of such an approach has resulted in it not being feasible in practice.

The wheel on which the mobile robot is based is provided with rollers that rotate freely about their axis, at an acute angle to the wheel axis. The roller angle varies from 30° to 90°. In most designs the rollers are identical, but they can be made of different sizes (see Fig. 2.8a). In the Unimation wheel design [Carlisle'83] use is made of eight rollers, comprising of alternating long and short ones. In this design the rollers axes are at 90° to the main wheel axis. The design helps to reduce the roller gap that is inherent in compound wheels, and which



produces an intermediate state when ground contact is transferred from one roller to the next.

#### Operation of Ilonator Wheeled Mobile Robot.

If the rollers' mounting angle is not  $90^\circ$ , their axes can be inclined either side of the normal, which makes the wheel to be considered as either 'left-bias' or 'right-bias' (see Fig. 2.9). The biasing indicates the direction in which the mobile robot can freely move based on the roller's angle, with only the roller rotation. For a forward or reverse movement of the wheel, the wheel behaves like a conventional wheel.

The way in which a mobile robot, based on the Ilonator wheel achieves different forms of motion can be analyzed by using Figs. 2.10 and 2.11. Fig. 2.10 shows a four-wheeled arrangement of a mobile robot, with the rollers axes displaced at  $45^\circ$  to the wheel hub longitudinal axis.

For a forward or reverse movement of the mobile robot (i.e.,  $\theta = 0^\circ$ ), only the wheels will turn. That is, there will not be any spinning of the rollers on their axes. And for  $\theta = 45^\circ$ , the wheel hub ceases to turn leaving only the rollers in contact with the ground to spin freely on their axes. Thus for an angle  $\theta$  which is neither  $0^\circ$  nor  $45^\circ$  the mobile robot movement is achieved by a combination of rotation of the rollers and the wheel hub [Daniel'85].

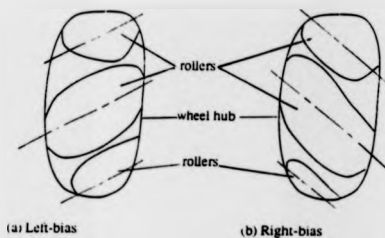


Fig. 2.9 Illustration of Ilonator wheel biasing.

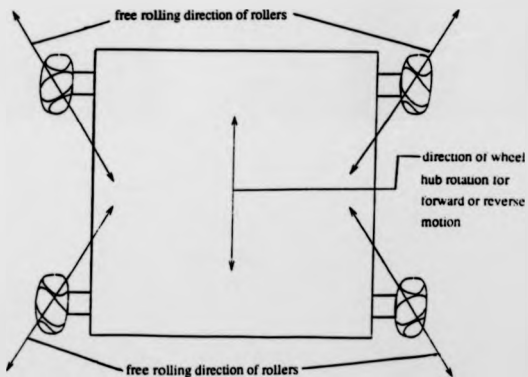
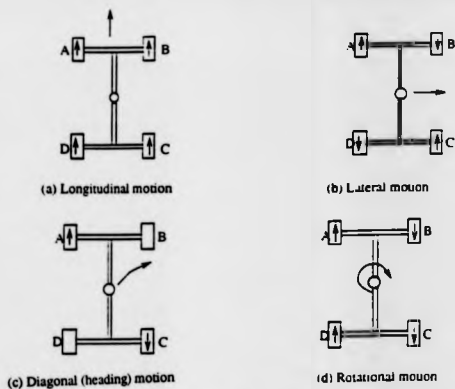


Fig. 2.10 A four-wheel Ilonator mobile robot with rollers placed at  $45^\circ$  to the wheel longitudinal axis.



A, B, C & D : Wheels

→ : Direction of travel.

Fig. 2.11 Attainment of basic motion for a four-wheel design.

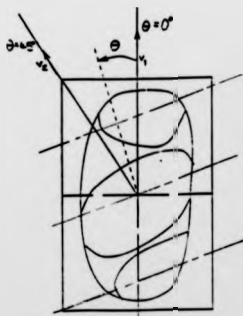


Fig. 2.12 Diagram showing the component velocities  $v_1$  and  $v_2$  of an omniscor wheel mobile robot.

By resolving the Ilonator wheel velocity into two components, having them directed along the line of  $\theta = 0^\circ$  and  $\theta = 45^\circ$  (see Fig. 2.12 above), moving the wheel in any direction  $\theta$  can be achieved by a combination of motion along these component vectors. The kinematics for the control are defined on the basis of the transformation of the mobile robot's velocities (i.e., translation and rotation velocities) into the wheel velocities [Daniel'85], [Muir'86].

#### 2.2.1.2 WHEEL COMPRISING OF ROLLER DRUMS.

Mobile bases have been developed by making use of wheels made of roller drums [Rose'83]. Such a wheel is shown in Fig. 2.13. Its motion analysis is similar to that of Ilonator wheel. Hence there is no further discussion on its operation.



Fig. 2.13 Roller drums arrangement showing driven and free rolling directions [Rose'89].

#### 2.2.1.3 ADVANTAGES AND DISADVANTAGES OF COMPOUND WHEEL.

The compound wheel has its advantages and disadvantages.

The advantages being that:

(a) Based on the roller's freedom to rotate of their own accord along their axes, compound wheels suffers none of the excessive frictional force suffered by conventional wheel which is caused by constant steering required to achieve change in heading [Carlisle'83].

(b) Because of smaller frictional force influences on the wheel during motion, there is minimum wear of both the rollers and floor surface.

Their disadvantages include:

(a) With compound wheels, the mobile robot tend to 'bounce' as the contact point of the wheel with floor translates discretely from one roller to the next roller. The extent of this effect is dependent on the distance between two adjacent rollers along the periphery of the wheel, but it can never be completely eliminated.

(b) The operation of an Ilonstor wheeled mobile robot requires continuous close monitoring and control of speed on all the wheels, if it is to achieve a small tracking error. This requirement brings the need for a precisely engineered wheel and a complex control algorithm.

(c) It has poor tolerance to surface irregularities, which is as a result of the effect of the peripheral rollers. This also influences their directional stability and efficiency.

(d) In an experiment carried out by Daniel, D.J. et al

[Daniel'85], on a mobile robot based on the compound wheel, the following are some of the results that were obtained:

- o Power requirement is dependent on direction of travel.
- o Most power is required for mobile robot lateral travel, indicating that roller bearing friction is greatest in the lateral direction of travel; and in most cases all the wheel motors are actuated.
- o Due to the fact that individual motors are required for each wheel, and they are in some cases driving against each other, its power consumption is generally high.
- o Even with servo braking incorporated there still exists substantial movement after braking, caused by the roller slippage.

(e) Control is achieved by transforming the mobile robots' velocities to that required by the respective wheels and rollers. Difficulties arise due to the inability to know the precise amount of drive motion occurring at the rollers.

(f) Additionally the wheel is considerably more expensive to manufacture than that of a conventional wheel.

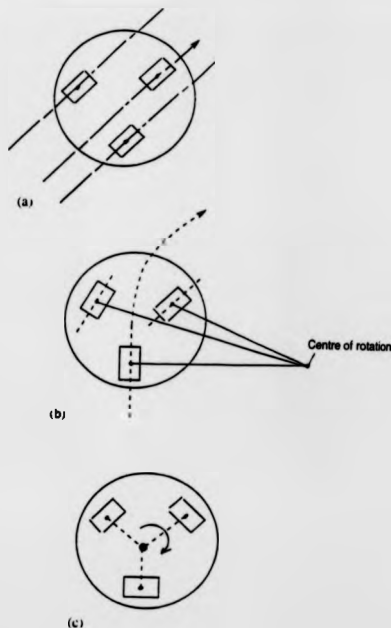
#### 2.2.2 CONVENTIONAL WHEEL SYNCHRO-DRIVE (ALL-WHEEL DRIVE/ STEERING) CONFIGURATION.

Due to the significant benefits in omnidirectional motion, and the basic simplicity in the fundamental design that achieves such a motion through all-wheel steering, it has attracted the interest of many researchers particularly in the United States [Holland'86], [Moravec'83b], [Flynn'88] and Japan [Nakano'83].

Omnidirectional translation coupled with rotation is only possible if a means of adjusting the relative alignment of individual wheels is provided. But the speed of the drive wheels also must be adjusted to avoid slip, except in the unique case of pure rotation about the mobile robot's own axis of symmetry. These three forms of motion are represented in Figs. 2.14a - 2.14c. An all-wheel drive and steer mobile robot capable of chassis rotation as well as omnidirectional translation must therefore have independent control of the drive and steering of each wheel rather than permanent synchronization. A three wheel mobile robot of this type has been built at CMU [Moravec'83], but the control of the three drive motors and three steering motors to ensure smooth path tracking has proved very difficult and is not considered in practice to offer advantage over a mobile robot with a separate orientable platform.

One of the attributes of the synchro-drive system is its fixed orientation as the mobile robot changes direction. This property of synchro-drive can serve the same purpose as a gyroscope for its directional reference [Holland'86]. Like a gyroscope, such a mobile robot under any mechanical systems error is liable to suffer from precession.

To reduce precession the following factors are crucial: mobile robot symmetry must be maintained; steering transmission system must have minimal backlash; wheels must be accurately aligned; wheel diameters have to be the same and tyre materials should offer identical frictional coefficients.



**Figs. 2.14 All-wheel steering system:**

- (a) All wheels aligned: Omnidirectional translation.
- (b) Relative misalignment of the wheels: Omnidirectional translation and rotation.
- (c) Unique case of misalignment: pure rotation about the mobile robot's centre of gravity.



One of the benefits of the synchro-drive system is that only two motors can be used to provide independent drive torque and steering torque for the wheels. The vector forces of the wheels are in principle in a permanent state of parallelism. This allows it to have good directional stability even on undulating surfaces. A mobile robot whose design is based on Synchro-Drive, using conventional wheels tends to have lower energy consumption, higher mobility efficiency and less control complexity, when compared to that of a compound wheel arrangement.

This research work is centred on the Synchro-Drive configuration, for two major reasons. These are:

(1) Synchro-drive appears to have a good combination of the performance characteristics considered desirable in a mobile robot, these being :

- ▷ Manoeuvrability
- ▷ Accuracy
- ▷ Energy efficiency
- ▷ Ease of control
- ▷ Directional stability

(2) Reported work on Synchro-Drive Mobile Robots (SDMR) lacks detailed analysis of its performance particularly with regards to accuracy, stability and the demand on the control system. It is generally assumed to have good accuracy and good directional stability even with simple control. Therefore there is need to test and validate such accepted notions.

For the above two reasons the rest of this thesis is concentrated

on evaluation of mobile robot designs that achieves omnidirectional locomotion through the *Synchro-Drive mechanism*.

### 2.2.3 DESIGNS OF SYNCHRO-DRIVE MOBILE ROBOT (SDMR).

The synchro-drive technique is not very popular among researchers working in the field of mobile robotics because most have simply employed the most readily available platform as a means of investigating issues in navigation and autonomous intelligent decision making. But varying types of synchro-drive configurations that have been implemented are depicted in Figs. 2.15 - 2.18. Differences exist between these designs in the areas such as; transmission system, wheel assembly, location of drive and steering motors, and techniques employed in reducing/eliminating inherent design drawbacks.

As there are differences in designs, so there are in performance. Each of the above factors affect; mechanical complexity, control complexity, energy efficiency, and production cost. For instance, the design shown in Fig. 2.18 can achieve different motion modes, namely; omnidirectional mode, car mode and rotation mode mechanically by use of clutch engagement [Arai'81]. The multi-mode mobile robots so far built are research machines and intended to display the attributes of each mode. It is the authors view that modes other than omnidirectional are unnecessary and the reasons can be seen in Appendix A.1. In this work the mobile robot was designed to be operational in only the omnidirectional mode, and the objective was to investigate the factors affecting performance when operating in this mode.

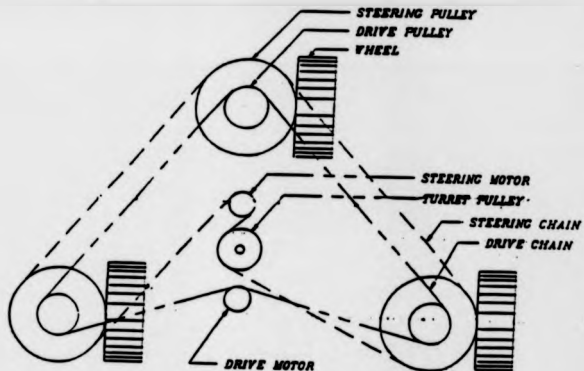


Fig. 2.15 Synchro-drive by continuous means [Holland'86].

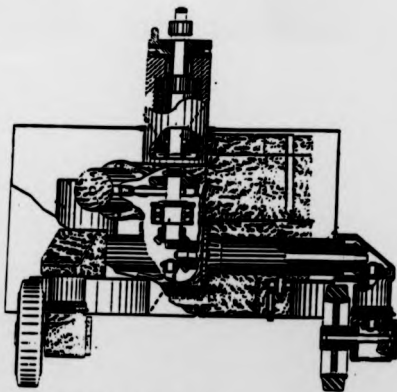


Fig. 2.16 Cut-away view of the K2A drive mechanism [Holland'86]

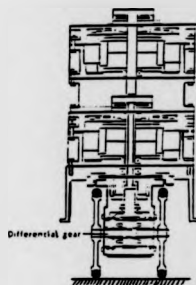


Fig. 2.17 Differential wheel assembly design (Moravec'83).

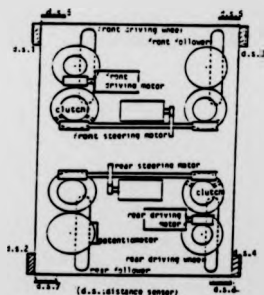


Fig. 2.18 The structure of the ODV (Arai'81).

Investigation revealed that there are three major ways in which a conventional wheel assembly can be configured, in order to achieve omnidirectional motion. They are as follows:

- (i) Wheel-offset from the steering axis of the wheel assembly (see Fig. 2.19), referred to as Type-1.
- (ii) Differential gear coupled wheel set (see Fig. 2.20), referred to as Type-2.
- (iii) Wheel-set on the steering axis of the wheel assembly (see Fig. 2.21), referred to as Type-3.

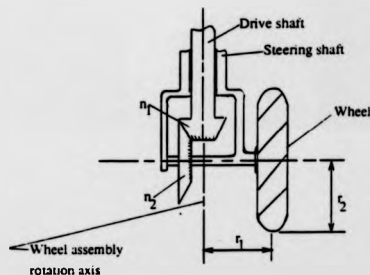


Fig. 2.19 Illustration of design of the wheel-offset from the wheel assembly vertical axis (Type-1).

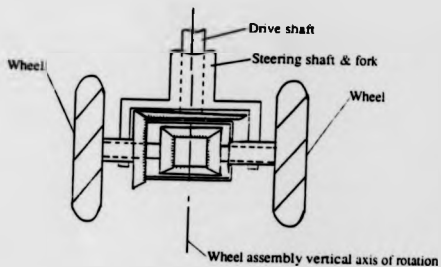


Fig. 2.20 Illustration of design of the differential coupled wheel set (Type-2).

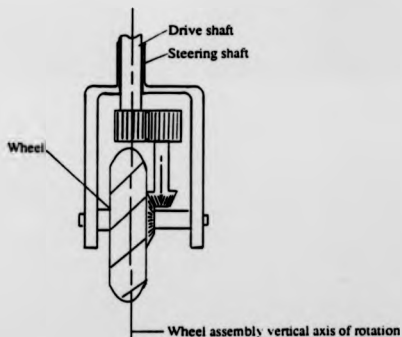


Fig. 2.21 Illustration of design of the wheel-set on the wheel assembly vertical axis (Type-3).

### 2.2.3.1 WHEEL ASSEMBLY, WITH WHEEL-OFFSET FROM THE STEERING

#### AXIS (TYPE-1).

Type-1 has been implemented by some researchers [Nakano'81], [Holland'86] (see Figs. 2.16 and 2.18) working on an omnidirectional mobile robot. The schematic illustration of such a technique is shown in Fig. 2.19.

One of the main benefits of the technique is that by offsetting the tyre/floor contact point from the vertical axis of wheel assembly rotation, the wheel can in theory rotate on its own axis without any slip or 'scuffing' occurring at the floor contact when turning. Using Fig. 2.19 it can be shown that if a correct offset distance  $r_1$  is used and all other factors remain correct, the wheel assembly has the tendency to spin about the point where the wheel assembly vertical axis intersects the floor, instead of round a small circle.

In this arrangement the wheel radius  $r_2$  is a function of the offset distance  $r_1$ , for a given gear ratio. That is;

$$r_2 = \xi r_1 \quad (2.1)$$

where,

$\xi$ , is the gear ratio given by,

$$\xi = n_2/n_1 \quad (\text{see Fig. 2.19}).$$

The wheel radius dependency on the offset distance is a source of limitation for such technique, in that a wheel with radius other than that on which the design was based cannot easily be used. This is because change in wheel radius, changes the point of

rotation of the wheel assembly and therefore increases the potential for errors. Also the assumption is made that the tyre makes a line contact with the ground which is fixed relative to the steering axis. Tyres must therefore be very narrow and stiff to resist lateral deflection.

Another drawback is that offsetting the wheel from the steering axis increases the tendency for the wheel to steer when a drive motion is initiated. The effect of the drawback can be limited by making use of a worm gear set, which has a self-locking function [Arai'81]. The worm gear locks the steering subsystem when there is no power supply from its motor (the same locking effect takes place in the drive subsystem). The closer the worm gear arrangement is to the wheel the more effective will be the resistance to induced steering.

#### 2.2.3.2 WHEEL ASSEMBLY, WITH DIFFERENTIAL GEAR COUPLED WHEEL SET (TYPE-2).

This wheel configuration technique has been implemented by researchers in USA [Moravec'83] (see Fig. 2.17). In this technique a differential gear unit is placed directly under the vertical axis of rotation of the wheel assembly (steering axis), with two wheels coupled to the two ends of the differential gear unit (see Fig. 2.20). The two parallel placed wheels at the ends of the differential gear allows steering of the wheel with a low frictional force even when stationary, and the symmetry of the wheel assembly removes the problems evident in Type-1.



In this configuration the mobile robot direction of travel is the resultant of the angle of the heading of the individual wheel assemblies. Forward and backward motion is achieved only if the drive shaft is rotated by the steering action; so one requires a separate drive motor for each wheel. Forward and backward movement is achieved by turning the inner shaft (drive shaft). While turning the outer shaft (steering shaft) (see Fig. 2.20) steers the wheel assembly, with the two wheels rolling in small circles [Moravec'83].

This technique generally produces a mobile robot with wheel assembly that is mechanically complex, expensive, and requiring a complex control system [Moravec'83], [Muir'86] with lower energy efficiency.

#### 2.2.3.3 WHEEL ASSEMBLY, WITH WHEEL-SET ON STEERING AXIS (TYPE-3)

This third technique, which has the wheel located on the SDMR steering axis, has been explored as a part of this work. From the investigations that have been carried out at the time of writing this thesis, there is no reported work that is implementing this technique. The wheel assembly design is depicted in Fig. 2.21.

By locating the tyre/floor contact point on the SDMR's wheel assembly steering axis, the problem of the wheel having the tendency to steer when drive motion occurs is in theory reduced. This is because there are no offset link forces that introduces a moment about the steering axis. But on the other hand, this

configuration introduces a tendency for the SDMR to drive when steering motion occurs. This is caused by the coupling of the steering and drive subsystems that allows the wheel to be both driven and steered. Steering causes the wheel to drive about a small circle. The value of the drive introduced is dependent on the wheel assembly gear ratio.

It has been discovered that the above drawback can be compensated for by incorporating worm gears and a differential gear arrangement into the drive/steering system of the SDMR (details on how it function is presented in chapter 4 and 5) . Another drawback, though not as significant, is that this technique requires a marginally greater number of gears than the first technique.

This configuration tends to produce a slightly higher rate of tyre wear than the other two techniques, if the mobile robot executes a turn when it is in a stationary state. Nevertheless such a wheel assembly provides an improved stability when compared with Type-1. This comes from two main sources which are; the tyre/floor contact and the wheel assembly steering axis have their z-axis coincidental, and there is a fixed relationship between the mobile robot's centre of mass and the wheels contact with the floor irrespective of the direction of travel (details are in the chapter 4 and 5).

### 2.3 TRANSMISSION SYSTEM.

The transmission system represents an important part in a mobile

robot system. This is borne out of the fact that if one uses the various transmission elements appropriately, one will achieve an overall design, which may be: compact; reliable; easy to maintain and competitive both in terms of performance and cost. Also gaining high power transmission efficiency; accurate and fine movement; and suitability regarding weight and size requirements [Duggan'71].

The transmission elements that may be implemented are:

- Belts with pulleys
- Chains with sprockets
- Shafts with gears.

The shaft, belt and chain transmission elements have their respective benefits and limitations, which are presented below.

Shaft transmission elements have the following advantages: They have definite velocity ratio. They can achieve high load application. They can operate at high speed. With it a compact design is possible [Holland'86].

The shaft transmission element disadvantages include: It cannot usually be obtained as a standard component. It is not easy to isolate or absorb shock and vibration. It requires consideration regarding lubrication. It does not generally accept bending deflection - gears cannot accept misalignment due to shaft deflection [Duggan'71]. It can be difficult to minimize weight while maintaining adequate stiffness. Unlike chains and belts it

is not adjustable when used in a system. Backlash is a problem unless very expensive antibacklash elements are used. It can be a costly option. Most of the shafts disadvantages are not particularly significant when they are used in mobile robots.

The relative merits of timing belt are given as: Being suitable for relatively long or variable centre distances. Ability to absorb shock and vibration. Lubrication and protection are not usually required. It is simple and flexible with low noise level. It provides positive drive with a constant velocity ratio. They do not usually slip or creep.

Timing belt limitations include: Though they come in standard lengths (loop), the lengths are not usually adjustable like chains, except by tensioning. When compared to chain, they are more prone to stretch, wear and elongation with usage. Comparatively they are more expensive.

Timing belts are equally used in SDMR [Barry'89]. They can require frequent maintenance, mainly due to excess belt stretching, which creates a reliability problem.

Chain drives are considered to be intermediate between belts and shaft gear drives. The type of chain considered is the standard single steel roller chain. Other types of chain includes; multistrand and silent chains [Duggan'71]. The benefits of a chain are as follows: If properly selected and installed, chain drives will operate with a very high efficiency, a figure in the

region of 98% can be achieved in an ideal conditions [Duggan'71]. It has the ability to absorb shock and vibration. It is suitable for either medium, short or variable centre distances. It provides a compact and positive method of transmitting power. A single chain may be arranged to drive more than one unit.

Chains, unlike shafts which are generally design specific, are readily available as standard commercial units. This is also the case with belts. But unlike belts, chain length can easily be modified as required. Therefore easy experimentation with various design concepts and the goal of a modular design are better served by chain drives.

The limitations of chain transmission include: The requirements for good shaft alignment. Power chains must articulate over the sprockets, thus giving rise to wear and possibly elongation with usage. The rise and fall due to radial motion of the chain in an attempt to follow the circular pitch line of the sprockets [Greenwood'62] can cause the chain section to have a fluctuating speed. It can also be noisy.

The effect of the radial motion is dependent on the number of teeth of the sprocket [Greenwood'62]. As for the rate of wear and chain elongation, this depends on several factors, that includes: Chains' tension force; state of contact surfaces (hardness); presence or absence or quality of lubrication; area of contact between pins and bushing (pin diameter times bushing length). Chain noise can be reduced by using smaller pitch.

This review shows that components of transmission system will greatly influence the overall performance that a mobile robot can achieve. Thus the use of a certain type of transmission should be application related.

This chapter has reviewed mobile robots in general and those capable of omnidirectional motion in particular. The *synchro-drive mechanism* has been identified as being of particular interest and worthy of in-depth analysis with regard to its potential performance. Hence the rest of this thesis concentrates on providing an in-depth knowledge of operation and performance of the Synchro-Drive Mobile Robot (SDMR).

The next three chapter deals with modeling and further analysis of synchro-drive mobile robots in terms of the factors that influence performance with particular emphasis on tipping stability and trajectory execution.

## CHAPTER 3

### ANALYSIS OF FACTORS THAT INFLUENCE PERFORMANCE

Synchro-Drive Mobile Robot (SDMR) performance with respect to position accuracy, trajectory execution and stability are influenced by; the interactions between the SDMR wheel and the floor surface, the mechanical systems error, and the SDMR response to drive and steering input. In this chapter the factors that influence performance are analyzed in three different sections as:

- o Wheel force/torque analysis.
- o Error types, sources and effects.
- o SDMR behaviour under a command input.

#### 3.1 WHEEL FORCE/TORQUE ANALYSIS.

Most of the forces that affect the motion of a mobile robot are applied at the wheel/floor surface interface. This gives rise to the need to understand the basic characteristics of the interaction that occurs. Such an understanding will assist in explaining the behaviour of the SDMR when it executes a particular command.

##### 3.1.1 COMPONENT FORCES, MOMENTS AND ANGLE OF A WHEEL.

Fig. 3.1 shows the forces and moments that act on any wheel. The coordinate system ( $X_c$ ,  $Y_c$  and  $Z_c$ ) used for the analysis has its origin at the wheel/floor contact. Forces acting on the wheel through the floor surface are:

- ▷ Tractive force (or longitudinal force),  $F_x$ .
- ▷ Lateral force,  $F_y$ .
- ▷ Normal force,  $F_z$ .

The moments acting on the tyre are:

- ▷ Overturning moment,  $M_x$ .
- ▷ Rolling resistance moment,  $M_y$ .
- ▷ Aligning torque,  $M_z$ .

Angles that are associated with a rolling tyre are:

- ▷ Slip angle,  $\alpha$ .
- ▷ Camber angle,  $\gamma$ .

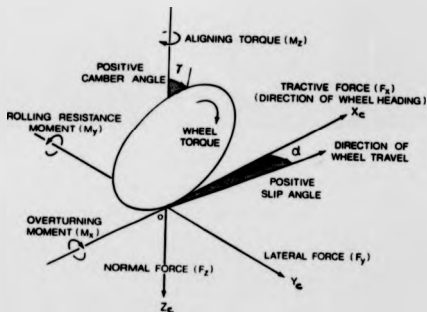


Fig. 3.1 Coordinate system of a wheel showing forces, moments and attached angles [Wong'78].



Among these forces, moments and angles, the ones whose effects can be identified during the operation of a mobile robot are; the tractive force, lateral force, normal force, aligning torque and slip angle.

The Normal force is the component of the resultant force that acts in the negative  $z$  direction of the wheel/floor coordinate system. It represents that proportion of the mobile robot's weight that is supported by the wheel.

The elastic nature of the tyre is such that the centre of normal load on wheel/floor contact is not at the origin of the coordinate system of tyre-floor axes [Wong'78]. Hence the three forces ( $F_x$ ,  $F_y$  and  $F_z$ ) that act on the tyre are displaced by certain distance. These displacements give rise to moments about the origin of the coordinate system. The three moments as already stated above are (see Fig. 3.1); Overturning moment,  $M_x$ , Rolling resistance moment,  $M_y$ , and Aligning moment,  $M_z$ . The magnitude of these moments in mobile robots are generally very small. This is because the shift of the point of contact of the normal load is very small when hard solid tyres are used. Their effects in first order analysis of mobile robots are deemed negligible [Wong'78], [Collins'87], particularly those of overturning and rolling resistance moments. But in the different mobile robot designs the aligning moment can play a role, as will be explained later in chapter 5.

The other important parameters of a wheel are the slip angle,  $\alpha$ ,

and camber angle,  $\gamma$ . The angle that exists between the direction of wheel travel and the line through the intersection of the wheel plane and the floor surface is called the slip angle (see Fig. 3.2a). The angle that also exist between the yz plane and the wheel plane is called the camber angle (see Fig. 3.2b).

The component of the resultant force on the wheel by the floor surface that acts in the x-direction is known as the tractive force (or longitudinal force). The x-direction represents the direction of the wheel heading. The tractive force is created by the application of drive torque to the wheel. This is through the friction between the tyre and the floor. It occurs at the wheel/floor contact area (contact area instead of contact point exists in reality, because of the tyre compression and deformation under load). The shape of the contact area is approximately elliptical and its size depends on the load, material and construction of the tyre.

A tyre that is not subjected to any force that acts perpendicular to its wheel plane (i.e., no side force) will have a rolling direction that coincides to that of the wheel plane. The Lateral force is the component of the resultant force that acts in the y-direction of the tyre coordinate system. The lateral force is a function of the two tyre angles, the slip and camber angle. For any slip angle that is not zero, tyre deformation occurs due to tyre elasticity, which allows the tyre to move through an unnatural path. The tendency for the tyre to slide is resisted

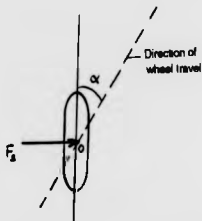


Fig. 3.2a Illustration of slip angle  $\alpha$  (top view).

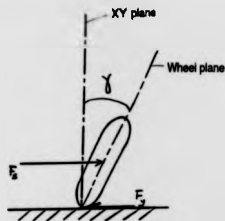


Fig. 3.2b Illustration of camber angle  $\gamma$  (side view).

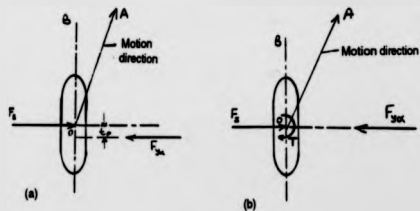


Fig. 3.3 Behaviour of wheel under the influence of side force (top view).

by the lateral force, whose direction of operation opposes the axis velocity component in the y-direction.

### 3.1.2 SDMR WHEEL.

In the case of most SDMR's where there are no camber angles introduced in the wheel assembly design, the lateral force is equivalent to the cornering force. With the existence of a side force  $F_s$ , a lateral force is developed at the contact area. The lateral force will cause the tyre to travel along a path at an angle  $\alpha$  to the wheel plane (see Fig. 3.2a). In mobile robots hard tyres are invariably used, hence slip angle tends to be very minimal. The angle referred to as angular 'free-play'  $\sigma$  has the most significant effect. Free-play angle is a function of the characteristics of the power transmission system and the wheel assembly.

The relationship between the lateral force and the free-play angle is very important to SDMR directional control and stability. What happens between cornering force and slip angle is similar to that between lateral force and free-play angle. Thus understanding one analysis helps to understand the other. Consider a wheel moving at a uniform speed in the direction OA (see Fig. 3.3), the side force  $F_s$  applied at the wheel centre and the cornering force  $F_{y,\alpha}$  in the ground contact are usually not colinear. For small slip angle, cornering force has been established to be slightly behind the applied side force [Wong'78]. The cornering force generates a torque (or couple),  $F_{y,\alpha} t_p$  acting on the wheel and it tends to align the wheel plane

with its direction of motion. If the wheel plane is to be kept parallel to the line OB; an equal and opposite couple must be applied to it by some other mechanism. For a mobile robot such a mechanism could be the steering system, or the suspension system where there is one.

The torque  $F_{ya} t_p$  is commonly known as self-aligning torque and it is one of the main restoring moments that helps a steered wheel to return to its original position after negotiating a turn. With reference to Fig. 3.3a, the horizontal distance between the  $F_y$  and  $F_{ya}$ ,  $t_p$  is known as the tyre trail. The tyre trail and the cornering force determines the self-aligning torque. The situation taking place in Fig. 3.3a can be represented in an alternative way as in Fig. 3.3b, consisting of force  $F_{ya}$  acting in the wheel plane where the wheel axis is located, together with a torque  $T$  acting about the vertical wheel axis.

The relationship between cornering force and slip angle for a solid rubber tyre has been investigated [Collins'87] (see Fig. 3.4). The test result shown in Fig 3.4, indicates that for small slip angle of up to about  $2.5^\circ$ , the cornering force increases approximately linearly as the slip angle increases. Above that cornering force increases at a lower rate until it reaches a value where lateral sliding sets in. At the on-set of sliding, the peak cornering force is determined by the coefficient of road adhesion  $\mu$  and the vertical load  $F_z$  ( $\mu F_z$ ) [Stead'60].

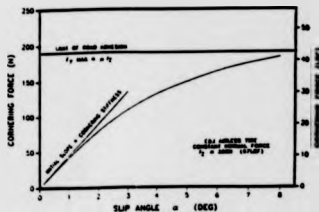


Fig. 3.4 Solid rubber tyre plot, showing relationship between cornering force and slip angle (Collins'78).

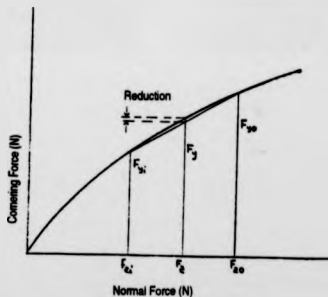


Fig. 3.5 Cornering force changes due to the effect of lateral load transfer (Wong'78).

Results reported in Wong [Wong'78] and by Collins [Collins'87] have shown that a number of factors influence the cornering behaviour of tyres and hence that of a mobile robot. The factors include; the vertical load on the tyre - for a given slip angle, increasing the vertical load results in increase in the cornering force. But it is noted that the relationship between the cornering force and the vertical load is nonlinear.

The results showed an important phenomenon, which is the transfer of load from the inside to the outside of a pair of wheels during heading change. This results in reducing the total cornering force that a pair of wheel can develop. This is illustrated with Fig 3.5. Consider a case where a pair of wheels on a mobile robot with a beam axle, each having vertical load  $F_{zi}$ , have a cornering force  $F_{yi}$  for a given slip angle. Assuming that the mobile robot is undergoing a steady-state turn, owing to lateral load transfer, the normal load on the inside tyre will be reduced to  $F_{zi}$  and that on the outside tyre will be increased to  $F_{zo}$ . The total cornering force of the two tyres will be  $F_{yi} + F_{yo}$ , which is less than  $2F_{yi}$ , as Fig 3.5 above shows. The implication of this phenomenon, is that there is a resultant increase in the slip angle of the tyres, because of the need for such pairs of tyre to develop the required amount of cornering force to balance a given centrifugal force.

Another aspect revealed by the test is that cornering force is highly independent of forward speed. When the forward speed is varied there is no noticeable changes in the shape of the tyre's

cornering force curves. Also cornering stiffness (cornering stiffness,  $C_\alpha$  is defined as the derivative of the cornering force  $F_{ya}$  with respect to slip angle,  $C_\alpha = \partial F_{ya} / \partial \alpha$ ) is highly dependent on choice of tyre. This implies that the sort of tyre used in a mobile robot also plays a part in determining its stability. For good performance, it is recommended that the tyre to be used should be one that gives low cornering stiffness, while maintaining good rolling resistance and low tyre wear.

### 3.2 ERRORS THAT AFFECTS THE SDMR PERFORMANCE.

Investigations show that there are several causes of errors that affect the mobile robot's performance. These sources of error create a situation where the mobile robot does not respond accurately to the specified command. The discussion will focus on two main aspects, namely:

- o The types of errors.
- o Sources of errors.

#### 3.2.1 TYPES OF ERROR.

The errors that affect the performance of the mobile robot can be classified into two main classes, namely:

- (a) Predictable or Systematic errors and
- (b) Non-predictable or Random errors.

##### 3.2.1.1 PREDICTABLE ERRORS.

Factors like, wheel misalignment and tyre wear produces error of this type. Error is considered to be predictable if it is consistent in a given direction of travel.



The effect of predictable error can be seen by considering a situation where a misalignment of one or more of the wheel(s) exists (see an illustration in Fig. 3.6 - with one wheel misaligned). Such a situation, may result in the SDMR moving in an arc of distance  $L_2$  and radius  $R$  instead of in a straight line of distance  $L_1$  as desired (see Fig. 3.7).

The path taken by the mobile robot and its radius is a function of angle of misalignment. The radius of the circular path is inversely proportional to the angle of misalignment;

$$\text{i.e., } R \propto 1/\alpha' \quad (3.1)$$

$$\text{As } \alpha' \rightarrow 0, \quad R \rightarrow \infty.$$

Relating these phenomenon to the two main position errors that arises from the SDMR's movement (lateral error,  $\delta y$  and longitudinal error,  $\delta x$ ) gives;

$$\text{if, } \alpha' \rightarrow 0, \quad R \rightarrow \infty$$

as  $R$  becomes very large,  $L_2$  gets closer to  $L_1$ ,

$\Delta \delta x$  and  $\delta y$  becomes smaller.

Any finite value of  $R$  caused by wheel misalignment could cause slip to occur. This is due to the fact that all the wheels are being driven at the same angular velocity but are moving on paths of differing radii.

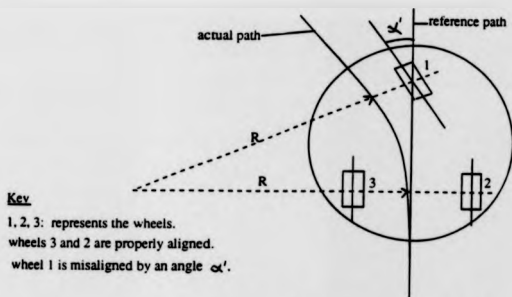


Fig. 3.6 Illustration of a misaligned wheel, reference path and the resultant SDMR's actual path.

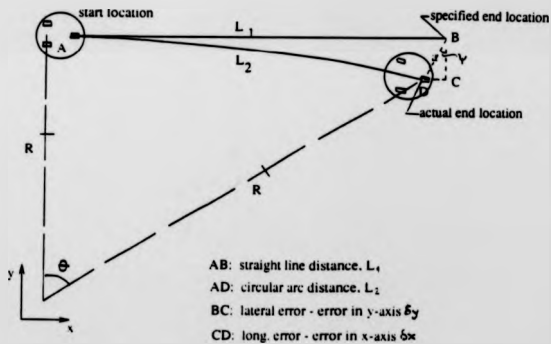


Fig. 3.7 Illustration of predictable error.

### 3.2.1.2 NON-PREDICTABLE ERRORS.

A non-predictable error is one that arise from events that are unforeseen from the onset of the SDMR's motion. They are contributed by events such as, wheel slip, arising from factors that include; floor surface roughness and state of the power transmission system, quantization error in the feedback system, etc.. They are classified as purely random errors, which may be expected to produce a cumulative mean error of zero, over many samples, but which can contribute large interim errors.

The impact of non-predictable error can be shown, by considering a situation where a bump exists along the path specified for the SDMR to follow. If the SDMR keeps to the specified path, under such circumstance one of the wheels may climb the bump. If this happens a drift in the SDMR's motion may occur and the resultant movement may be as shown in Fig. 3.8. Lateral error,  $\delta y$  and longitudinal error,  $\delta x$  will appear due to the drift (see Fig. 3.8).

The magnitude of the errors  $\delta y$  and  $\delta x$  depends on two factors; where along the path the error source was encountered, and the impact of the error source on the SDMR system.

The two above factors imply that non-predictable error can be either greater than, equal to or less than the predictable error. The unpredictability of this error makes it much more difficult to eliminate, or develop a compensation system to cater for it.

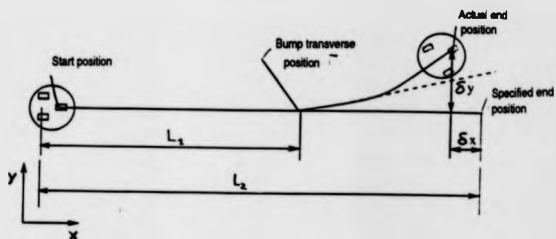


Fig. 3.8 Illustration of non-predictable error.

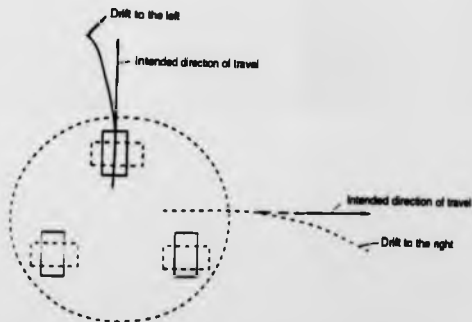


Fig. 3.9 Illustration of drift inconsistency due to principle of synchro-drive system.

### 1.2.2 SOURCES OF ERROR.

The errors that affects the mobile robot may be generated by one of a number of sources that include:

- (1) Power transmission mechanism.
- (2) Tyre.
- (3) Wheel alignment.
- (4) Nature of floor surface.
- (5) Sensors and Computation.

The mechanical system's error sources are of particular interest and they are covered by (1) to (3) above. How the five sources create error are briefly discussed below.

#### 1.2.2.1 POWER TRANSMISSION MECHANISM.

The transmission mechanism, which transmits the drive and steering power to the wheels are made of chains, sprockets, shafts and gears. They have the benefit of normally allowing no slip or stretch but there is inevitably some degree of slack and backlash. They do also suffer from imperfect manufacture partly due to dimensional tolerances.

##### (a) Transmission System.

Some slack is normally evident in chain drive systems because it is not possible to provide sufficient tension without causing undue strain on bearings and the chain itself. Similarly geared systems cannot be in a constant perfect mesh without resulting in a high contact forces. These requirements for compromise create a source of error.

If slack exists in the steering mechanism it will introduce 'play' of the wheels about the z-axis and may result in the wheels having different headings. In the same vein, if slack occur in the drive mechanism the wheels will exhibit 'play' about their respective y-axis and this may result in slip. The errors generated by the transmission mechanism are generally considered as non-predictable errors, because slack and backlash varies with the state of adjustment and tolerances of the transmission system.

(b) Drive and Steering subsystems meshing.

The drive subsystem and the steering subsystem meshes through the spur and bevel gears (see Fig. 3.10). It is through these meshing that the induced drive action caused by the steering torque creates an error in the mobile robot's position.

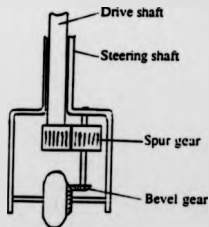


Fig. 3.10 Diagram showing drive and steering subsystem meshing through the spur and bevel gears.

The value of the error,  $\delta m$ , created by the above phenomenon is a function of: the gear ratio,  $\xi$  from the point of meshing of the two subsystems; the wheel diameter,  $D$ ; and the turned angle,  $\phi_*$ . This can be expressed as;

$$\delta m = f(\xi, D, \phi_*) \quad (3.2)$$

$$\delta m = (D/\xi) (\phi_*/360) \quad (3.3)$$

This form of error is predictable and hence can be compensated.

### 3.2.2.2 TYRE.

The tyre contributes its own share of errors from; tyre size, tyre slip, tyre creep, material and structure. The variation in wheel size can arise from; tyre wear, manufacturing tolerance, loading effect, etc. The tyre size error is considered predictable error for it can be measured.

Tyre slip that may have a noticeable influence on the SDMR can be seen to be a function of the parameters, such as; steer angle, braking torque, and driving force acting on the tyre. Braking torque and driving torque induces slip, only if the traction force exceeds the friction forces and normally acceleration and deceleration rates can be limited to remove this possibility.

The extent of tyre creep is dependent on the tyre material and structure. Tyre creep produces area contact instead of point contact necessary for perfect rolling. Its effect has been discussed earlier.

#### 3.2.2.3 WHEEL ALIGNMENT.

Any misalignment of any of the three wheels introduces an error in the mobile robot movement. The misalignment of the wheels would produce a drift from the desired path. The exact path taken will be a curve and it is dependent on; the extent of the misalignment, the number of wheels involved, the relative wheel displacement, and the direction of travel in relation to the wheel heading relative to the SDMR chassis.

#### 3.2.2.4 NATURE OF FLOOR SURFACE (ROUGHNESS).

Nature of floor surface problems arises in the form of; bumps or cavities in the floor, and slippery floor or floor slope. Each of these induce an error into the mobile robot system, which shows up as tyre slip or creep or wheel misalignment. Due to the random nature of their occurrence, the error created by the nature of the floor surface is considered to be a non-predictable error.

#### 3.2.2.5 SENSORS AND COMPUTATION.

Sensors for 'dead-reckoning' position determination gives two form of errors; quantization error [Banta'87] represented as;  $\zeta = \pi D/D$ , where  $D$ , is the wheel diameter and  $D$  is the number of divisions that the sensor gives for one wheel rotation. The second sensor error arises in the way in which the sensor is coupled to the unit that is to be sensed. Where it is not possible to connect it directly to the moving part, for example the wheel, then it become necessary to measure instead the movement of some part of the transmission system leading to the



wheel, and any phase difference in the transmission system will cause error.

Computation error arises mainly from integration errors [Banta'87]. The accuracy of the integration process is influenced by the extent to which they represent the actual motion of the mobile robot. It also depends on the number of significant figures which the computer uses to carry out its computation.

### 3.3 SDMR BEHAVIOUR

The intention of this section is to explain why the SDMR trajectory when there is no steering input can result in curved path. The nature of the curve is identified with the aid of the analysis of the equation of motion of the centre of mass that give rise to such a trajectory. With the developed equations a general qualitative analysis of motion can be offered.

Also discussed is the behaviour of the SDMR when there is a steering input. Here the SDMR behaviour under steady-state and the transient state are of interest.

#### 3.3.1 BEHAVIOUR UNDER DRIVE INPUT ONLY.

For the SDMR not to translate in a straight line when requested to do so, there must be an error in its geometry. For instance, the SDMR is designed to be symmetrical, with the wheels' 'point' of floor contact forming an equilateral triangle. This symmetry in most cases is not achieved because instead of 'point' contact

at the wheel/floor interaction, we have area contact whose shape is ellipsoidal [Wong'78]. This area contact can cause the SDMR to lose symmetry. Fig. 3.11 shows a case where there may be symmetrical area contact but no contact point symmetry. Also the transmission mechanism which is observed to be characterized by slack and backlash can cause loss of symmetry.

Once symmetry is lost, the tractive forces acting at the three wheels either become unequal in magnitude or become non-parallel. This will cause a twisting moment resulting in precession about the z-axis. Frame rotation while the SDMR is in motion implies that the motion of the entire system is no longer uniform. The motion that results depends on the tractive force  $F$ , resistance force  $K$ , and the SDMR structure as defined by the moment of inertia  $I$ , mass  $m$ , and relevant dimensions (see Fig. 3.12). Having identified some of the factors that may cause the SDMR not to translate in a straight line it is therefore worth investigating what the trajectory should be under different conditions.

#### 3.3.1.1 EQUATIONS OF MOTION AND TRAJECTORY ANALYSIS.

The errors under investigation causes the SDMR to undergo body frame rotation about the z-axis of the centre of mass. Therefore the resulting motion is considered as a combination of the rotation of the frame about the centre of mass and a translatory displacement. Using Fig. 3.12 an equation of the motion of the centre of mass, as referred to the tangent to the path taken by the SDMR can be represented as;



$$\begin{aligned}
 m \frac{d^2 s}{dt^2} &= F_1 + F_2 + F_3 - K \\
 I \frac{d^2 \alpha}{dt^2} &= \frac{\sqrt{3}}{6} l (F_1 + F_3) - \frac{\sqrt{3}}{3} l (F_2) - M_o
 \end{aligned}
 \tag{3.4}$$

where,  $l$ , is the wheelbase in a tricycle configuration,

$s$ , is the distance moved by the SDMR,

$\alpha$ , is the angle between the specified path and the tangent to the path taken by the SDMR.

$F_1$ ,  $F_2$ , and  $F_3$  are the wheels' tractive force,

$K$ , is the motion resistance acting on each wheel, with

$K = 3K$  (for the three wheels),

$M_o$ , is the moment of resistance to the frame rotation about the centre of mass,

$m$ , is mass of the SDMR,

$l$ , is the horizontal distance between the first and the last wheel location.

Considering a situation where at time  $t = 0$ , the linear velocity of the centre of mass is  $v_R$  and the angular velocity  $\omega$  is zero, then;

$$\begin{aligned}
 \frac{ds}{dt} &= \frac{F_1 + F_2 + F_3 - 3K}{m} t + v_R \\
 \frac{d\alpha}{dt} &= \frac{0.29l(F_1 + F_3) - 0.58l(F_2) - M_o}{I} t
 \end{aligned}
 \tag{3.5}$$

For convenience let,

$$\begin{aligned}
 \frac{F_1 + F_2 + F_3 - 3K}{m} &= (\lambda), \\
 \frac{0.29l(F_1 + F_3) - 0.58l(F_2) - M_o}{I} &= (\lambda)
 \end{aligned}
 \tag{3.6}$$

Substituting equations (3.6) in (3.5) yields;

$$\begin{aligned}\frac{ds}{dt} &= (l)t + v_R \\ \frac{dx}{dt} &= (\lambda)t\end{aligned}\quad (3.7)$$

The radius of curvature,  $r_c$ , of the path executed by the SDMR is given by  $r_c = ds/d\alpha$ . From this, equations (3.7) yields;

$$r_c = \frac{(l)}{(\lambda)} + \frac{v_R}{(\lambda)t} \quad (3.8)$$

And the length of the path segment is,

$$ds^2 = dx^2 + dy^2 \quad (3.9)$$

with the path tangent,  $\tan(90-\alpha) = dx/dy$ .

At time = 0 and  $\alpha = 0$ , integrating the second of the equations in (3.7) yields,

$$\alpha = \frac{1}{2}(\lambda)t^2 \quad (3.10)$$

With the aid of triangle ABC attached to the SDMR path in Fig. 3.12;

$$ds = \frac{dy}{\sin \alpha} \quad \text{or} \quad ds = \frac{dx}{\cos \alpha}$$

substituting for  $ds$  and  $\alpha$  using equations (3.7) and (3.10), the following expression emerges;

$$\begin{aligned}\frac{dy}{\sin^{\frac{1}{2}}(\lambda)t^2} &= [(l)t + v_R]dt \\ \frac{dx}{\cos^{\frac{1}{2}}(\lambda)t^2} &= [(l)t + v_R]dt\end{aligned}$$

Integrating the expression yields;

$$\begin{aligned}
 y &= -\frac{(t)}{(\lambda)} \cos_{\frac{1}{2}}(\lambda)t^2 + u_n \int \sin_{\frac{1}{2}}(\lambda)t^2 dt + \frac{(t)}{(\lambda)} \\
 x &= \frac{(t)}{(\lambda)} \sin_{\frac{1}{2}}(\lambda)t^2 + u_n \int \cos_{\frac{1}{2}}(\lambda)t^2 dt
 \end{aligned}
 \tag{3.11}$$

Using the following expansions,

$$\begin{aligned}
 \int \sin_{\frac{1}{2}}(\lambda)t^2 dt &= \int \frac{\left[ \sin \frac{\pi}{2} \left( \sqrt{\frac{(\lambda)}{\pi}} t \right)^2 \right] \sqrt{\frac{(\lambda)}{\pi}}}{\sqrt{\frac{(\lambda)}{\pi}}} dt \\
 \int \cos_{\frac{1}{2}}(\lambda)t^2 dt &= \int \frac{\left[ \cos \frac{\pi}{2} \left( \sqrt{\frac{(\lambda)}{\pi}} t \right)^2 \right] \sqrt{\frac{(\lambda)}{\pi}}}{\sqrt{\frac{(\lambda)}{\pi}}} dt
 \end{aligned}$$

and making the substitution,  $u = t\sqrt{(\lambda)/\pi}$ , from which  $du = \sqrt{(\lambda)/\pi} dt$ , gives;

$$\begin{aligned}
 y &= -\frac{(t)}{(\lambda)} \cos_{\frac{1}{2}}(\lambda)t^2 + u_n \sqrt{\frac{\pi}{(\lambda)}} \int \sin_{\frac{\pi}{2}} u^2 du + \frac{(t)}{(\lambda)} \\
 x &= \frac{(t)}{(\lambda)} \sin_{\frac{1}{2}}(\lambda)t^2 + u_n \sqrt{\frac{\pi}{(\lambda)}} \int \cos_{\frac{\pi}{2}} u^2 du
 \end{aligned}
 \tag{3.12}$$

The integral  $\int \sin_{\frac{\pi}{2}} u^2 du$  and  $\int \cos_{\frac{\pi}{2}} u^2 du$  are known as Fresnel's integral [Itô'87] and has been determined. Equation (3.12) can be expressed as follows;

$$\left[ y - \left( \frac{t}{\lambda} \right) + v_{rv} \sqrt{\frac{\pi}{(\lambda)}} \int \sin \frac{\pi}{2} u^2 du \right]^2 = \left[ - \left( \frac{t}{\lambda} \right) \cos \frac{1}{2}(\lambda) t^2 \right]^2 \quad (3.13)$$

$$\left[ x - v_{rv} \sqrt{\frac{\pi}{(\lambda)}} \int \cos \frac{\pi}{2} u^2 du \right]^2 = \left[ \left( \frac{t}{\lambda} \right) \sin \frac{1}{2}(\lambda) t^2 \right]^2$$

Adding the two equations of equation 3.13, yields;

$$\begin{aligned} & \left[ y - \left( \frac{t}{\lambda} \right) + v_{rv} \sqrt{\frac{\pi}{(\lambda)}} \int \sin \frac{\pi}{2} u^2 du \right]^2 \\ & + \left[ x - v_{rv} \sqrt{\frac{\pi}{(\lambda)}} \int \cos \frac{\pi}{2} u^2 du \right]^2 = \left[ \left( \frac{t}{\lambda} \right) \right]^2 \end{aligned} \quad (3.14)$$

Equation (3.14) which results represents a family of curves with constant radius given as  $(t)/(\lambda)$ . The centres of the circles are located on a curve determined by Fresnel's integral, as;

$$\begin{aligned} y' &= v_{rv} \sqrt{\frac{\pi}{(\lambda)}} \int \sin \frac{\pi}{2} u^2 du + \left( \frac{t}{\lambda} \right) \\ x' &= v_{rv} \sqrt{\frac{\pi}{(\lambda)}} \int \cos \frac{\pi}{2} u^2 du \end{aligned} \quad (3.15)$$

Equation (3.15) represents that of cornu spiral (see Fig. 3.13). The implications of equations (3.14) and (3.15) is that; the path which the SDMR centre of mass executes when undergoing frame rotation can be represented as a curve whose centre is located using equation (3.15).

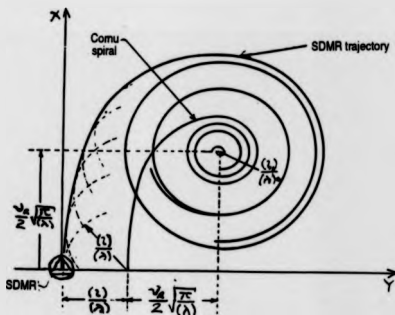
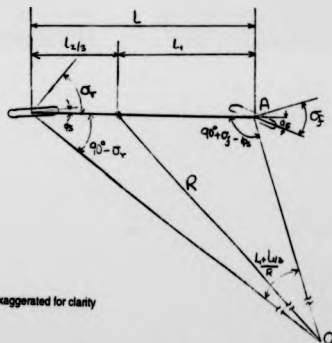


Fig. 3.13 Illustration of possible trajectory of SDMR.



Note:  
Angles are exaggerated for clarity

Fig. 3.14 Two wheel model of the SDMR.



### Effects of $(\iota)$ and $(\lambda)$

When  $(\iota) = (\lambda) = 0$ , the motion of the SDMR is a straight line along the x axis. Here equations (3.11) reduces to  $y = 0$  and  $x = v_R t$ . If for  $t = 0$ ,  $da/dt = \omega_R$ , then having  $(\iota) = (\lambda) = 0$ , gives  $da/dt = \omega_R$  and  $ds/dt = v_R$ . This establishes the radius of curvature  $r_c$ , as  $r_c = v_R/\omega_R$ . Under this condition the SDMR executes a circular path of radius  $v_R/\omega_R$ .

If the situation is such that  $(\iota) > 0$  and  $(\lambda) > 0$ , the SDMR path is represented as in Fig. 3.13. If on the other hand  $(\iota) < 0$  and  $(\lambda) = 0$ , the SDMR moves along the x axis with an acceleration or deceleration  $(\iota)$ . Given that  $(\lambda) > 0$  and that  $(\iota) = 0$ , equation (3.12) may be expressed in the form;

$$y = v_R \sqrt{\frac{\pi}{(\lambda)}} \int \sin \frac{\pi}{2} u^2 du$$

$$x = v_R \sqrt{\frac{\pi}{(\lambda)}} \int \cos \frac{\pi}{2} u^2 du$$

and the curve which this establishes will be identical to the cornu spiral.

In a situation where  $(\iota) < 0$  and  $(\lambda) > 0$ , the radius of the circle in equation (2.14) takes the form;

$$\left[ y - \frac{(\iota)}{(\lambda)} \right]^2 + x^2 = \left[ \frac{(\iota)}{(\lambda)} \right]^2$$

This implies that the path executed by the SDMR is transformed into a circle, the centre of which is located on the y axis at a distance  $(\iota)/(\lambda)$  from the origin.

The analysis has shown that where the orientation of the SDMR frame is monitored and with the ability to determine the motions of respective wheel the nature of trajectory executed by the SDMR centre of mass can be determined by checking the values of ( $\iota$ ) and ( $\lambda$ ).

The discussion here covers a general phenomenon, and they describe the behaviour of the SDMR in an equilibrium state. It is worth noting that the discussion makes simplified assumptions. For instance the forces  $F_1$ ,  $F_2$  and  $F_3$  are assumed constant, which in reality they are not. They are dependent on the motor torque and the transmission system inequalities. Also in reality the effect of centripetal and coriolis forces cannot be neglected, especially if high operating speed is considered. These facts need considering if greater accuracy is essential. However this analysis serves the purpose of understanding SDMR trajectory and characterization of its error, and for that the extent covered is deemed adequate. Also it has to be recognized that even the theoretical analysis discussed will be very difficult to implement in practice, because of problems of measuring and controlling ( $\iota$ ) and ( $\lambda$ ) parameters.

### 3.3.2 BEHAVIOUR UNDER A STEERING INPUT.

The analysis here deals with the way the SDMR responds to a steering input that changes its direction of motion. The issues that are of interest are;

- ▷ the control of mobile robot to its desired path, and

- ▷ the stabilization of the direction of motion against external disturbances.

The discussion is concerned with the steady-state and transient performance of SDMR. A two wheel geometrical model of the system is used for the analysis (see Fig. 3.14 above). The two wheel system is assumed by considering two of the wheels combined to form a single wheel. Considering that all the wheels of a SDMR are driven and steered in unison under a fixed chassis orientation, such an assumption is seen as valid for the purpose of evaluating SDMR behaviour.

#### 3.3.2.1 STEADY-STATE BEHAVIOUR.

The performance in terms of directional behaviour when the SDMR is negotiating a turn under non-time varying conditions is of concern. Steady-state operation of a mobile robot can be represented by a mobile robot turning through a curve of constant radius at a constant forward speed. Inertia properties of the SDMR are not of interest in the steady-state performance analysis.

The steering characteristics depends on the relationship between the 'free-play' angles of the wheels  $\sigma_l$  and  $\sigma_r$  (Fig. 3.14), where free-play is the angular wheel displacement from the specified, due to error sources, such as chain slack, gear backlash, bearing tolerances, tyre slip angle, etc. The relationship that exists between the steer angle  $\phi_s$ , turning radius  $R$ , wheel base  $l$  ( $l = l_1 + l_{2/1}$ ), and the free-play angles  $\sigma_l$  and  $\sigma_r$  has been

established by Bundorf [Bundorf'68] as;

$$\phi_s = \sigma_f - \sigma_r + \frac{L}{2R} \quad (3.16)$$

Equation (3.16) indicates that the actual steer angle is a function of the turning radius  $R$ , and the free-play angles of the wheels ( $\sigma_f$  and  $\sigma_r$ ). The cornering forces acting on the front and rear wheels ( $F_{yf}$  and  $F_{yr}$ ) can be determined by using the equilibrium equation of the SDMR in the lateral direction. Considering the situation for small steer angle, the cornering forces acting at the front and the rear wheels are approximately given by;

$$F_{yf} = \frac{W}{g} \frac{u^2}{R} \left( \frac{L_1}{L} \right) \quad (3.17)$$

$$F_{yr} = \frac{W}{g} \frac{u^2}{R} \left( \frac{L_{2/3}}{L} \right) \quad (3.18)$$

where;  $W$  is the total weight of the SDMR,

$g$  is the acceleration due to gravity,

$u$  is the SDMR forward speed.

When the SDMR is in a static state, the front and rear wheels normal supported loads,  $N_f$  and  $N_r$ , are approximated as;

$$N_f = \frac{WL_1}{L}$$

$$N_r = \frac{WL_{2/3}}{L}$$

Substituting  $N_f$  and  $N_r$  in equations (3.17) and (3.18) gives;

$$F_{yf} = N_f \frac{u^2}{gR} \quad (3.19)$$

$$F_{yr} = N_r \frac{U^2}{gR} \quad (3.20)$$

The free-play angles  $\sigma_f$  and  $\sigma_r$  depends on the tractive (or braking) force, side force acting on the wheels and their cornering stiffness. They are expressed as;

$$\sigma_f = \frac{F_{yf}}{C_{\sigma f}} \quad (3.21)$$

$$\sigma_r = \frac{F_{yr}}{C_{\sigma r}} \quad (3.22)$$

It should be noted that cornering stiffness  $C_{\sigma}$ , of a given wheel varies with a number of operational parameters, such as; normal load, slack and backlash in the steering system, tractive (or braking) effort, and lateral force. However within a limited range of operation it can be regarded as being constant [Wong'78].

Substituting equations (3.19) and (3.20) in (3.21) and (3.22), and  $\sigma_f$  and  $\sigma_r$  in (3.16), the steer angle becomes;

$$\begin{aligned} \phi_s &= \left( \frac{N_f}{C_{\sigma f}} - \frac{N_r}{C_{\sigma r}} \right) \frac{U^2}{gR} + \frac{L}{R} \\ \phi_s &= K_c \frac{U^2}{gR} + \frac{L}{R} = \frac{K_c U^2 + gL}{gR} \end{aligned} \quad (3.23)$$

where  $K_c$  can be regarded as the steering angle modifier, and it is expressed in radians.

The steering behaviour of the SDMR under steady-state is governed by equation (3.23). It can be deduced from the equation that for a given curve, the steer angle required to accomplish the turn is

dependent on the forward speed, weight distribution, wheel base and wheel cornering stiffness.

The analysis here goes to show that the actual angle turned by the SDMR is modified by factors such as free-play, the way the load is distributed and the wheel base. The implication this has on SDMR performance is that, because of its fixed chassis orientation, for different wheel heading, the wheels' actual turn angle for the same steering input differs. The steering angle modifier  $K_s$  also assists in determining directional stability as will be seen in section 3.3.2.3.

#### 3.3.2.2 TRANSIENT STATE BEHAVIOUR.

A transient state occurs between the application of a steering input and the accomplishment of a steady-state motion. Under transient response the inertia properties of the SDMR are considered. When a SDMR is negotiating a turn, its wheels are in a state of translation as well as rotation, while its chassis is only in a state of translation for a perfect system. In reality as experimental results show (see chapter 7), there is a small amount of chassis rotation about the centre of mass. This occurs even without any steering input. This makes it necessary to consider the motion of the SDMR as comprising of translation, and a small (error) rotation about the centre of mass.

Let  $x_a$  and  $y_a$  represent the longitudinal and lateral axes fixed to the frame of the SDMR with the origin placed at the centre of mass, C. (see Fig 3.15). Let  $u_a$  and  $v_a$  represent the components

of velocity  $v$  of the centre of mass along the axes  $x_n$  and  $y_n$ , respectively, at time  $t$  (see Fig. 3.15). The state of the SDMR at time  $t + \Delta t$  is also shown in Fig. 3.15. The changes in velocity that takes place between time  $t$  and time  $t + \Delta t$  can be represented component-wise as

Velocity component parallel to  $x_n$  axis, is expressed as;

$$\begin{aligned} & \left( v_x + \Delta v_x \right) \cos \Delta \theta_n - v_x - \left( v_y + \Delta v_y \right) \sin \Delta \theta_n \\ &= v_x \cos \Delta \theta_n + \Delta v_x \cos \Delta \theta_n - v_x - v_y \sin \Delta \theta_n - \Delta v_y \sin \Delta \theta_n \quad (3.24) \end{aligned}$$

Consider  $\Delta \theta_n$  to be small, and neglecting second-order terms, expression (3.24) becomes,

$$\dot{x}_n = \Delta v_x - v_y \Delta \theta \quad (3.25)$$

By dividing equation (3.25) by  $\Delta t$ , we obtain the absolute acceleration of the centre of mass of the SDMR along the longitudinal axis, and is given as;

$$a_x = \frac{dv_x}{dt} - v_y \frac{d\theta}{dt} = \dot{v}_x - v_y \dot{\theta}_n \quad (3.26)$$

$dv_x/dt$  (or  $\dot{v}_x$ ) component of the acceleration is caused by the changing magnitude of the velocity component  $v_x$  and its direction is along  $x_n$  axis. The  $v_y d\theta/dt$  (or  $v_y \dot{\theta}_n$ ) component is caused by the rotation of the velocity vector  $v_y$ . Similarly, the component of the absolute acceleration of the centre of mass of the SDMR along the lateral axis is given as;

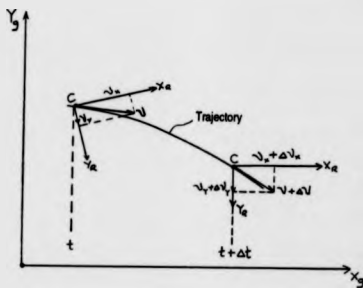


Fig. 3.15 SDMR centre of mass trajectory at time  $t$  and  $(t + \Delta t)$ .

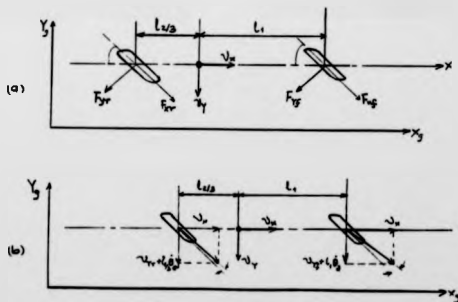


Fig. 3.16 Two wheel model of SDMR for transient behaviour analysis.



$$a_y = \frac{du}{dt} + u \frac{d\phi}{dt} = \dot{u}_y + u \dot{\phi}_z \quad (3.27)$$

Using the wheel model of the SDMR (see Figs. 3.16 above), the equation of motion that is based on the SDMR coordinate system can be developed. The equation of motion is given as;

$$m(\dot{u}_x - u_y \dot{\phi}_z) = F_{xr} \cos \phi_{sr} + F_{xr} \cos \phi_{sr} - (F_{yr} \sin \phi_{sr} + F_{yr} \sin \phi_{sr}) \quad (3.28)$$

$$m(\dot{u}_y + u_x \dot{\phi}_z) = F_{yr} \cos \phi_{sr} + F_{yr} \cos \phi_{sr} + F_{xr} \sin \phi_{sr} + F_{xr} \sin \phi_{sr} \quad (3.29)$$

$$I_x \dot{\omega}_x = I_1 F_{yr} \cos \phi_{sr} + I_1 F_{xr} \sin \phi_{sr} \\ = (I_{2/3} F_{yr} \cos \phi_{sr} + I_{2/3} F_{xr} \sin \phi_{sr}) \quad (3.30)$$

where  $m$  is the mass of the SDMR and  $I_x$  is the mass moment of inertia of the SDMR about the  $z$  axis.

For the case where there is no acceleration or deceleration in the longitudinal direction, equation (3.28) will not be necessary. The lateral motion of the SDMR will be governed by equations (3.29) and (3.30). A case such as this is very useful when directional stability is analyzed, as will be seen later.

The free-play angles  $\sigma_r$  and  $\sigma_r$  of a SDMR can be expressed in terms of the motion parameters  $\dot{\phi}_z$  and  $u_y$ , (see Fig. 3.16, with small angle assumption) as thus;

$$\sigma_r = \phi_{sr} - \frac{L_1 \dot{\theta}_s + v_{yr}}{u_x} \quad (3.31)$$

$$\sigma_r = \phi_{sr} - \frac{L_{2/3} \dot{\theta}_s + v_{yr}}{u_x} \quad (3.32)$$

Cornering forces  $F_{yr}$  and  $F_{xr}$  can be expressed as a function of free-play angle and cornering stiffness, given as;

$$F_{yr} = C_{\sigma r} \sigma_r \quad (3.33)$$

$$F_{xr} = C_{\sigma r} \sigma_r \quad (3.34)$$

When equations (3.29) to (3.34) are combined, with the assumption that the steer angle is small and  $F_{sr}$  is zero, the equation of lateral motions of the SDMR having only the steer angle as input variable will be;

$$m \dot{v}_y + \left( m u_x + \frac{C_{\sigma r} L_{2/3} + C_{\sigma r} L_1}{u_x} \right) \dot{\theta}_s + \left( \frac{C_{\sigma r} - C_{\sigma r}}{u_x} \right) v_y = 2 C_{\sigma r} \phi_s(t) \quad (3.35)$$

$$I_x \dot{\omega}_x + \left( \frac{C_{\sigma r} L_1^2 - C_{\sigma r} L_{2/3}^2}{u_x} \right) \dot{\theta}_s + \left( \frac{C_{\sigma r} L_1 + C_{\sigma r} L_{2/3}}{u_x} \right) v_y = \left( C_{\sigma r} L_1 - C_{\sigma r} L_{2/3} \right) \phi_s(t) \quad (3.36)$$

where,  $\phi_{sr} = \phi_{sr} = \phi_s$ , and  $\phi_s(t)$  represents the steer angle of the wheel as a function of time.

Any other external forces or moments acting on the mobile robot forms part of the systems' input variables and will be reflected on the right-hand side of equations (3.35) and (3.36).

The lateral equations of motion developed above will now be used to study the conditions for directional stability of a SDMR.

### 3.3.2.3 DIRECTIONAL STABILITY.

Directional stability is concerned with the mobile robot's ability to stabilize its direction of motion against an unwanted external influence. When a mobile robot returns to a state of steady-state within a finite time, when the systems' source of disturbance has been removed, the system is said to be directionally stable.

Removing the source of disturbance to the systems' state, the rate of change of chassis orientation and lateral velocities,  $\dot{\theta}$  and  $\dot{v}_y$  will vary with time exponentially  $e^{\psi t}$  [Segel'57], [Wong'78] and the system's stability is determined by the value of  $\psi$ . Having  $\psi$  as a real and positive value,  $\dot{\theta}$  and  $\dot{v}_y$  will have values that increases exponentially with time, making the mobile robot to be directionally unstable.

A real and negative value of  $\psi$  indicates that motion of the SDMR converge to a steady state in a finite time and that the mobile robot is directionally stable. For complex  $\psi$  with positive real part, an oscillatory motion takes place with increasing amplitudes. A directionally unstable mobile robot motion results

under such conditions.

What the above paragraph indicate is that by determining the value of  $\psi$ , we can evaluate the directional stability of the SDMR. In evaluating directional stability we are interested in motion of the mobile robot after disturbance, hence the steering input and the likes are taken to be zero. In order to obtain the value of  $\psi$ , the solution of the differential equations of (3.35) and (3.36) is assumed to be;

$$\dot{v}_y = A_1 e^{\psi t} \quad (3.37)$$

$$\dot{\theta}_x = A_2 e^{\psi t} \quad (3.38)$$

Differentiating equations (3.37) and (3.38) gives;

$$\ddot{v}_y = A_1 \psi e^{\psi t} \quad (3.39)$$

$$\ddot{\theta}_x = A_2 \psi e^{\psi t} \quad (3.40)$$

Substituting for  $v_y$ ,  $\dot{v}_y$ ,  $\theta_x$ , and  $\dot{\theta}_x$  in equations (3.35) and (3.36) and setting the right-hand sides of the equation to zero, the equations become;

$$mA_1 \psi + \left( \frac{C_{\sigma r} - C_{\sigma r}}{u_x} \right) A_1 + \left( \frac{mu_x^2 + C_{\sigma r} L_{2/3} + C_{\sigma r} L_1}{u_x} \right) A_2 = 0 \quad (3.41)$$

$$I_x A_2 \psi + \left( \frac{C_{\sigma r} L_1 + C_{\sigma r} L_{2/3}}{u_x} \right) A_1 + \left( \frac{C_{\sigma r} L_1^2 + C_{\sigma r} L_{2/3}^2}{u_x} \right) A_2 = 0 \quad (3.42)$$

Equations (3.41) and (3.42) can be rewritten as;

$$m\lambda_1\psi + \beta_1\lambda_1 + \beta_2\lambda_3 = 0 \quad (3.43)$$

$$I_x\lambda_2\psi + \beta_3\lambda_1 + \beta_4\lambda_3 = 0 \quad (3.44)$$

where,

$$\beta_1 = \frac{C_{\sigma r} - C_{\sigma r}}{u_x}$$

$$\beta_2 = \frac{mu_x^2 + C_{\sigma r} l_{2/2} + C_{\sigma r} l_1}{u_x}$$

$$\beta_3 = \frac{C_{\sigma r} l_1 + C_{\sigma r} l_{2/2}}{u_x}$$

$$\beta_4 = \frac{C_{\sigma r} l_1^2 + C_{\sigma r} l_{2/2}^2}{u_x}$$

To obtain a nontrivial solution of  $\psi$  from equations (3.43) and (3.44), the determinant of the linear homogeneous equations must equal zero. This gives;

$$\begin{bmatrix} m\psi + \beta_1 & \beta_2 \\ \beta_3 & I_x\psi + \beta_4 \end{bmatrix} = 0 \quad (3.45)$$

A characteristic equation of the system is obtained by expanding the determinant, which is given as;

$$mI_x\psi^2 + (I_x\beta_1 + m\beta_4)\psi + (\beta_1\beta_4 - \beta_2\beta_3) = 0 \quad (3.46)$$

If the values of  $(I_x\beta_1 + m\beta_4)$  and  $(\beta_1\beta_4 - \beta_2\beta_3)$  are both positive, it implies that  $\psi$  will be either a negative real number

or a complex number with a negative real part. It should be noted that the terms  $I_x \beta_1$  and  $m \beta_4$  are always positive. This indicates that if  $\beta_1 \beta_4 - \beta_2 \beta_3$  is a positive value, the SDMR will be directionally stable. The condition for  $\beta_1 \beta_4 - \beta_2 \beta_3 > 0$  is represented by;

$$I + \frac{u^2}{g} \left( \frac{N_f}{C_{\sigma f}} - \frac{N_r}{C_{\sigma r}} \right) > 0$$

or

$$I + \frac{u^2}{g} K_c > 0 \quad (3.47)$$

where  $K_c$  is the steering angle modifier. Equation (3.47) shows that analyzing directional stability of a mobile robot is equivalent to determining the conditions under which the equation is satisfied. A positive steering angle modifier always satisfies the equation. Therefore a mobile robot with positive  $K_c$  is always directionally stable. With negative  $K_c$  implying that the mobile robot is directionally stable only if the forward speed is below its critical value  $V_{crit}$ . Inspecting equation (3.47)  $V_{crit}$  is represented by  $\sqrt{\frac{gl}{-K_c}}$ . Hence for a mobile robot whose angle modifier is zero, it will always remain directionally stable.

In a situation where the load on the wheels are evenly distributed, the steering angle modifier depends on the value of the free-play angle  $\sigma$ . If the free-play angle of the wheels are equal, it gives a situation where  $K_c$  is zero. With  $K_c$  zero, the SDMR will always remain directionally stable, and at the same

time, the steering angle  $\phi_c$  required to negotiate a given curve will be independent of the drive velocity. But where such is not the case, the SDMR can run into directional instability if the drive speed is greater than the critical speed.

Satisfying equation (3.47) and thus directional stability depend also on the mobile robot's length parameters (see equations (3.17) and (3.18)). The length parameters of the SDMR varies as change in heading occurs (further details on change in length parameters can be seen in the next chapter). This means that a SDMR can run into directional instability for given heading, while being directional stable in another.

This chapter has analyzed the forces and moments of a wheel and exposed the implication of such forces and moments to the performance of mobile robots. Detailed discussion on the effects of the wheel forces and moments to different SDMR design can be seen in chapter 4 and 5. The error types which has been classified as predictable and non-predictable error with their sources identified and analyzed, highlighting the effects that fixed chassis orientation have on the errors. For instance because of fixed chassis orientation most SDMR errors can be classified as non-predictable. The analysis of its behaviour in recognition of the errors arising from the system have also been dealt with, identifying the form of trajectories that can be obtained during path execution. Insight has been given into directional stability determination together with formulae to calculate whether an SDMR is running into directional

instability.

The next chapter deals with modeling and further analysis of SDMR through the investigation of control space aimed at preventing dynamic instability and identifying SDMR control requirements.



## CHAPTER 4

### KINEMATIC MODELING AND BOUNDARIES OF CONTROL SPACE

In this chapter consideration is given to the kinematic modeling of two different designs of SDMR - one with a wheel assembly having the wheel-offset from the steering axis (Type-1) and another with a wheel assembly having its wheel set on the steering axis (Type-3). Type-2 wheel assembly which is that with two wheels coupled together through a differential gear is not considered. This is because its mode of operation is not just limited to omnidirectional mode, and it requires  $2n$  motors (where  $n$  is the number of wheel assemblies used) to operate. Another reason being that some work has been done in the kinematic modeling and control of a mobile robot based on this sort of wheel assembly (Type-2) [Moravec'83], [Muir'86]. Investigations revealed such a wheel assembly design not to be practically feasible and hence the work was discontinued [Muir'86]. Therefore it was not considered necessary for this work to investigate it any further.

The control requirements of a SDMR are considered based on establishing the boundaries of the control space which will ensure that the SDMR remains stable. A SDMR using wheel assembly design, Type-3 is the focus of the research, and such a design has not been implemented in any other reported work.

#### 4.1 SYNCHRO-DRIVE MOBILE ROBOT'S (SDMR's) KINEMATICS.

The proposed mobile robot is a three wheel drive and three wheel steering system. Briefly it is a mobile robot that has its wheels arranged permanently parallel to each other and spaced equidistance from one another. The wheels are also equidistant from the mobile robot's centre of area. The mobile robot geometry is shown in Fig. 4.1. Fig. 4.2 shows the variables associated with a conventional steerable wheel. The SDMR's considered here are of two types, namely:

- (1) Wheel-offset from the wheel assembly steering axis (Type-1 - Fig. 4.3).
- (2) Wheel-set on the wheel assembly steering axis (Type-3 - Fig. 4.4).

#### Assumptions.

The following assumptions are made in order to facilitate production of a model:

(1) Motion is considered only in a plane parallel to the floor surface. Thus the motion that can be achieved is constrained to rotation about an axis normal to the surface ( $\theta$ ), and the translational motion in the x-y plane. This assumption removes the effect of floor surface roughness.

(2) At the point of wheel and floor contact the friction in the drive direction is considered to be very large and the steering friction is considered to be extremely small. This removes the effect or occurrence of translational slip while allowing the steering of the wheel about the point of contact.

(3) The effect of slack, backlash, bearing and gear friction in the transmission system is assumed negligible.

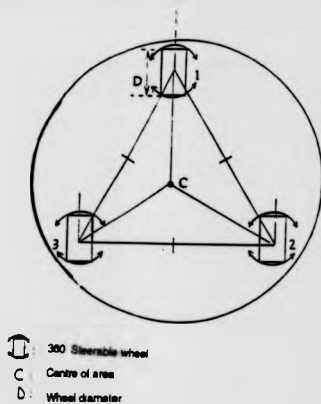


Fig. 4.1 Mobile robot geometry.

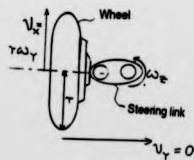


Fig. 4.2 Parameters of a conventional steerable wheel.

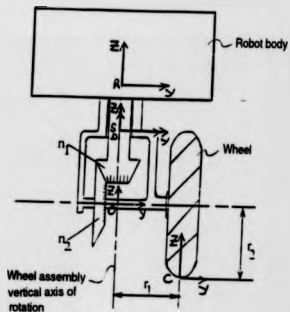


Fig. 4.3 Type-I SDRM with its coordinate systems.

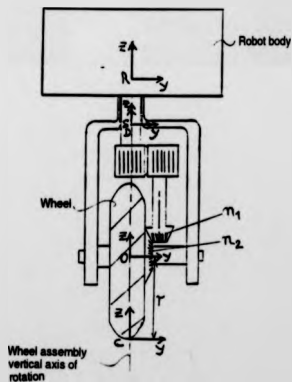


Fig. 4.4 Type-3-A SDRM with its coordinate systems.

(4) In cases where we have a three-wheel dsm. all driven by one electric motor and steered by another electric motor, it can be assumed that the motion of the mobile robot is represented by that of any one of the three wheels. That is the SDMR can be modeled as a one wheeled system.

(5) There is no rotation of the SDMR's frame. That is the effect of precession is negligible. The frame translates in the x-y plane only.

Considering Fig. 4.2, the kinematic relationship for the wheel (where the translation is in the x-direction) is given as;

$$\begin{aligned} v_y &= 0 \\ v_x &= \omega_y r \\ \omega_x &= \omega_y \end{aligned} \quad (4.1)$$

Equation (4.1) gives the wheel equation-of-motion, where;

$v_x$  and  $v_y$ : x and y components of the linear velocity at the point of wheel and floor contact.

$\omega_z$ : z components of the angular velocity of the wheel at the point of contact with the floor.

r: radius of the wheel.

#### 4.1.1 COORDINATE SYSTEM ASSIGNMENT.

The SDMR is considered as a three body mechanism, comprising of;

- the wheel,
- the steering assembly, and
- the body of the SDMR.

The coordinate system assignment is defined in table 1.

Table 4.1: Coordinate system assignment.

Frame name	Description
F, Floor:	Reference coordinate system fixed to the environment.
R, Robot:	SDMR frame coordinate system. It moves with the robot's body, with its z-axis orthogonal to the floor surface.
S, Steering:	Coordinate system that is attached to the steering shaft of the wheel assembly.
D, Driving:	Coordinate system that is attached to the driving shaft of the wheel assembly.
O, Wheel axle:	Coordinate system attached to the axle of the wheel with its origin coincident with the assembly vertical axis.
C, Contact point:	Coordinate system that has its origin at the point of contact between the wheel and the surface, with its x-axis parallel to the wheel and the x-y plane tangential to the floor.

The placement of the coordinate assignment defined in table 4.1 is shown in the two configurations of Figs. 4.3 and 4.4.

#### 4.1.2 SDMR KINEMATIC VELOCITIES AND ACCELERATIONS.

Kinematic velocities for three different designs of SDMR are analyzed. The designs are of:

- (1) Wheel-offset from wheel assembly steering axis; Type-1 (Fig. 4.3).

- (2) Wheel-set on wheel assembly steering axis; Type-3:a (Fig. 4.4).
- (3) Wheel-set on wheel assembly steering axis with decoupling unit incorporated; Type-3:b (Fig. 4.5).

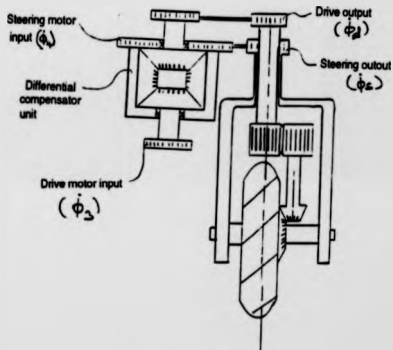


Fig. 4.5 Type-3:B SDMR incorporating mechanical compensator unit.

#### 4.1.2.1 WHEEL-OFFSET FROM WHEEL ASSEMBLY STEERING AXIS (TYPE-1).

At a fixed rotation of the steering shaft about  $S_z$  coordinate system (Fig. 4.3);  $\omega_y = 0$  and  $\omega_z = \dot{\phi}_s$ . If the wheel is driven with the steering shaft held fixed, we have;

$$\dot{\phi}_s = 0, \quad \dot{\phi}_d = -\frac{n_2}{n_1} \omega_y, \quad \text{and} \quad \omega_y = -\frac{n_1}{n_2} \dot{\phi}_d.$$

∴ the wheel assembly matrix representation becomes;

$$\begin{bmatrix} \dot{\phi}_d \\ \dot{\phi}_s \end{bmatrix} = \begin{bmatrix} -\frac{n_2}{n_1} & 1 \\ 0 & 1 \end{bmatrix} \begin{bmatrix} \omega_y \\ \omega_z \end{bmatrix} \quad (4.2)$$

$$\begin{bmatrix} \omega_y \\ \omega_z \end{bmatrix} = -\frac{n_1}{n_2} \begin{bmatrix} 1 & -1 \\ 0 & -\frac{n_2}{n_1} \end{bmatrix} \begin{bmatrix} \dot{\phi}_d \\ \dot{\phi}_s \end{bmatrix} \quad (4.3)$$

The velocities at the wheel/floor contact point ( $\dot{x}_c$  and  $\dot{y}_c$ ) gives;

$$\begin{bmatrix} \dot{x}_c \\ \dot{y}_c \end{bmatrix} = \begin{bmatrix} \cos \theta_z \\ -\sin \theta_z \end{bmatrix} r_z \omega_y \quad (4.4)$$

where;

$\omega_y$ : wheel drive speed about the y-axis,

$\omega_z$ : wheel steering rate about the z axis,

$\theta_z$ : wheel steering angle.

The wheel velocities with respect to Type-1 wheel assembly axis ( $\dot{x}_o$  and  $\dot{y}_o$ ) gives;

$$\begin{bmatrix} \dot{x}_o \\ \dot{y}_o \end{bmatrix} = \begin{bmatrix} \cos \theta_z \\ -\sin \theta_z \end{bmatrix} r_1 \omega_z \quad (4.5)$$



The SDMR velocities ( $\dot{x}_R$  and  $\dot{y}_R$ ) are given by;

$$\begin{bmatrix} \dot{x}_R \\ \dot{y}_R \end{bmatrix} = \begin{bmatrix} \dot{x}_c \\ \dot{y}_c \end{bmatrix} - \begin{bmatrix} \dot{x}_o \\ \dot{y}_o \end{bmatrix} \quad (4.6)$$

Substituting equation (4.4) and (4.5) in equation (4.6) gives;

$$\begin{bmatrix} \dot{x}_R \\ \dot{y}_R \end{bmatrix} = \begin{bmatrix} r_2 \cos \theta_s & -r_1 \cos \theta_s \\ -r_2 \sin \theta_s & r_1 \sin \theta_s \end{bmatrix} \begin{bmatrix} \dot{\omega}_s \\ \dot{\omega}_s \end{bmatrix} \quad (4.7)$$

$$\begin{bmatrix} \dot{x}_R \\ \dot{y}_R \end{bmatrix} = -\frac{n_1}{n_2} \begin{bmatrix} r_2 \cos \theta_s & -(r_2 - r_1 \frac{n_2}{n_1}) \cos \theta_s \\ -r_2 \sin \theta_s & (r_2 - r_1 \frac{n_2}{n_1}) \sin \theta_s \end{bmatrix} \begin{bmatrix} \dot{\phi}_s \\ \dot{\phi}_s \end{bmatrix} \quad (4.8)$$

Equation (4.8) shows that in Type-1 wheel assembly, coupling exist between the drive and steering subsystems. This makes it difficult to predict correctly the SDMR's motion and hence controllability is affected. However in this configuration, the effect of coupling can be eliminated if the equation  $(r_2 - r_1 \frac{n_2}{n_1})$  is zero. This may be achieved by making the ratio,  $r_2:r_1$  equal to  $n_2:n_1$  (see fig. 4.1). If this is the situation, the SDMR velocities will be directly related to the drive speed and steering rate.

Differentiating equation (4.8) gives the expression for the acceleration of the SDMR, which yields;

$$\begin{aligned} \ddot{x}_R = & \left( \frac{n_1}{n_2} r_2 - r_1 \right) \ddot{\phi}_s (\cos \theta_s) - \left( \frac{n_1}{n_2} r_2 \right) \dot{\phi}_s^2 (\sin \theta_s) \\ & + \left( \frac{n_1}{n_2} r_2 \right) \dot{\phi}_s \dot{\theta}_s (\sin \theta_s) - \left( \frac{n_1}{n_2} r_2 - r_1 \right) \dot{\phi}_s^2 (\sin \theta_s) \end{aligned} \quad (4.9)$$

$$\ddot{y}_s = \left( \frac{n_1}{n_2} r_2 \right) \ddot{\phi}_d (\sin \theta_z) - \left( \frac{n_1}{n_2} r_2 - r_1 \right) \ddot{\phi}_s (\sin \theta_z) + \left( \frac{n_1}{n_2} r_2 \right) \dot{\phi}_d \dot{\phi}_s (\cos \theta_z) - \left( \frac{n_1}{n_2} r_2 - r_1 \right) \dot{\phi}_s^2 (\cos \theta_z) \quad (4.10)$$

In the acceleration equations three types of terms exists. The inertia term which is proportional to the drive and steering acceleration. The centripetal term which is proportional to the square of the steering velocity. Finally the coriolis term that is proportional to the product of drive and steering velocities.

#### 4.1.2.2 WHEEL-SET ON WHEEL ASSEMBLY STEERING AXIS (TYPE-3:A).

At a fixed position of the drive shaft, with rotation of the steering shaft about  $S_s$  coordinate system (Fig. 4.4),  $\omega_y = 0$  and  $\omega_s = \dot{\phi}_s$ . If the steering shaft is held fixed, with drive shaft rotation about  $D_x$ , we have  $\dot{\phi}_s = 0$ ,  $\dot{\phi}_d = \frac{n_2}{n_1} \omega_y$  and  $\omega_y = \frac{n_1}{n_2} \dot{\phi}_d$ .

the wheel assembly matrix representation becomes;

$$\begin{bmatrix} \dot{\phi}_d \\ \dot{\phi}_s \end{bmatrix} = \begin{bmatrix} \frac{n_2}{n_1} & 1 \\ 0 & 1 \end{bmatrix} \begin{bmatrix} \omega_y \\ \omega_s \end{bmatrix} \quad (4.11)$$

$$\begin{bmatrix} \omega_y \\ \omega_s \end{bmatrix} = \frac{n_1}{n_2} \begin{bmatrix} 1 & -1 \\ 0 & \frac{n_2}{n_1} \end{bmatrix} \begin{bmatrix} \dot{\phi}_d \\ \dot{\phi}_s \end{bmatrix} \quad (4.12)$$

In Type-3:A wheel assembly configuration, the SDMR's velocities are directly represented by the wheel contact velocities, and are given as;

$$\begin{bmatrix} \dot{x}_R \\ \dot{y}_R \end{bmatrix} = \begin{bmatrix} \dot{x}_c \\ \dot{y}_c \end{bmatrix} = \begin{bmatrix} r \cos \theta_z & 0 \\ -r \sin \theta_z & 0 \end{bmatrix} \begin{bmatrix} \omega_y \\ \omega_s \end{bmatrix} \quad (4.13)$$

Substituting for  $\omega_y$  and  $\omega_s$  in equation (4.13) results in;

$$\begin{bmatrix} \dot{x}_R \\ \dot{y}_R \end{bmatrix} = \frac{n_1}{n_2} \begin{bmatrix} r \cos \theta_1 & -r \cos \theta_2 \\ -r \sin \theta_1 & r \sin \theta_2 \end{bmatrix} \begin{bmatrix} \dot{\phi}_d \\ \dot{\phi}_s \end{bmatrix} \quad (4.14)$$

Equation (4.14) shows that there exists a coupling between the drive and steering motions. Hence Type-3 wheel assembly configuration of the SDMR will be difficult to accurately control without decoupling the drive and steering motions. In the work presented here, a method is proposed to decouple these motions. It is based of differential gear system, and the way it operates is discussed in the next section.

Differentiating equation (4.14) gives the expression for the acceleration of the SDMR, which yields;

$$\begin{aligned} \ddot{x}_R = & \left( \frac{n_1}{n_2} r \right) \ddot{\phi}_d (\cos \theta_1) - \left( \frac{n_1}{n_2} r \right) \ddot{\phi}_s (\cos \theta_2) \\ & - \left( \frac{n_1}{n_2} r \right) \dot{\phi}_d \dot{\phi}_s (\sin \theta_1) + \left( \frac{n_1}{n_2} r \right) \dot{\phi}_s^2 (\sin \theta_2) \end{aligned} \quad (4.15)$$

$$\begin{aligned} \ddot{y}_R = & \left( \frac{n_1}{n_2} r \right) \ddot{\phi}_s (\sin \theta_1) - \left( \frac{n_1}{n_2} r \right) \ddot{\phi}_d (\sin \theta_2) \\ & - \left( \frac{n_1}{n_2} r \right) \dot{\phi}_d \dot{\phi}_s (\cos \theta_1) + \left( \frac{n_1}{n_2} r \right) \dot{\phi}_s^2 (\cos \theta_2) \end{aligned} \quad (4.16)$$

#### 4.1.2.3 WHEEL-SET ON WHEEL ASSEMBLY STEERING AXIS WITH

##### MECHANICAL COMPENSATOR UNIT (TYPE-3:B).

The function of the differential gear unit is to add or subtract drive wheel rotation depending on the direction in which the wheel is being steered. Other unwanted motions in the power

transmission system are eliminated using the self-locking property of the worm gears which prevent motion being transmitted back through the system. This subsystem that eliminates the unwanted motions is referred to as *mechanical compensator unit*.

The mechanical compensator gives a situation where the SDMR's velocities are directly proportional to the angular rate of change of the drive and steering motor shafts (say  $\dot{\phi}_3$  and  $\dot{\phi}_4$  - see Fig. 4.5). The effect of the differential gear unit (or mechanical compensator unit) is represented in a matrix form as;

$$\begin{bmatrix} \dot{\phi}_3 \\ \dot{\phi}_4 \end{bmatrix} = \begin{bmatrix} 1 & 1 \\ 0 & 1 \end{bmatrix} \begin{bmatrix} \dot{\phi}_3 \\ \dot{\phi}_4 \end{bmatrix} \quad (4.17)$$

Substituting for  $\dot{\phi}_3$  and  $\dot{\phi}_4$  in equation (4.14) results in;

$$\begin{bmatrix} \dot{x}_s \\ \dot{y}_s \end{bmatrix} = \frac{n_1}{n_2} \begin{bmatrix} r \cos \theta_z & 0 \\ r \sin \theta_z & 0 \end{bmatrix} \begin{bmatrix} \dot{\phi}_3 \\ \dot{\phi}_4 \end{bmatrix} \quad (4.18)$$

The operation of the mechanical compensation unit is described below using equations (4.14) and (4.18) and Fig. 4.5. Consider a situation where there is a requirement to steer, but not to drive. This implies that  $\dot{\phi}_4$  is zero, but from equation (4.14) a drive speed exist, which can be expressed as;

$$\begin{bmatrix} \dot{x}_s \\ \dot{y}_s \end{bmatrix} = \frac{n_1}{n_2} \begin{bmatrix} -r \cos \theta_z \\ r \sin \theta_z \end{bmatrix} \begin{bmatrix} \dot{\phi}_3 \end{bmatrix} \quad (4.19)$$

The motion achieved by equation (4.19) is the induced motion which is unwanted if the SDMR is to translate accurately when steering of the wheels occur. To eliminate the induced motion (or induced error) the Jacobian matrix of equation (4.19) must be made zero at all times. This is achieved using a differential

unit whose action is represented mathematically by equation (4.17). The outcome is equation (4.18) in which there is no induced drive motion when there is no drive motion provided by the drive motor. Hence the action of differential unit makes it possible to decouple the motions, which will allow for accurate control of position and heading of the SDMR. This novel approach makes it possible to implement wheel-set on steering axis (Type-3) successfully. Mobile robots whose design are based on Type-3 wheel assembly have never been reported in all the literature reviewed.

Differentiating equation (4.18) gives the expression for the acceleration of the SDMR, which yields;

$$\ddot{X}_x = \left(\frac{r_1}{n_2}r\right)\ddot{\theta}_2(\cos \theta_x) - \left(\frac{r_1}{n_2}r\right)\dot{\theta}_2\dot{\theta}_4(\sin \theta_x) \quad (4.20)$$

$$\ddot{Y}_x = -\left(\frac{r_1}{n_2}r\right)\ddot{\theta}_2(\sin \theta_x) - \left(\frac{r_1}{n_2}r\right)\dot{\theta}_2\dot{\theta}_4(\cos \theta_x) \quad (4.21)$$

#### Observation:

SDMR with Type-1 and Type-3 wheel configurations are kinematically equivalent under the following conditions;

- (a) where the ratios  $n_1:n_2$  and  $r_1:r_2$  are equal for Type-1 wheel configuration, and
- (b) when the differential compensation unit is incorporated in the drive/steering subsystem of Type-3 wheel configuration.

If we assumes no errors such as those from different wheel radius, backlash, slip, etc, their dynamic behaviour is also alike. For the Type-3 wheel configuration it is apparent that

the induced torque at the wheel centre is zero, because the radius at which any force present can act is zero. For the Type-1 wheel configuration, the torque (Q) is given by (see Fig. 4.3 for the variables);

$$Q = f_a n_1 a - f_c r_1 \quad (4.23)$$

where;  $f_a$  represents the actual drive force,

$f_c$  represents the reactive force

To determine  $f_c$ ,

$$f_c r_2 = f_a n_2 a$$

$$\therefore f_c = f_a \frac{n_2 a}{r_2}$$

but with  $\frac{n_1}{n_2} = \frac{r_1}{r_2}$ , substituting for  $f_c$  in equation (4.23) gives;

$$Q = f_a n_1 a - f_a n_1 a = 0$$

$\therefore$  the resultant torque about the steering axis is zero.

The Jacobian matrix in equations (4.8) and (4.18) that relates the wheel velocities through the rate of change of angular displacement of the electric motors to the mobile robot velocities contains elements with different variables for the different configurations. For this reason the mobility behaviour of the different configurations under real conditions where influences of factors such as; different wheel radius, backlash, slip, etc are evident will not be alike. These differences are further exposed by considering the implications of the wheel forces and moments analyzed in chapter 3. This is issue considered as part of the next chapter.

#### 4.2 BOUNDARIES OF THE CONTROL SPACE.

The SDMR considered is that powered by two DC motors, which are used for driving and steering. These two motors have independent motion controllers that control their velocities. The velocities which they provide are the drive shaft velocity,  $\dot{\phi}_d (\omega_d)$  and the steering shaft velocity,  $\dot{\phi}_s (\omega_s)$ . These in turn provides the SDMR centre of mass drive speed and acceleration (see section 4.1.2 for expression of the SDMR kinematic velocities and accelerations).

The velocities which the motors demand in order to execute a given users request may be constrained by the SDMR kinematics and dynamics, if a stable state is to be maintained. These constraints are limits imposed by factors such as acceleration and frictional forces. The implication of such a request is that the motors may provide SDMR drive speed which in turn generates an acceleration and its force/torque components that if executed by the SDMR will cause it to slide or overturn. If such phenomenon occurs the SDMR in the short run will suffer from path execution error, while in the long run will remain in a permanent state of error, caused by factors such as excessive wear and strain in the mechanical components. For these reasons, the need to prevent such events happening becomes paramount.

The approach advocated in this thesis to tackle the problem of occurrence of sliding or overturning is to establish what is considered as 'boundaries of the control space'. These are the boundaries that sets limits on the acceleration and force/torque requirements. These limits through the inverse of the kinematics

developed in section 4.1.2 sets limits on the velocity requirements of the two motors.

The importance of investigating the boundaries of the control space for the SDMR is further enhanced by two other factors, which are;

(1) The limits are affected by the configuration of the mobile robot. Hence different designs achieve different levels of performance.

(1i) SDMRs can exhibit very high turning rates due to low mass involved when turning caused by fixed chassis orientation. Only the wheel assembly mass are required to be overcome by the steering force (Appendix B). This makes SDMR designs potentially more vulnerable to sliding and overturning if the capability it possesses is used in the wrong circumstance.

The boundaries of the control space are established based on the following conditions:

(1) Condition of no sliding occurring. Sliding comprises of longitudinal and lateral slip (slip is used for the rest of the text to stand for either lateral or longitudinal slip or both). This condition is investigated on the basis of the required acceleration to initiate slip. The parameters that affects the slip condition are; the steering rate  $\dot{\phi}_s$ , drive velocity  $v$  ( $\dot{\phi}_d$ ), and drive acceleration  $a$  ( $\ddot{\phi}_d$ ).

(2) Condition of no overturning occurring. Here limits on acceleration is investigated and the D'Alembert principle of forces is used to obtain the dynamic situation. The parameters that affect overturning conditions are; the steering angle



$\theta_s(\phi_s)$ , steering rate  $\omega_s(\dot{\phi}_s)$ , drive velocity  $v(\dot{\phi}_d)$ , and drive acceleration  $a(\ddot{\phi}_d)$ .

For the SDMR to remain in a state of dynamic equilibrium, it is required that under no circumstance shall it slip or overturn. This will be possible only if; the frictional force is sufficiently high to prevent the wheel from slipping either longitudinally or laterally when accelerating, and that the SDMR will never under any condition pivot about any of the wheel/floor contact points.

The constraints that establish the conditions of no slip and no overturning at the wheel/floor contact 'points' are derived. Using the relevant expressions developed it is possible to derive;

- ▷ the motion outcome for a given input in a given circumstance and,
- ▷ the inputs necessary to execute a desired motion without violating the SDMR stability conditions.

#### 4.2.1 NO SLIPPING CONDITION.

Forces that affect wheel slipping are the frictional forces at the wheel/floor surface contact 'points' and the reaction (coupling) forces between the SDMR frame and the wheels. The reaction forces are represented in the coordinate system with its origin at the wheel contact point  $(x_c, y_c)$ . At wheel 1 contact point, the reaction force components are  $F_{1x}$  and  $F_{1y}$  (see Figs. 4.6 and 4.7); the reaction force components at wheel 2 are  $F_{2x}$  and  $F_{2y}$  and that at wheel 3 are  $F_{3x}$  and  $F_{3y}$ .

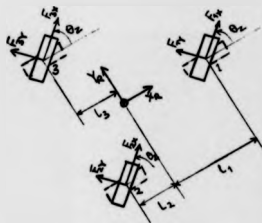


Fig. 4.6 Illustration of 3-wheel model of SDM (free-body diagram).

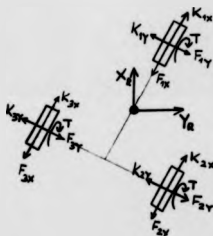


Fig. 4.7 Representation of reaction and frictional force components from a top view.

The equations of motion of the centre of mass  $x_n$  and  $y_n$  are given by;

$$\begin{aligned} m\ddot{x}_n = & F_{1x}(\cos \theta_{1x}) - F_{1y}(\sin \theta_{1x}) + F_{2x}(\cos \theta_{2x}) \\ & - F_{2y}(\sin \theta_{2x}) + F_{3x}(\cos \theta_{3x}) - F_{3y}(\sin \theta_{3x}) \end{aligned} \quad (4.24)$$

$$\begin{aligned} m\ddot{y}_n = & F_{1x}(\sin \theta_{1x}) + F_{1y}(\cos \theta_{1x}) + F_{2x}(\sin \theta_{2x}) \\ & + F_{2y}(\cos \theta_{2x}) + F_{3x}(\sin \theta_{3x}) + F_{3y}(\cos \theta_{3x}) \end{aligned} \quad (4.25)$$

where,  $m$  is the mass of the SDMR. The moment expression in the  $x_n, y_n$  frame gives;

$$\begin{aligned} I_n \ddot{\theta}_x = & F_{1x}l_1(\sin \theta_{1x}) + F_{1y}l_1(\cos \theta_{1x}) - F_{2x}l_2(\sin \theta_{2x}) \\ & - F_{2y}l_2(\cos \theta_{2x}) - F_{3x}l_3(\sin \theta_{3x}) - F_{3y}l_3(\cos \theta_{3x}) \end{aligned} \quad (4.26)$$

where  $I_n$  is the mass moment of inertia of the SDMR about its z-axis and  $l_1, l_2$  and  $l_3$  are distances from wheel 1, 2 and 3 (see Fig. 4.6) to the SDMR centre of mass measured in the x-direction.

The dynamic equations for wheel 1 (which is similar to that of wheels 2 and 3) is expressed as;

Wheel 1;

$$\begin{aligned} m_{w1}\ddot{x}_{1x} = & [K_{1x} - F_{1x}] \cos \theta_{1x} - [K_{1y} - F_{1y}] \sin \theta_{1x} \\ m_{w1}\ddot{x}_{1y} = & [K_{1x} - F_{1x}] \sin \theta_{1x} - [K_{1y} - F_{1y}] \cos \theta_{1x} \\ I_{w1}\dot{\omega}_1 = & T_0 - K_{1x}r_w \end{aligned} \quad (4.27)$$

where;  $\dot{\omega}_1$  represents wheel 1 angular accelerations  $\left( \dot{\omega} = \frac{\dot{\theta}_{1x}}{r_w} \right)$ ,

$m_w$ , the wheel assembly mass and  $r_w$ , the wheel radius,  
 $T_d$ , is the applied drive torque.

Under no slip conditions, the SDMR should satisfy the following;

(i) The velocity of the wheel's contact point must be zero. This implies that the velocities at the wheel's centre point must be directed at the steering angle  $\theta_z$ .

(ii) For a SDMR there is no frame rotation, therefore the translation of the wheels have to be equal to one another and equal to that of the centre of mass.

$$\text{i.e., } F_x = F_{1x} = F_{2x} = F_{3x} \text{ and } F_y = F_{1y} = F_{2y} = F_{3y}$$

where,  $F_x$  and  $F_y$  are force components at the centre of mass.

(iii) The magnitude of the product of the acceleration  $|a|$  of the centre of mass must be less than that of the coefficient of friction  $\mu$  and the gravitational acceleration  $g$ ;

$$\text{i.e., } |a| < \mu g \quad (4.28)$$

$$\text{since } ma = \mu mg$$

$$\text{and } \mu \leq b/h \quad (4.29)$$

where  $h$  is the vertical height of the centre of gravity and  $b$  is the horizontal distance between the centre of gravity and wheels' line of action measured along the wheel contact  $y$ -direction. For a SDMR this distance is variable (see Fig. 4.8a and 4.8b - it varies from 0.291 to 0.581).

The acceleration  $a$ , of the centre of mass ( $a_x = \ddot{X}_R$  and  $a_y = \ddot{Y}_R$ ) have been determined (see section 4.1.2). The SDMR control should ensure that the SDMR does not accelerate at a value higher than that given by equation (4.28).

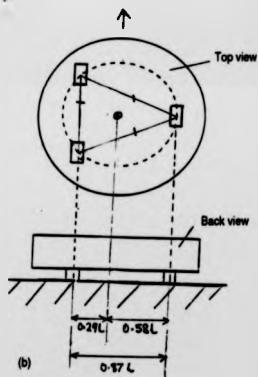
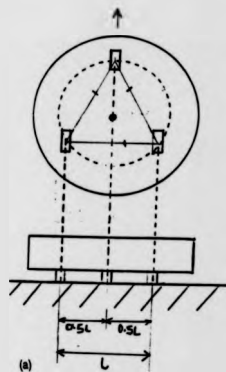


Fig. 4.8 Illustration of varying wheel to centre of mass distances.

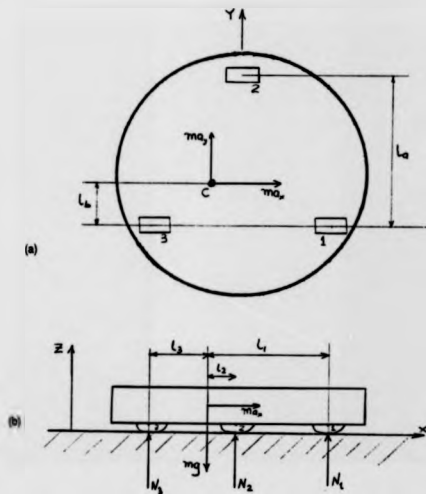
However it should be noted that equation (4.28) sets condition for no slipping of the three wheels. It is generally accepted that the principle of the synchro-drive mechanism guarantees zero wheel slip at a single wheel [Meriam'87]. It is assumed that if it does occur, all wheels must slip in unison, because it assumes identical conditions at each wheel. No reported work has revealed whether it is possible for only two wheels to slip first if the conditions on each wheel is not identical. As part of establishing the boundaries of control space within which no slip occurs, such a condition has been investigated.

Non-identical wheel conditions for the wheels of a SDMR can occur if the load is not evenly distributed on the wheels or if the point of wheel/floor contact is not symmetrical with respect to the centre of mass. Therefore the intention is to find if and under what condition slip at two wheels can occur if  $|a| < \mu g$ .

#### DETERMINATION OF ACCELERATION WHERE TWO OF THE THREE WHEELS ARE ABOUT TO SLIP.

If two of the three wheels are about to slip, the SDMR will possess both translation and rotation about the third wheel. Taking a case where the load is not evenly distributed, the forces and moments that arise can be analyzed with the aid of Fig. 4.9a and 4.9b.

Assume that wheel 1 and wheel 2 are about to slip. The slipping frictional force on wheel 1 and wheel 2 will develop moments about wheel 3. The D'Alembert force acting at the centre of mass will also develop a moment about wheel 3. The approach taken



1.2.3: Wheel and their numbers  
C: Centre of mass

Figs. 4.9 SDMR Model:

(a) Top view.

(b) Side view.

does away with the unknowns that are of no interest to the analysis.

Taking moment about the y-axis of wheel 3;

$$mg l_3 = N_2 (l_2 + l_3) + N_1 (l_1 + l_3) \quad (4.30)$$

Taking moment about the z-axis of wheel 3;

$$m a_y l_3 - m a_x l_b = \pm \mu (N_1 + N_2) (l_1 + l_3) \quad (4.31)$$

Taking moments about the x-axis of wheel 3;

$$mg l_b = N_2 l_a$$

$$\Delta \quad N_2 = mg \frac{l_b}{l_a} \quad (4.32)$$

Substituting for  $N_2$  in equation (4.30) gives,

$$N_1 = \frac{mg [l_3 - l_b / l_a (l_2 + l_3)]}{l_1 + l_3} \quad (4.33)$$

Substituting for  $N_1$  and  $N_2$  in equation (4.31) gives,

$$a_y l_3 - a_x l_b = \pm \mu g \frac{l_b}{l_a} (l_1 - l_2 + l_3 \frac{l_a}{l_b}) \quad (4.34)$$

The expression of equation (4.34) represents the acceleration to which the SDMR will have to be limited, in order to prevent wheel 1 and wheel 2 from slipping. Taking,

$$\pm \mu g \frac{l_b}{l_a} (l_1 - l_2 + l_3 \frac{l_a}{l_b}) = \gamma_3$$

the x-directional and the y-directional acceleration boundaries are given as;  $a_x = \pm \frac{\gamma_3}{l_b}$ , and  $a_y = \pm \frac{\gamma_3}{l_3}$  which is represented in Fig. 4.10a.



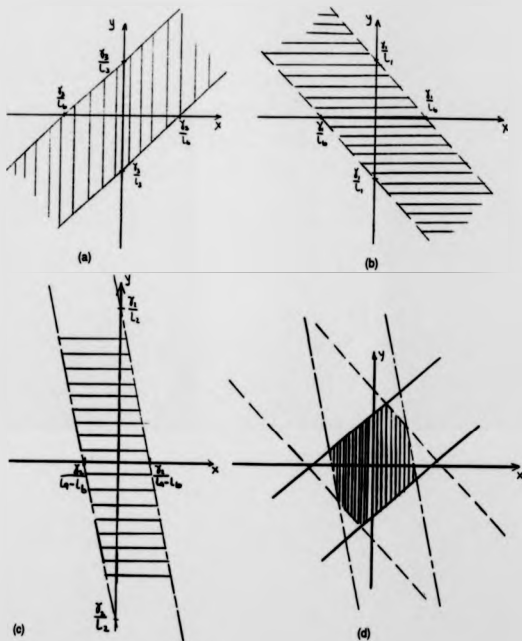


Fig. 4.10 SDMR boundaries of acceleration that prevents wheel slip:

(a) For wheel 1 and wheel 2 not to slip.

(b) For wheel 2 and wheel 3 not to slip.

(c) For wheel 1 and wheel 3 not to slip.

(d) For none of the wheels not to slip.

Similarly with wheel 2 and wheel 3 about to slip, the expression for the acceleration becomes;

$$a_y l_1 + a_x l_b = \pm \mu g \frac{l_b}{l_a} \left( l_1 \frac{l_b}{l_a} + l_2 + l_3 \right) \quad (4.35)$$

The expression of equation (4.35) represents the acceleration to which the SDMR will have to be limited, in order to prevent wheel 2 and wheel 3 from slipping. Taking,

$$\pm \mu g \frac{l_b}{l_a} \left( l_1 \frac{l_b}{l_a} + l_2 + l_3 \right) = \tau_1$$

the x-directional and the y-directional acceleration boundaries are given as;  $a_x = \pm \frac{\tau_1}{l_b}$ , and  $a_y = \pm \frac{\tau_1}{l_1}$  which is represented in Fig. 4.10b above.

Likewise with wheel 1 and wheel 3 about to slip, the acceleration of the SDMR that can prevent that happening is given by the expression (derived by taking moments about wheel 2);

$$a_y l_2 - a_x (l_a - l_b) = \pm \mu g \frac{(l_a - l_b)}{l_a} (l_1 + l_3) \quad (4.36)$$

The expression of equation (4.36) represents that which the SDMR acceleration will have to be limited to in order to prevent wheel 1 and wheel 3 from slipping. Taking,

$$\pm \mu g \frac{(l_a - l_b)}{l_a} (l_1 + l_3) = \tau_2$$

the x-directional and the y-directional acceleration boundaries are given as;  $a_x = \pm \frac{\tau_2}{l_a - l_b}$ , and  $a_y = \pm \frac{\tau_2}{l_2}$  which is represented in Fig. 4.10c above.

The three limiting accelerations when combined determines the acceleration boundaries that will limit two of the three wheels from slipping.

In order to get a clearer picture of the situation and the boundary of the combined event that will prevent wheel slipping an example is considered. Take a case where the parameters  $L_b$ ,  $L_1$ ,  $L_2$  and  $L_3$  of the SDMR are given as;  $L_b = 16\text{cm}$ ,  $L_1 = 17\text{cm}$ ,  $L_2 = 21\text{cm}$ ,  $L_3 = 1.5\text{cm}$  and  $L_3 = 18.75\text{cm}$ . Also let the acceleration due to gravity  $g$ , be  $9.81\text{m/s}^2$  and the coefficient of friction  $\mu$ , be 0.8.

For the travel position represented by Figs. 4.9a and 4.9b, the acceleration that will prevent wheel 1 and wheel 2 from slipping has to be,  $a_x \leq 13.2\text{m/s}^2$  and  $a_y \leq 11.8\text{m/s}^2$ . For wheel 2 and wheel 3 not to slip,  $a_x \leq 14.7\text{m/s}^2$  and  $a_y \leq 11.4\text{m/s}^2$ . While to prevent wheel 1 and wheel 3 the acceleration limit should be  $a_x \leq 9.0\text{m/s}^2$  and  $a_y \leq 84.8\text{m/s}^2$ . To prevent the three wheels from slipping  $|a| < \mu g$ , which in this case gives  $7.8\text{m/s}^2$ .

The acceleration commanded by the controller must fall within the shaded area of Fig. 4.10d. The boundary represented by the shaded area is the control space boundary that will prevent any two wheels from slipping. This implies that by changing the SDMR wheel heading relative to chassis orientation the acceleration requirements of the SDMR changes. Hence an acceleration that may be accommodated in a given heading may lead to violation of the control space in another heading. But the example shows that if the imbalance in conditions of the wheels is not severe, the

acceleration that allows slip at any of the wheels irrespective of heading relative to chassis orientation is above that required for the three wheels to slip.

#### 4.2.2 NO OVERTURNING CONDITION.

For the no overturning condition, the relevant major external forces that affect the SDMR are considered (see Fig. 4.11a). They consist of the force due to gravity  $mg$ , supporting forces  $N_1$ ,  $N_2$  and  $N_3$ , the tractive force  $F_x$ .

The position of the centre of mass is located by considering the system as a single rigid body. The velocity and acceleration of the centre of mass have already been established (see section 4.1.2). Using the D'Alembert force principle [Meriam'87], a dynamic system can be considered in the static state, if D'Alembert forces at the centre of mass of the SDMR act in the opposite direction to the acceleration of the centre of mass (see Fig. 4.11b). The D'Alembert forces for the SDMR consists of the inertia force, the centripetal force and the Coriolis forces. These forces are contributed by the corresponding terms in the SDMR acceleration equations derived earlier in section 4.1.2.

The no overturning condition demands that the net force, which is the vector sum of all external forces acting on the SDMR, be directed in a way that ensures that the line of action of the resultant force intersects the sides of the triangular cone. The cone is formed by the three wheel/floor contact points and the SDMR centre of mass ABCD (see Fig. 4.12). The point of intersection on the floor surface should be within the area of

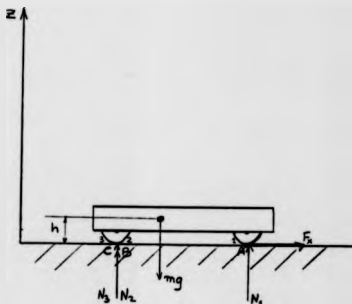


Fig. 4.11a External forces acting on the SDMR.

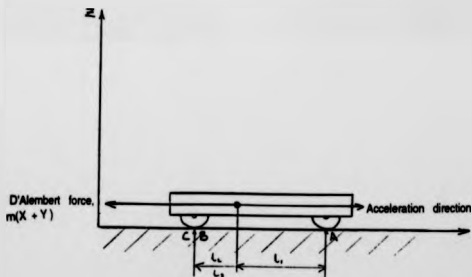


Fig. 4.11b Side view of SDMR showing D'Alembert force representation.

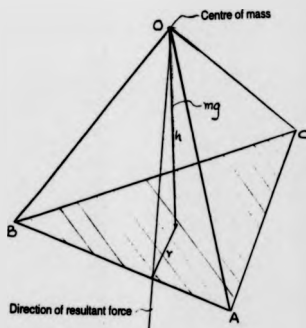


Fig. 4.12 Triangular cone showing volume for no SDMR overturning.

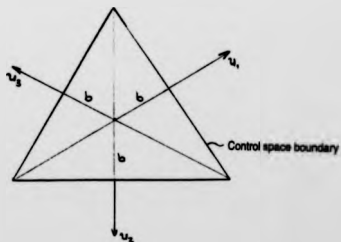


Fig. 4.13 Area showing acceleration boundary for no SDMR overturning.

the triangle formed between point A, B and C, that represents the wheel/floor contact points. The three points establish the limits of the stability region associated with maintaining vertical equilibrium.

The condition for stability can therefore be expressed as requiring that the sum of torques generated by  $F$ ,  $mg$  and the D'Alembert force about, for example, the potential pivot (supporting) point A (see Fig. 4.11b and 4.12) be of positive value and that at point B and C be negative simultaneously. The positive value of the net torque about point A prevents the SDMR from tipping over forward and the negative values about point B and C prevents it from tipping over backward for the situation under consideration.

If the force  $F$  is resolved in the X and Y axes as  $F_x$  and  $F_y$  and the distance between the centre line of the SDMR centre of mass and either of the supporting point A, B and C be  $l_1$ ,  $l_2$  and  $l_3$  (see Fig. 4.11b). The criteria for establishing the boundary of the control space with respect to overturning is obtained by forcing the sum of the torques of the external force about A to be positive and those about point B and C to be negative, simultaneously. Mathematically this implies that;

$$-F_x(l_3 - l_2) + F_y(l_1 + l_2) - mgl_1 + m a_y y_R - m a_y l_1 < 0 \quad (4.37)$$

$$-F_x(2l_2 + l_3) + F_y(l_1 + l_2) - mgl_2 + m a_y y_R - m a_y l_2 > 0 \quad (4.38)$$

$$-F_x(2l_3 + l_2) + F_y(l_1 + l_3) - mgl_3 + m a_y y_R - m a_y l_3 > 0 \quad (4.39)$$

Note: The values of  $L_1$ ,  $L_2$  and  $L_3$  are dependent on the SDMR chassis orientation and wheel heading (see Figs. 4.8).

Equations (4.37) to (4.39) are criteria for dynamic stability of the SDMR. If the acceleration is made zero it reduces to the case of static stability.

The acceleration value that ensures no overturning of the SDMR can be determined by using simple geometry. Similar triangles yields (see Fig. 4.12);

$$\frac{|a|}{g} = \frac{|r|}{h} \quad (4.40)$$

For no overturning,

$$|a| < \frac{|r|g}{h} \quad (4.41)$$

The acceleration can be derived from the rate of change of drive speed or from the steering rate expressed as  $(v^2/R)/t$ , where  $R$  represents the radius of the curve path and  $t$  the time. These values for the acceleration account for both longitudinal and lateral overturning.

For the three wheels, considering that the sides of the triangle which they form has unit vectors  $u_1$ ,  $u_2$  and  $u_3$  (see Fig. 4.13 above), it implies that;

$$\begin{aligned} a \cdot u_1 &< \frac{bg}{h} \\ a \cdot u_2 &< \frac{bg}{h} \\ a \cdot u_3 &< \frac{bg}{h} \end{aligned} \quad (4.42)$$



The magnitude of the acceleration is dependent on the distance  $b$ .  $b$  has a coefficient that varies from 0.29 to 0.58 depending on the chassis orientation and wheel heading. This signifies that SDMR stability requirement is dependent on wheel heading relative to chassis orientation and speed of travel. For the controller to achieve stable motion it has to plan ahead of time required to execute the control command, in order to make necessary adjustments to the control parameters.

Equations (4.37) to (4.42) have to be satisfied at all times in order to achieve dynamic stability. It should be borne in mind, that the conditions under which the boundary for no slip or overturning occurring as established, and derived above are sufficient conditions, which would guarantee that there is no tendency for the SDMR to slide or overturn.

The combination of the regions that guarantee no slip and no overturning sets out the zone within which the controller will allow the SDMR to operate. This zone is what is called the boundaries of the control space. The criteria for the boundaries of the control space also affects the solution to the inverse kinematics and dynamics. Therefore any solution to the inverse kinematic and dynamic problems which violates the control space criteria expressed by the equations (4.28) to (4.42) should be ruled out. This should ensure that the SDMR does not deviate from its desired trajectory.

The control space expression derived in this chapter is seen as the controller limiter and essential for accuracy and stability

of operation. Any control strategy that incorporates the established boundaries of control space (which ensure no slip or overturning of the SDMR) has to always check the user requested acceleration against that established by the control space at all times. If that established by the control space is less than that specified by the user, the users requested acceleration should be discarded for that given by the control space, or an error state reported as need be.

A new method of kinematic modeling of SDMR have been implemented in analyzing different wheel assembly designs. The analysis has identified analytically the source of steering induced error which characterizes Type-1 wheel assembly design. Through the modeling it is revealed how the induced error can be eliminated. Also some dynamic considerations of the SDMR have been given enabling the study of control space and requirements. To avoid the SDMR becoming unstable in operation, the acceleration limits which the controller should allow for have been investigated and established. The next chapter deals with the construction of prototypes and further wheel design comparison.

## CHAPTER 5

### PROTOTYPE DEVELOPMENT AND FURTHER ANALYSIS OF DIFFERENT WHEEL ASSEMBLY DESIGNS

This chapter discusses the construction of the prototype SDMRs, and the effect of wheel forces/torque and steering input on two main design of SDMR. The designs investigated are those based on wheel assembly, with wheel-offset from the steering axis and that with wheel-set on the steering axis.

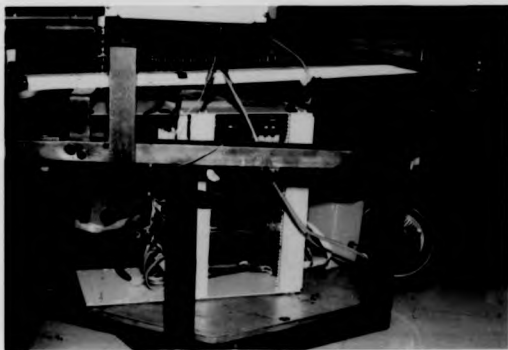
#### 5.1 PROTOTYPE DEVELOPMENT.

This section deals with the SDMR structure, power transmission mechanism, and layout implemented in the prototypes used to conduct experimental tests.

There are two versions of the prototype SDMR Type-3 used in conducting tests. Version 1 is the modified original design represented as Type-3:A SDMR in chapter 4, section 4.1.2.2, without the design-error compensation mechanism (see Fig. 5.1). Version 2 is the Type-3:B SDMR, which incorporates a design-error compensator unit (Fig. 5.2). The specifications of the two versions are given in Appendix C.

##### 5.1.1 STRUCTURE AND LAYOUT OF THE PROTOTYPE SDMR.

A requirement of the mobile robot that has been developed is that it should be able to carry loads on its 'platform'. The overall shape of Version 1 prototype SDMR is shown pictorially in Fig. 5.3.



**Fig. 5.1** SDMR Version 1 showing part of the inside construction.



**Fig. 5.2** SDMR Version 2 which incorporates the design-error compensator mechanism.

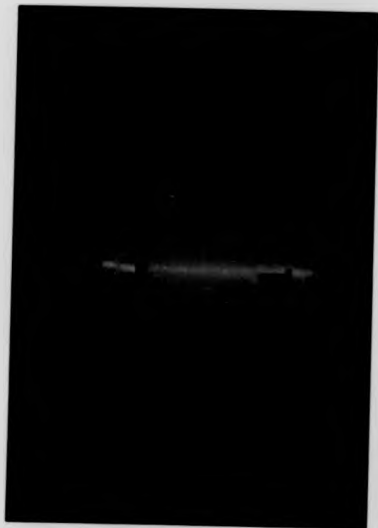


Fig. 5.3 Pictorial view of the overall shape of the SDMR Version 1

It is made up of three removable sections and they are: The platform, for carrying loads. The mid-section, where the user controls, emergency stops and the danger signaling lights are located. The main body/bumper section, where the main components such as battery, motors, etc. are accommodated.

The power transmission system employs steel chains for the section between the motor shafts and the wheel assembly shafts (see Fig. 5.1). Chains were used for that section of the transmission system for the reasons, given in chapter 2.

#### LAYOUT OF THE FIRST PROTOTYPE SDMR.

The structural layout of the mobile robot is shown in Fig. 5.4. The approach chosen is to drive the three wheels from one electric motor and steer the three wheels using another electric motor. This creates an efficient and economical system.

With the three wheel assemblies driven by one motor; for the motor to exert equal effects on the three wheels, the wheel to motor linkages must have an equal effect on their respective wheels. If this is not achieved it will mean that when a drive torque is applied by the drive motor, on each wheel, it will tend to exert different forces. If this happens there will be a tendency for wheel slip to occur. Any slip could introduce an arc movement when straight line movement is intended or vary the radius of any intended curved path.



Fig. 5.4 SDMR Version 1 without the 'platform', showing the chain transmission system.



In the same vein, in order to make effective use of the All-wheel steering principle, which helps to achieve omnidirectionality, the three wheels steered by one motor must have equal rates of turn at all times. To achieve this, the steering motor to wheel linkage must exert the same steering force on the three wheels in order to accelerate them. If the wheels' turn rates differ from each other, due to unequal response, this will result in temporary misalignment of the wheels and this will affect the desired SDMR heading.

To prevent unequal response to steering input, there must be a total synchronization of the response of the transmission system. This implies no slack or backlash, which is however not attainable. Though the construction must attempt to minimise slack and backlash. The effects of the error due to slack and backlash are discussed later in chapter 8.

Bearing in mind that the mobile robot design implemented is that which achieves true omnidirectional motion, there is no preferred direction of travel. The only perceived requirements to control orientation occur if;

- sensors are mounted on the mobile robot, which must be aligned with the direction of travel,
- objects are transported on the mobile robot, which must be carried or delivered in a specified orientation, or
- a manipulator is mounted on the SDMR which must interact with objects anywhere in the environment.

Consideration of these requirements has shown that it is

unnecessary for the chassis itself to possess the ability to rotate with respect to the environment. Provided that a rotary platform is fitted which can rotate with respect to the chassis. This will make it possible for the orientation of the platform to be linked to the direction of travel, or it may be dissociated from the direction of travel as required by the application.

The platform, which is rotatable, is designed to be driven in a number of ways depending on the application. The ways in which the platform can function are as follows:

- (i) It can be connected to the steering mechanism, in which case it turns with the wheels and maintains an orientation that is related to the heading of the SDMR.
- (ii) It can be disconnected via a clutch system, in which case it maintains a fixed orientation regardless of SDMR heading.
- (iii) Alternatively the platform could be powered by a separate electric motor, which has been fitted solely to provide platform orientation, independent of the heading of the mobile robot. In this case it can be electronically synchronized with the steering if required.

#### 5.1.2 METHODS TO COMPENSATE WHEEL ASSEMBLY DESIGN-ERROR.

The effect of coupling in the wheel assembly has been discussed in section 4.1.2. Fig. 5.5 shows that the drive and steering subsystems are linked through spur gears and bevel gears. The drive motion is transmitted through spur gears to the bevel gear, which then allows the wheel to rotate as a result of the drive motion. It is also through the bevel gears that the steering

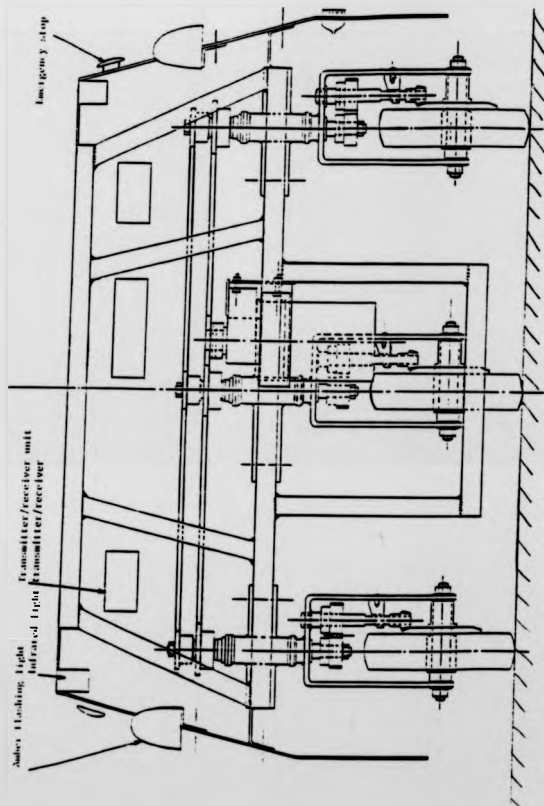


Fig. 5.5 Side view of the general assembly of the SDMR.

motion induces the rotation of the wheel about its horizontal axis when steering of the wheel occurs. This rotation of the wheel, when steering, causes position error.

The kinematic modeling presented in section 4.1.2 shows that the induced motion which is an outcome of the wheel assembly design can be eliminated. Investigation revealed that to retain such a design there are two major ways through which the design-error can be eliminated. They are through:

- o Software Compensation.
- o Hardware Compensation.

#### 5.1.2.1 SOFTWARE COMPENSATION.

Software compensation can be achieved by building into the control algorithm a subroutine that is called once a steering action takes place. The subroutine should determine what the value of the error is, which is dependent on the value of the angle turned. It will then generate a value that will be equal in magnitude to the induced drive but opposite in direction.

However this compensation method is less effective because it is itself error driven. It relies on the effectiveness of the dead-reckoning navigation systems, which is error prone. And compensation takes place mostly in the transient state, which is when the system is less stable.

#### 5.1.2.2 HARDWARE COMPENSATION.

The hardware compensation is achieved by creating another meshing point for the drive and steering subsystems. This new meshing

point is through a differential mechanism called 'mechanical compensator unit'. The mathematical expression of the operation has been discussed earlier in section 4.1.2. The mechanical compensator unit is implemented in the Version 2 prototype SDMR (see Fig. 5.6)

The way it operates is thus: When a steering output is sent out through the steering motor shaft via a worm gear set, the steering output passes through the differential gear arrangements. Through the end of the differential shaft that is directly connected to the drive chains a drive output of opposite sign is activated. The magnitude of the drive output is dependent on the differential gear ratio. The ratio is made such that the amount of drive motion which is caused by steering the wheel is the same as that which the differential generates.

The development of the SDMR discussed above highlights some construction difficulties, such as exerting equal amount of torque on the three wheels through the power transmission mechanism. In view of these limitations in achieving a perfect system it is deemed necessary to theoretically and experimentally investigate what the behaviour will be. The experimental consideration starts from the next chapter. The theoretical study has been covered earlier. The next section is concerned with the further theoretical evaluation of Type-1 and Type-3 SDMR.

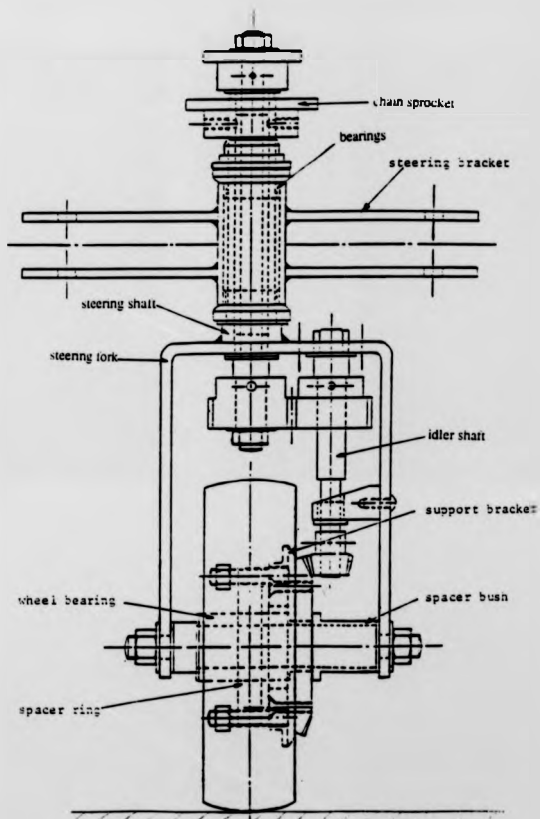
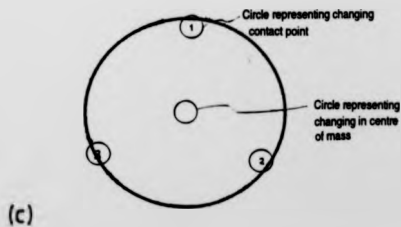
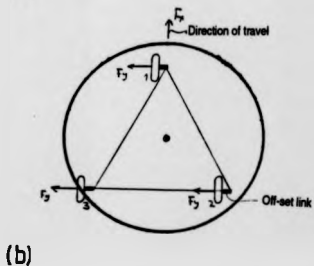
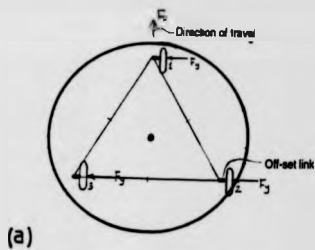


Fig. 5.6 Complete schematic diagram of the drive/steering wheel assembly.

## 5.2 THE IMPACT OF WHEEL FORCES/TORQUE AND STEERING INPUT ON SDMR PERFORMANCE.

The effect of tractive force on both wheel configurations of the SDMR is the same. But when the lateral force and self-aligning torque effects are considered the result becomes different. The self-aligning torque is given by the product of the cornering force and the tyre trail  $(M_s = F_y t_s)$  (see chapter 3, section 3.1). The torque developed by the lateral force has the tendency to align the wheel plane with the direction of motion. Side force is proportional to the lateral force.

For a Type-1 wheel assembly; The magnitude of the self-aligning torque is directionally dependent. The major factor that affects it is the positioning of the offset link (see Figs. 5.7a and b). In the positioning shown in Fig. 5.7a, with the direction of travel shown with its drive force represented by  $F_x$ , the magnitude of the self-aligning torque is at its maximum. This is caused by the fact that the side force generated by the drive force on the tyre and that generated by the force acting on the offset link add to each other in such position. Under such circumstances a higher 'free-play' angle and lateral force are produced. When motion of the wheel reverses by steering the wheels through  $180^\circ$  (as illustrated by Fig. 5.7b with the offset link on the left side of the wheel), the side force generated by the two different source opposes each other. There is a resultant side force which invariably is less than either of the two original side forces. The value of the lateral force by this resultant side force will be at its minimum value and hence the self-aligning torque value will also be at its minimum.



Figs. 5.7 Illustration of changes in the self-aligning torque and the contact points.



Such changes in the magnitude of the self-aligning torque with respect to reversal of direction of motion does not occur in the case of wheel-set on steering axis wheel assembly configuration. This is primarily due to lack of the offset link, because here the tyre contact area is under the steering axis of the wheel assembly.

The lateral force also helps to establish another moment known as twisting moment. This tends to twist the body/frame of the mobile robot. The twisting moment acts about the vertical axis through the centre of gravity (C of G) of the mobile robot. Twisting moment is given as  $M_t = F_l l$ , where  $l$  is the perpendicular distance from the wheel assembly vertical axis to the mobile robot's C of G. The twisting moment can affect the mobile robot's directional stability. For example in the case of a conventional designed mobile robot that uses an idler (caster), if the idler is placed in the front of the mobile robot, it gives rise to directional stability when moving forward. If it is at the rear it causes directional instability as witnessed in wheelchairs [Collins'87].

For all SDMR's, the effect of twisting torque does not give rise to a straight forward state of stability or instability. This is due to the ability of the wheels of SDMR to swivel through  $360^\circ$  and head in any direction. In certain wheel positions (see Figs. 6. for illustration of different wheel heading with respect to the SDMR chassis), with the wheels equidistance from one another and also symmetrical, the resultant of the twisting torque is zero. This is on the assumption that other conditions such as

evenly distributed load and no slack, backlash are met.

Using Fig. 5.8 to illustrate this fact; assume the perpendicular distance between,

wheel 1,  $w_1$  and C of  $G = s_{a1}$

wheel 2,  $w_2$  and C of  $G = s_{a2}$  and

wheel 3,  $w_3$  and C of  $G = s_{a3}$ ,

lateral force of each of the three wheels =  $F_y$ .

The twisting moment produced by wheel 1 is given by,

$$M_1 = s_{a1} F_y, \quad (5.1)$$

and it is acting say anti-clockwise.

The twisting moment produced by wheel 2 given by,

$$M_2 = s_{a2} F_y, \quad (5.2)$$

and acting say clockwise.

The twisting moment produced by wheel 3 given by,

$$M_3 = s_{a3} F_y, \quad (5.3)$$

and acting say clockwise.

Knowing that  $s_{a1} = s_{a2} + s_{a3}$  and  $s_{a2} = s_{a3}$ , it implies that;

$$M_1 = 2s_{a2} F_y \text{ and } M_{23} = 2s_{a2} F_y$$
$$M_1 = M_{23} \quad (5.4)$$

Thus the resultant twisting moment is zero. Under such circumstance directional stability is achieved and maintained by the SDMR configuration, and self-aligning torque developed, with no twisting moment effects.

In reality there is a resultant twisting moment because of differences in load distribution, power transmission (caused by

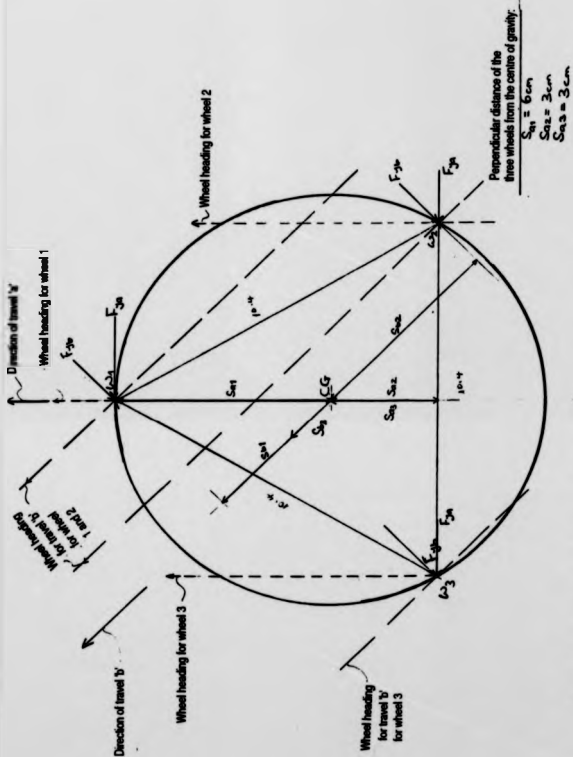


Fig. 5.6 Illustration of varying wheel contact point to centre of mass distances.

things such as slack, backlash), wheel alignment, etc. The effects of such twisting moment are dependent on two main factors, namely;

- ▷ wheel heading with respect to the SDMR chassis and free-play angle,
- ▷ the type of wheel assembly implemented and the direction of travel.

However Type-1 wheel configuration has a tendency for lesser directional stability and can approach directional instability more easily than the Type-3 wheel configuration. This is because of changing C of G of the mobile robot as it changes heading. The changing C of G of the mobile robot causes lateral load transfer between the inside and outside wheel. The analysis of lateral load transfer has been presented earlier in chapter 3, section 3.1. The lateral load transfer reduces the overall lateral force developed by the SDMR.

The load transfer that occurs with the Type-1 wheel assembly based SDMR has two major effects on the behaviour of the mobile robot. First it affects the magnitude of the self-aligning torque developed in each of the wheels. As the load transfers from the inside wheel to the outside wheel, so does the lateral force. Thus making the lateral forces developed on each of the three wheels to be unequal. As the lateral force on the three wheels differs so does the self-aligning torque which they generate. This phenomenon will actually cause the wheels to travel at slightly different angles and therefore the possibility

of different direction of motion. With the wheels traveling in different directions the actual direction of travel of the SDMR will not in general be a straight line but an arc.

The second effect of the load transfer concerns the twisting moment. The C of G changes because of the wheels that are offset from the wheel assembly steering axis. The twisting moment also changes because of changes in the values of the lateral force and the perpendicular distance of the wheels from the C of G. This phenomenon affects the SDMR directional stability and control. The load transfer taking place on the SDMR based on wheel-offset wheel assembly configuration makes the overall error motions of the SDMR to be highly unpredictable.

The wheel-offset (Type-1) configuration therefore has the tendency for lesser directional stability, because of changing C of G and reduced overall lateral force. Thus it can be said that SDMR based on such a wheel assembly is more prone to error if poor quality components are used in the construction.

The wheel-set on wheel assembly steering axis (Type-3) configuration does not suffer from any load transfer during manoeuvres. This causes the cornering force to remain fixed and maintain its acquired value. Hence its motion is predictable to a certain degree. This is because the self-aligning torque and its twisting moment in certain cases (such as in an ideal tricycle wheel positions with equal free-play angle) can be known.

Having said this the overall motion of a SDMR motion and behaviour in generally cannot easily be predicted. This is because all the wheels are driven and steered in unison, and once there is a different response of any of the wheels, its effect on the SDMR behaviour cannot be easily identified or isolated.

The steady-state handling characteristics of a SDMR is highly influenced by;

- ▷ the relative displacement of the wheels with respect to the SDMR chassis and direction of travel,
- ▷ the weight distribution and
- ▷ cornering stiffness, which is defined as the derivative of cornering force with respect to slip angle.

Significant changes in any of these factors alter the SDMR handling behaviour. Some of these factors are affected by design and operational parameters. For instance the sort of wheel assembly implemented can influence weight distribution, and conversely the handling behaviour. This implies that though the behaviour of the two different SDMR may be similar under the same operational parameters, their level of stability is not necessarily the same.

The wheel analysis has indicated that Type-3 based SDMR has the tendency for more predictable handling behaviour than that of Type-1 based. This is mainly attributed to the limited load transfer taking place during manoeuvres and the twisting torque.

However the level of stability achieved by both design varies as

the SDMR heading varies. This is due to changes in wheelbase value. As the value changes so does other factors such as cornering stiffness, overall weight distribution, etc. Hence though an SDMR may be generally directionally stable, its level of stability varies with wheel heading.

This chapter has dealt with the development of SDMR using Type-3 wheel assembly design. It has described how Type-3 wheel assembly design-error can be compensated, and has shown the practical implementation of the design-error compensator mechanism. Also covered, is the further evaluation of Type-1 and Type-3 SDMR highlighting some major practical differences through the understanding of their theoretical behaviour. The next two chapters concentrate on actually testing the developed SDMRs, in order to know what the sources, causes and sort of influence the errors identified have on them. Also it helps to verify the behaviour predicted from the theoretical study.

EXPERIMENTAL TECHNIQUE TO DETERMINE SDMR ERRORS AND BEHAVIOUR

This chapter discusses the objectives of the experiments that were conducted and the methods used to acquire results.

6.1 EXPERIMENTAL OBJECTIVES.

The experiments were conducted to provide data for error analysis and also serve as an information base for understanding the behaviour of a SDMR. These aims in collaboration with the earlier theoretical evaluation helped establish mathematical models that expressed the characteristics and the boundaries of the control space of a SDMR. The models achieved and other information which the experiments provided are anticipated to be very helpful for designers of mobile robots in general and Synchro-Drive Mobile robots in particular.

Mobile robots possess errors originating from two major sources. They are the mechanical system and control system errors. It is the purpose of this work to investigate errors which originate from the mechanical system.

Mechanical system errors can be caused by design, construction and assembling of the system, friction, backlash/slack in the mechanisms, and tolerances. When any of these error sources are present, data recorded from the control system will not reflect the actual physical behaviour of the robot.



Some of these errors may be repeatable and others random. Among the objectives of the work is to identify the sort of errors possessed by SDMR. Also the sources, magnitude, direction (including reversibility) and relative importance of the identified errors are identified with a view to fully assessing the overall performance of the SDMR.

Measures of performance are expressed in terms of accuracy of the path and the nature of trajectory executed by the SDMR. The measurable performance variables are; the lateral error ( $\delta y$ ), the longitudinal error ( $\delta x$ ), precession angle ( $\beta$ ). The nearer these variables are to zero the better the mobile robots' performance. The performance variables are affected by effects of; backlash/slack, wheel misalignment, different wheel radii, weight distribution, component tolerances, and control system parameters and strategy

The data from the tests formed the basis upon which observational (qualitative) analysis as well as statistical analysis were conducted. With various states under which results were recorded, statistical inferences were made. This assisted in explaining the behaviour of the SDMR, and the reasons for the observed results.

## 6.2 EXPERIMENTAL PROCEDURE.

Experiments were conducted with the SDMR having the wheel-set on the wheel assembly steering axis configuration only (Type-3). Previous analysis has identified the differences and similarities

that exist when compared with other designs.

Path information was supplied to the SDMR in two different modes. Both modes employ radio communications. The two modes were as follows:

(a) Manually controlled radio transmitter. In this mode, there was no on-board processing of path information. The SDMR motion was wholly open loop controlled. With known input the path errors resulting are predominantly from the mechanical system.

(b) Autonomous control by means of a pre-prepared program, down loaded over a radio link into the memory of the SDMRs' on-board computer. The path was then executed by means of dead-reckoning navigation using feedback from the motor mounted encoders. In this mode the path errors result from a combination of control system error and mechanical system error.

These two different control modes were implemented on two different versions of the Type-3 SDMR. Version 1 represents Type-3:A SDMR, which is a design without the design error compensation unit. Version 2 is the Type-3:B SDMR, which has a design error compensation unit.

#### 6.2.1 TESTS CONDUCTED.

The test performed were of two forms;

- (1) Those in which the SDMR were adjusted to reduce the mechanical error as far as was reasonably practicable, and it was considered as 'Form-1' test.

- (2) Those in which deliberate errors were introduced in order to identify the contribution made by such errors. This was considered as 'Form-2' test.

The SDMRs were driven around within a defined space measuring approximately 7m by 5m in the laboratory where the research was been conducted. The floor surface consisted of smooth thermoplastic floor tiles and was level to within 1mm in 1m. Fig. 6.1 shows the plan view of the test area. The test paths consisted of mainly straight lines.

For the straight line paths the SDMRs were driven forward and backward. The return journey was accomplished by reversing the direction of the drive motor rather than by steering the wheels through 180°. This eliminated the possibility of error arising from rotating the steering axis by exactly 180°, but did reverse the direction of all the drive forces through the transmission system. Based on the path execution, it was possible to establish the main sources of mechanical system error present in the mobile robots under test.

In order to isolate the sources of errors and identify the contribution which they made, several different types of test runs were conducted. These tests included;

- (a) Travelling with different SDMR orientation with respect to wheel heading relative to the fixed global frame of reference, otherwise known as 'posture'.
- (b) Travelling under different states of adjustment known

as 'Form-1' and 'Form-2' (defined earlier).

(c) Travelling at different speeds and accelerations.

(a) Due to the SDMR's ability to travel in any direction regardless of chassis orientation, there was a need to know the influence of chassis orientation on the errors in the path. The chassis may be orientated in any direction with respect to a global coordinate system which has its origin on the laboratory floor. Fig. 6.2 shows just twelve possible SDMR postures, but an infinite number of postures are possible.

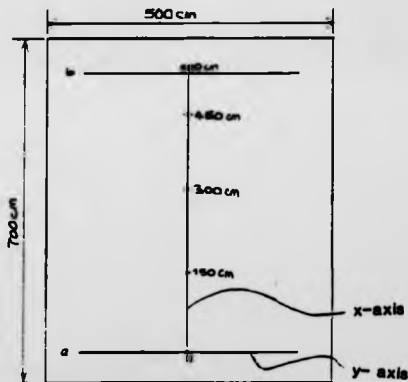
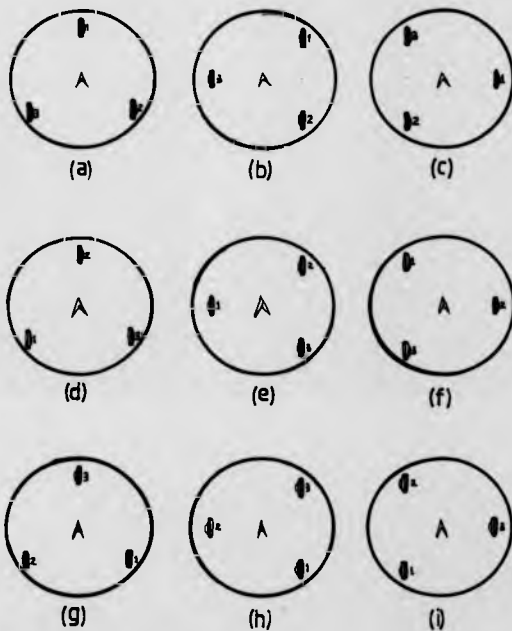


Fig. 6.1 Plan view of the experimental test area.



A: Chassis orientation

1, 2 or 3: Wheel and the wheel number

Figs. 6.2 Twelve possible SDRM postures.

For any chassis orientation the wheels may be steered to any direction (Fig. 6.3). The significance of this fact is that SDMR chassis orientation and wheel heading are independent of each other. This characteristic is peculiar to mobile robots with omnidirectional motion, and creates an added source of error. Since the wheels may be steered in any direction with any chassis orientation, any errors associated with either wheel heading or orientation will cause the SDMR to move with path errors which vary as a function of orientation and wheel heading. Analysis in chapter 3 and 4 shows that changes in 'wheelbase' parameters due to change in posture influence behaviour and limits of the control space. Tests conducted under different chassis orientation and different wheel heading (SDMR posture) shows their effect on the path execution.

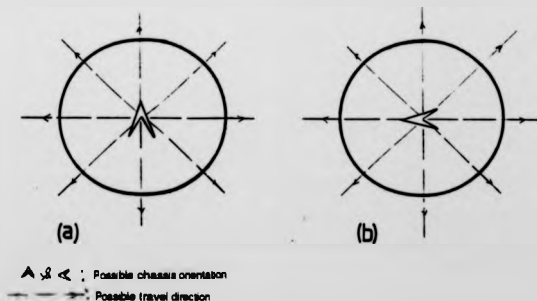


Fig. 6.3 Possible direction of travel of the SDMR under a given chassis orientation

Even if the SDMR is geometrically perfect such that the behaviour of wheels 1, 2 and 3 are identical in every way, the SDMR can still experience forces which will tend to deviate it from its prescribed path (for analysis see chapter 3, section 3.3.1). The magnitude of the deviation and the nature of the path changes as the chassis orientation and wheel heading changes.

(b) Tests under 'Form-1' condition establishes contributions made by major sources of errors such as design and construction, and the type of errors they were, such as reversible and/or repeatable. Tests in 'Form-2' helps identify what contributes most to a particular type of error, and what influence such an error source has on the overall performance. 'Form-1' and 'Form-2' tests were necessary in order to ascertain what source is contributing what and its overall impact.

(c) Conducting tests by travelling at different speeds and acceleration achieves the following;

- ▶ allow for the understanding of the dynamic behaviour of the SDMR,
- ▶ the implication of violating the boundaries of the control space, which allows wheel slip and skidding to set in.

The emphasis of the test is on SDMR behaviour in relation to change in any of the mechanical systems parameter, such as load distribution. For this reason the tests were conducted at a fixed speed and acceleration.

#### 6.2.2 METHODS USED TO RECORD PATHS AND SET THE SDMR STATES.

Paths executed by the SDMR were marked directly on the laboratory floor using a fine point fiber tipped marker pen. The design of the pen plotter is shown in Fig. 6.4. The pen was mounted at the precise centre of the SDMR, in order to record the trajectory of the SDMR and to eliminate effects of chassis precession. Chassis precession was monitored independently using an Autohelm electronic compass [Autohelm].

Test runs were executed slightly differently for the two versions of the SDMR tested. Version 1, which was tested only under manual remote control, had its path executed and monitored at only one constant speed of 40cm/s between two measured points. Version 2, which is both manual and computer controlled executed its path at two different speed of 40cm/s and 100cm/s. The tests were conducted under computer control. Due to no significant change in the outcome of the tests at the two different speeds, only test results at the speed of 40cm/s will be reported in the next chapter. The path specification incorporated start and stop at specified distances.

Before the tests in the 'Form-1' condition commenced, the wheels were aligned using the in-built wheel adjuster. In Version 1 SDMR, alignment screw adjusters (see Fig. 6.5 for the pictorial view) are mounted on two of the three wheel assemblies to permit alignment with the 3rd fixed wheel assembly. Wheel misalignment was identified using two 1.5 metres straight edges, clamped to steering fork of the three wheel assemblies.



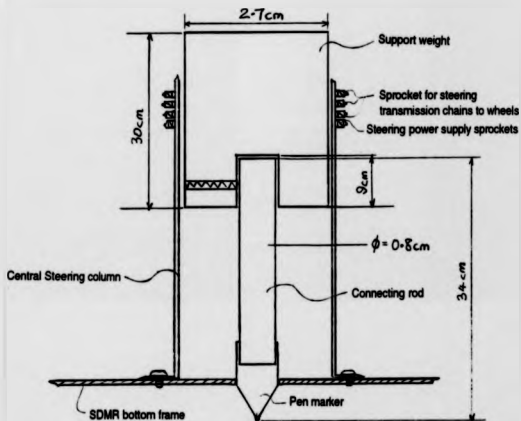


Fig. 6.4 Schematic diagram of the pen plotter mechanism.



Fig. 6.5 Pictorial view of one of the wheel alignment screw adjusters.

Measurements were made at points  $x_1$  and  $x_2$  (see Fig. 6.6). Any difference in reading between  $x_1$  and  $x_2$  indicates a wheel misalignment. A difference of 1mm corresponds to an angular error of less than  $0.05^\circ$ , thus making a steel tape a sufficiently accurate measuring instrument for wheel misalignment. If  $x_1$  and  $x_2$  differed, adjustments were made using the alignment screws until they were equal to within 1mm.

#### 6.2.3 MEASUREMENTS TAKEN AND EQUIPMENT USED.

The measurements taken were that of;

- (1) the SDMR frame rotation (precession) which was measured in degrees,
- (2) the y-direction (y-axis) deviation of the SDMR location, which is called the lateral error ( $\delta y$ ) measured in centimetres,
- (3) the x-direction (x-axis) deviation which is also called the longitudinal error ( $\delta x$ ) measured in centimetres,
- (4) the overall wheel angular displacement contributed by the backlash in the gears and slack in chains of the steering transmission mechanism and wheel assembly play- influenced by tolerances and dimension inaccuracy, which is hereby called the wheel 'free-play' angle,  $\sigma$  and it was measured in degrees,
- (5) the location of the centre of gravity measured in centimetres, from the centre of mass to wheel 1 location.
- (6) the radius of the wheels measured in centimetres.

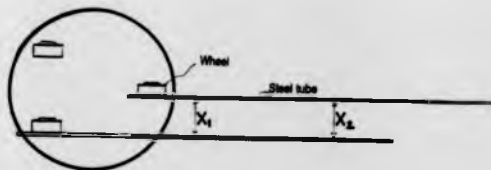


Fig. 6.6 Illustration of the method of checking individual wheel alignment.

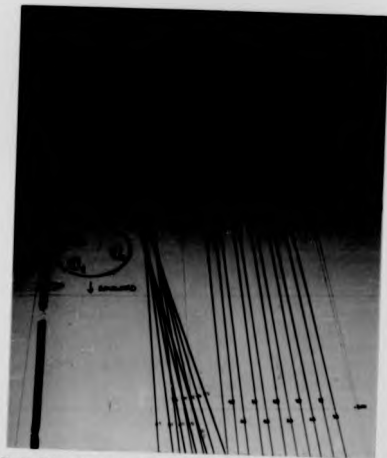


Fig. 6.7 Pictorial view of some of the trajectories executed by SDMR Version 1.

- (7) the 'play' in the wheel drive direction caused by backlash, slack and tolerances in the drive transmission mechanism measured in degrees.

Considering the fact that a synchro-drive system has a fixed frame of reference in principle (see section 6.2.1) irrespective of the direction of travel, it is important to know whether any precession of the frame occurred and if so to know its magnitude. Also any relationship between precession and the SDMR trajectory were observed.

The frame rotation was monitored using an Autohelm electronic compass [Autohelm], which has a resolution of 1'. The electronic compass was found to be effective for the purpose for which it was used, and its memory capability was particularly useful. Measurements were taken at the start and finish of each test run of the SDMR. At each instance nine readings were made and stored in the compass memory, after which the arithmetic mean was taken and recorded as the final reading. The difference between readings at start position and finish position represents the frame rotation (precession) for that particular run.

The trajectories which the SDMR exhibited were marked directly on the floor using the marker pen as a plotter as previously described. Fig. 6.7 above shows pictorial view of some of the trajectories made by the SDMR with different wheel positioning.

The lines plotted by the pen plotter which are the actual

trajectories of the SDMR for every run was then measured, recording their y-direction deviations at chosen interval in the x-direction. The deviation at the finished position plays a greater part in the analysis. In the data table, were recorded such values as longitudinal error ( $\delta x$ ) and lateral error ( $\delta y$ ) (explained further in the next chapter). All measurements were taken with a steel tape having a measurement accuracy of  $\pm 1\text{mm}$ .

Another form of taking measurements was considered. That considered was the use of camera system. The camera system [Appendix A, section A.2] was considered unsuitable because of low resolution and speed problems for a camera system that can operate over such a large area. Camera resolution deteriorates as the angle of view increases. In the sort of measurements being considered a wide angle lens is essential if the whole trajectory is to be traced (see Fig. 6.7). Also there is the problem of accurately mounting the camera without tilt of one form or another. These problems can create sufficient errors that are significant on their own, and therefore may produce errors, at least of the same magnitude as, if not larger than those of interest.

Another measurement taken was that of the transmission system's backlash, slack and play in the wheel assemblies, when swiveling the wheels, which together is called the wheel assembly 'free-play'. The slack in the power transmission system were generated by the chains used, while the gears used generated backlash. The play arises from manufacturing tolerance and

dimensional inaccuracies in components used (example is the bearings). The wheel steering free-play angle,  $\sigma$  was measured directly in degrees.

The measurement was accomplished using a precision protractor and rule. The measurements were taken by suspending the SOMR, using supports to raise the wheels above the floor. This was done in order to eliminate the effects of ground friction, which can reduce the overall wheel steering 'free-play' angle. The wheels were swiveled by hand until they could no longer steer, with the steering motor held in servo brake mode. The initial individual wheel heading was marked on the floor and a line drawn at a tangent to the virtual line of floor contact. At the end of swivel the same process was repeated for the finish heading. The angular difference between these two lines were measured using a protractor. Five such readings were made and their arithmetic mean recorded as the wheel steering 'free-play' angle of that particular wheel for that particular test case.

The radius of each of the wheels were measured using vernier calipers. The wheel displacement caused by backlash, slack and play in the drive transmission system were measured using a similar method to that of wheel steering 'free-play' angle. Here the wheels were individually turned forward and backward by hand, and the angular displacement produced were measured. For each wheel five readings were taken and the mean recorded as the displaced value, which was then converted to linear measure.

The location of the axis of the centre of gravity was identified by supporting the SDMR in the air using a steel rod 4cm in diameter. The location of the rod was varied until balance was obtained and this was taken as the location of the axis of centre of gravity. The position was measured with respect to wheel 1 using a steel tape. Locating the centre of gravity by this method was estimated to be accurate to within  $\pm 8\text{mm}$ . It was important to locate the centre of gravity, for it assisted in identifying the effect that weight distribution had on the performance of the SDMR.

The results obtained from the experimental runs for different parameters, whose method of measurements and equipment used for the measurements have been presented here, are now presented in the next chapter.



## CHAPTER 7

### EXPERIMENTAL RESULTS.

The experimental test results presented in this chapter were those obtained using the two versions of the prototype Synchro-Drive Mobile Robot (SDMR). These versions and their control modes were described in the last chapter.

The tests were to assess performance in terms of; position error-lateral error ( $\delta y$ ) and longitudinal error ( $\delta x$ ), precession ( $\beta$ ) which is the displacement of the chassis (or frame) about the z-axis of the centre of mass, and the trajectory (or path) exhibited. With Version 1 SDMR, only one form of experiment was conducted, which was the test in the 'normal operating state' (Form-1). 'Normal operating state' is the SDMR state where there was no deliberate intention to introduce any form of mechanical systems error. With Version 2, there were six categories of test conducted, namely;

- (A) Test with the SDMR in the normal operating state (Form-1).
- (B) Test in which the SDMR wheels bears uneven load (Form-2).
- (C) Test in which one of the wheels was misaligned (Form-2).
- (D) Test in which two of the wheels were misaligned inwardly toward the centre of mass (Form-2).
- (E) Test in which two of the wheels were misaligned outwardly from the centre of mass (Form-2).
- (F) Test in which one wheel radius was smaller (Form-2).

Test results presented are those obtained during the execution of straight line path. Preliminary tests conducted for bent paths comprising of straight lines and curved paths showed that the control system implemented had significant influence on its performance. Since this work is mainly interested in the mechanical systems error, there were no detailed tests conducted where the SDMR was deliberately executing bent paths. For straight line paths under the above mentioned test categories, both measured and calculated data are presented. Also given is the information produced from statistical analysis of the results.

The straight line path specified was between 4m and 5m in length. Complete tests involved repeated runs, forward and backward over the specified path. The SDMR has two different ways of reversing direction - one is to steer the wheels through  $180^\circ$  and the other is to reverse the direction of the drive motor current by polarity reversal. The latter method was used in order to minimize the effect of imprecise steering position control and to concentrate on detecting the effect of errors in the mechanical system.

The different SDMR postures symbols are explained in table 7.1 (their sketches are embodied in the plots of their respective trajectories given later);

Table 7.1: Definition of SDMR postures.

<u>Posture</u>	<u>Description</u>
1r	In this posture the wheel numbered 1 was in front with the three wheels forming a tricycle arrangement, and the drive gears were on the right hand side of the wheels with respect to the forward direction of travel.
1l	This is the same with above, except that the drive gears were on the left hand side of the wheels with respect to the forward direction of travel.
2r & 3r	The explanation for 1r stands, except that for 2r wheel numbered 2 was leading, and for 3r wheel 3 was leading.
13s	In this posture wheels 1 and 3 were on one side of the SDMR centre of mass with the x-axis of the two wheels' contact point coordinate systems coinciding. Here wheel 1 was leading wheel 3 in the forward direction of travel, with wheel 2 on other side of the centre of mass and located mid-way between wheel 1 and wheel 3.
21s	This posture is similar to 13s, except that here wheel 2 was leading wheel 1 in the forward direction of travel.
32s	Similar to above with wheel 3 leading wheel 2.
1rp	This posture was the same with 1r, except that here attempts were made to eliminate the slack in the transmission chains.

Notes for table 7.1:

(i) In some there are extension name, which defines the category the test results belong. Any recorded result with

extension name is for the SDMR Version 2. The meaning of these extension names are given below;

- e: This indicates that the posture and the test results are for SDMR test under normal operating state with evenly balanced load (Category A test).
- u: This indicates that the posture and the test results are for the SDMR operating in a state where the load is unevenly distributed on the wheels (Category B test).
- mone: This indicates that the posture and the test results were for the SDMR operating in a state where one wheel was misaligned (Category C test).
- min: The SDMR posture and the test results were for the SDMR operating in a state where two of the wheels were misaligned inwardly towards the centre of mass (Category D test).
- mout: The SDMR posture and the test results were for the SDMR operating in a state where two of the wheels were misaligned outwardly from the centre of mass (Category E test).
- rad: The SDMR posture and the test results were for the SDMR operating in a state where one wheel had a smaller radius (Category F test).

It should also be borne in mind that the changes to the state of the SDMR, namely uneven load, one wheel misaligned, etc. were implemented independently. The one change at a time was necessary for verification of the impact of each variable on the performance of the SDMR.

- (ii) In the schematic diagrams of the SDMR posture embodied

in the trajectory plots, the wheel numbers are given and the drive gear position are represented. /// symbol indicates that the drive gear on the wheels was on the right side for forward travel direction, while \\ indicates that it was on the left.

#### 7.1 TEST RESULTS WITH VERSION 1 SDMR.

The essence of the test conducted here when studied in conjunction with the results of that of Version 2 will aid in;

- identifying factors that influence performance,
- identifying the characteristics of the SDMR
- identifying the nature and relationships between error sources.

The SDMR was commanded to travel forward 5m and backward 5m. Five test runs for each direction of travel were measured and recorded. These runs were for different SDMR posture (i.e. different wheel heading relative to chassis orientation). The test runs were performed at a drive speed of 40cm/s. This speed was used mainly because that was the highest speed the electronic power drive unit could allow on the Version 1 SDMR.

The data recorded was that which described the SDMR trajectory, that is the x-y start point, intermediate x-y readings at x = 1.5m, 3m and 4.5m, and the SDMR x-y finish point. Also recorded was the precession angle ( $\beta$ ).

The plot of the trajectories which the measurements of the experimental test runs gave are shown in Figs. 7.1 to 7.9. The

plots show that the SDMR drift direction changes as the direction of travel changes and also as the SDMR posture changes. Fig. 7.10 shows how the drift occurring with the trajectories can be classified. It was evident from the plots that the error magnitude varies as the posture varies. With wheel 2 leading the errors were greater than when wheel 1 was leading, while least errors occurred in posture 3r. It was observed, and as the plots in the Figs. 7.1 to 7.9 shows; that although the SDMR in executing its paths drifts, the magnitude of the errors which arose and their trajectories for a given SDMR posture and runs were highly consistent and repeatable.

Fig. 7.1 Posture 1r: Forward and backward trajectories.

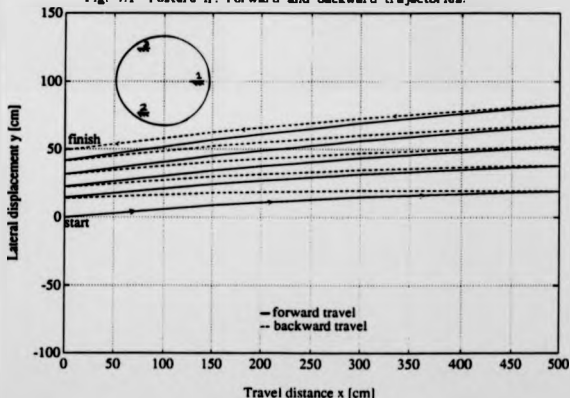


Fig. 7.2 Posture II: Forward and backward trajectories.

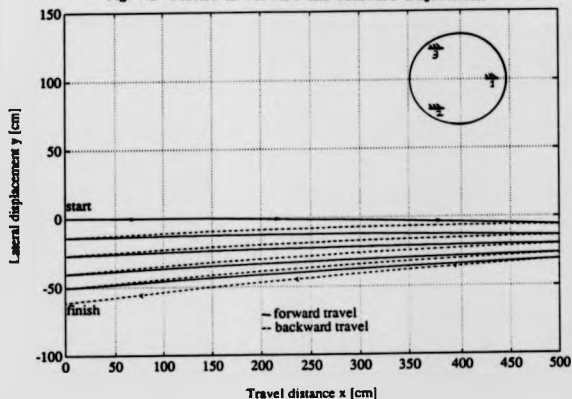


Fig. 7.3 Posture 2r: Forward and backward trajectories.

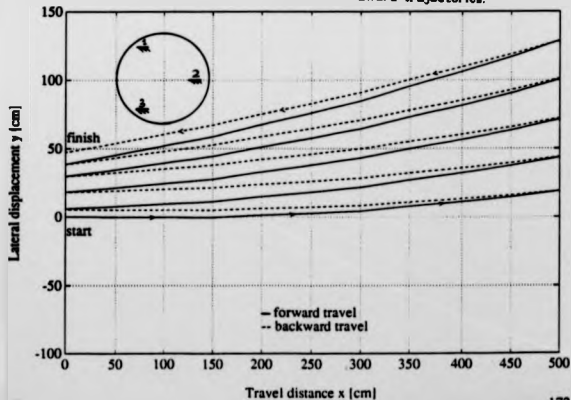


Fig. 7.4 Posture 3r: Forward and backward trajectories.

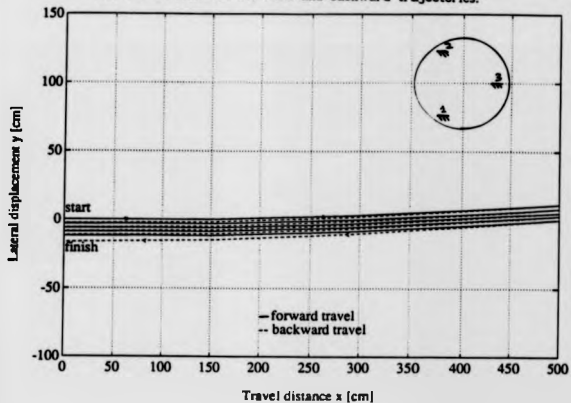


Fig. 7.5 Posture 3l: Forward and backward trajectories.

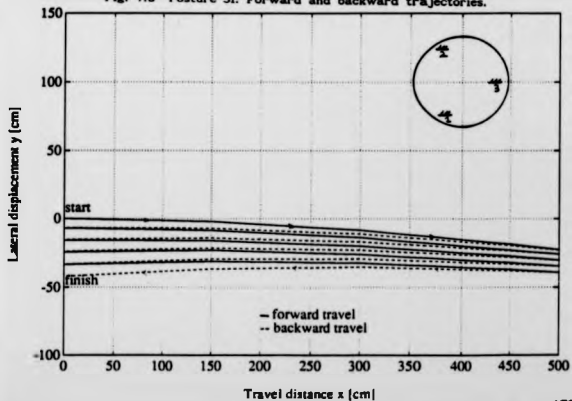




Fig. 7.6 Posture 13s: Forward and backward trajectories.

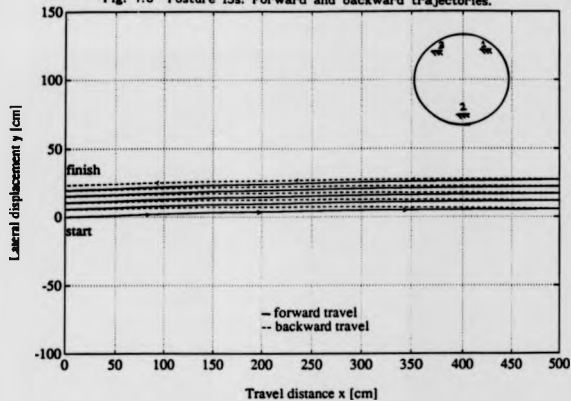


Fig. 7.7 Posture 21s: Forward and backward trajectories.

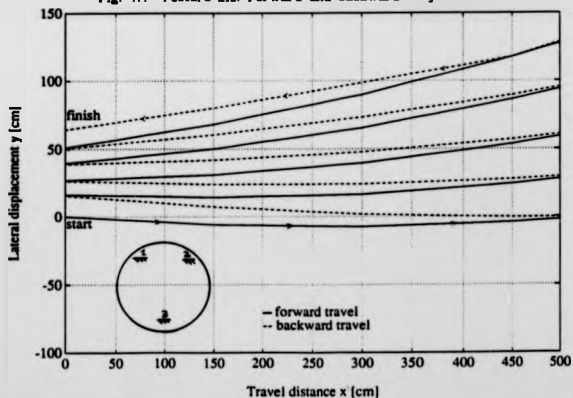


Fig. 7.8 Posture 32s: Forward and backward trajectories.

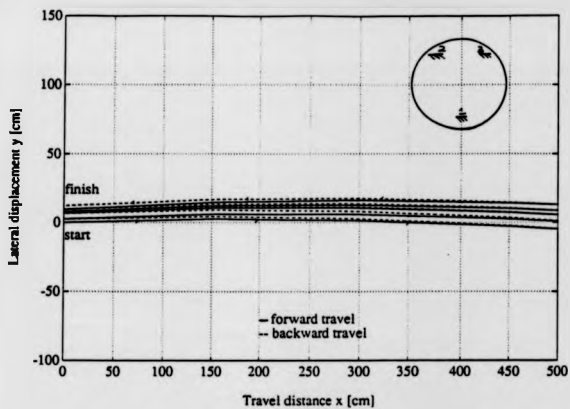
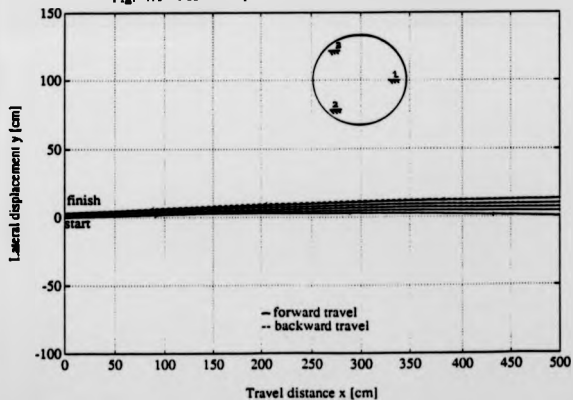


Fig. 7.9 Posture 1rp: Forward and backward trajectories.



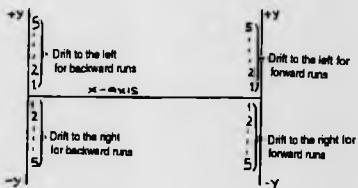
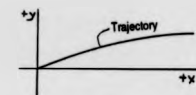


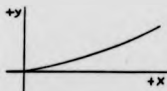
Fig. 7.10 Classification of trajectory drifts.



(a) Positive concave



(b) Negative concave



(c) Positive convex



(d) Negative convex

Fig. 7.11 Possible SDMR trajectory shapes.

The trajectories which the SDMR exhibited under different postures were that of a curved path. Measurement of the radius of curvature at various points showed them to be approximately a circular path. The circular path exhibited by different SDMR postures differed in nature. Their shapes are termed positive concave, negative concave, positive convex, and negative convex (see Figs. 7.11a to 7.11d for identification of the shapes). These results show that a given posture gives a consistent trajectory shape, while the trajectory shape changes with change in posture. The measurement of the 'free-play' angle,  $\sigma$  on each wheel also changes as the posture changes.

The magnitude of the position error, drift direction and trajectory shape is seen to differ for different SDMR posture (Figs. 7.1 to 7.8). Since the SDMR traveled on a circular arc it was necessary to determine the arc radius for the following reasons; to know whether it was constant for a given SDMR posture, and to know the sort of relationship which arc radius has with other measurable performance variables - precession, lateral error and longitudinal error.

Due to initial setting uncertainty and the very large value of arc radius, it was necessary for position error caused by the mechanical system and arc radius to be determined by calculation. How the lateral error, longitudinal error and arc radius (R) were determined are given in the next section. The same method was

used for the different categories of test conducted with Version 2 SDMR.

7.1.1 DETERMINATION OF LATERAL ERROR ( $\delta y$ ), LONGITUDINAL ERROR ( $\delta x$ ), AND ARC RADIUS (R). (R).

Using the Mathematica software package for solving mathematical problems, the data collected from the experimental tests were fitted to the equation of a second-degree curve expressed as;

$$y = a + bx + cx^2 \quad (7.1)$$

Differentiating the equation with respect to x yields;

$$dy/dx = b + 2cx \quad (7.2)$$

From the equation the slope of the tangent to the trajectory curve at the start point was determined. If there were no position errors when the paths were executed, the tangents would represent the trajectories of the SDMR, since the demand was for the SDMR to translate in a straight line.

The trajectory slope at the start point where  $x = 0$  is given by the parameter  $b$  in equation (7.2). The value of  $b$  is in radians. Having determined the trajectory slope, the lateral error, longitudinal error and arc radius were then determined using the observed data and the slope calculated. Their relationship is explained with the help of Fig. 7.12.

From Fig. 7.12, point P represents the required stopping position when the initial setting uncertainty is considered. P' represents the actual position where the SDMR stops. Distance OB = x, represents the fixed coordinate frame distance from which the



position measurements recorded were taken. The y-axis finish point measurement taken is represented by BP'. From the illustration the mechanical systems error contribution can be approximately given as;

$$\text{Lateral error } (\delta y) = BP' - BB' \quad (7.3)$$

$$\text{Longitudinal error } (\delta x) = OP - OB' \quad (7.4)$$

where,

BP': data collected from test,

BB': equal to  $OB * b$ , OB data collected and b the calculated slope,

OP: the specified travel distance,

OB': given as,  $OB/\cos(\arctan b)$ .

Arc radius (R) = CP'. CP' is determined from;

$$\begin{aligned} (CP')^2 &= (AC)^2 + (AP')^2 \\ &= (R - a)^2 + (x')^2 \\ CP' &= \left( a^2 + (x')^2 \right)^{1/2} / 2a \end{aligned} \quad (7.5)$$

The sign of the lateral error was determined based on the shape of the trajectory and the way the fixed coordinate system was considered for the forward and backward travel. For forward journeys the fixed coordinate system where the measurements were taken was considered as shown in Fig. 7.13a. That of backward journeys is given in Fig. 7.13b.

The values determined from SDMR Version 1 test results using the above method of calculation were used to conduct statistical analysis.

### 7.1.2 STATISTICAL ANALYSIS.

A model for the performance criteria was sought to relate - precession ( $\beta$ ), lateral error ( $\delta y$ ), longitudinal error ( $\delta x$ ) and arc radius ( $R$ ) were sort. The intention was to evaluate their relationship and investigate the ability to predict one knowing the others. The relationship was sought using correlation based on the Pearson product moment and regression process [Guttman'71]. Also, if prediction is possible, the aim was to find the model which gives the best prediction.

In conducting the analysis certain assumptions were made. The assumptions include:

- ▷ Though the errors in positioning the SDMR originate from different sources, the effect each of them creates is considered as originating from small variations in the geometric parameters of the SDMR mechanical system.

- ▷ Errors such as those of slack and backlash are deterministic in nature, but because of the difficulties in measuring them, their cumulative effect when added to those of other sources can be treated as a random variation in the SDMR geometrical parameters [Kumar'83]. Such variations can be assumed to be normally distributed.

In conducting the regression analysis the mean value of the calculated results for each SDMR posture was used. Using mean results the intention was to reflect an overall performance rating of different postures. It also helped to avoid undue bias that the results might contain.



Table 7.2: Mean values for precession, lateral error, longitudinal error and arc radius for the forward journeys in different postures for Version 1 SDMR.

SDMR Postures						
	1f	1l	2r	3r	3l	3a
Precession (p)	-3.10	-6.00	10.00	-0.20	-2.00	3.40
Lateral error (dy)	15.16	-6.96	30.36	16.90	-21.56	8.42
Longit. error (dx)	2.07	0.27	1.16	0.03	0.09	0.23
Arc radius (R)	83.41	-181.75	41.59	74.25	-58.43	149.25

Table 7.3: Mean values for precession, lateral error, longitudinal error and arc radius for the backward journeys in different postures for Version 1 SDMR.

SDMR Postures						
	1f	1l	2r	3r	3l	3a
Precession (p)	3.00	6.30	-9.20	-0.20	2.30	-3.20
Lateral error (dy)	-14.38	-9.18	-22.26	-13.16	19.94	-5.94
Longit. error (dx)	0.15	-0.17	5.12	0.77	0.75	0.01
Arc radius (R)	-88.14	-137.02	-57.52	-95.94	63.11	-211.95

Note: p in [degrees], dy and dx in [cm], and R in [a].

The correlation, analysis of variance and the regression equation models were determined using MINITAB Statistical software package. From individual posture results, tables 7.2 and 7.3 above were obtained making use of mean values of the performance variables. In the forward direction of travel, the correlation between the variables were determined as;

Correlation:

	Precession ( $\beta$ )	Lateral error ( $\delta y$ )	Long. error ( $\delta x$ )
Lateral error	0.62		
Long. error	0.16	0.45	
Arc radius (R)	0.37	0.61	0.26

For the backward journey the correlation between the variables were,

	Precession ( $\beta$ )	Lateral error ( $\delta y$ )	Long. error ( $\delta x$ )
Lateral error	0.48		
Long. error	-0.74	-0.46	
Arc radius (R)	0.10	0.68	0.15

Different forms of regression analysis were performed to determine the model that gives the best prediction based on the relationship between the variables. They were linear regression based on one input variable which was taken as the precession, and linear regression based on two input variables taken as the precession and arc radius. The third one was that of a quadratic polynomial also using precession and arc radius as input. Precession and arc radius were used as input variables because it is their existence which gives rise to position error.

From the analysis, the model that most closely relates the lateral error ( $\delta y$ ) and precession ( $\beta$ ) or/and arc radius (R) was;

$$\delta y = 6.0 + 0.1\beta + 0.1R + 0.06\beta^2 \quad (7.6)$$

The R-sq value (which represents the variation in lateral error represented in the equation) of equation (7.6) was about 57%. This implies that through the statistical relationship that exists between lateral error and precession or/and arc radius 43% of the variation could not be explained.

For longitudinal error and precession, and longitudinal error and arc radius, no significant relationship between these variables is evident. But a correlation coefficient of 0.449 tends to indicate a link between longitudinal error and lateral error.

From the correlation coefficient of arc radius and precession, which was 0.367, it cannot be said with any certainty that there was a significant relationship between the two variables. The regression evaluation gave no room for any conclusion as regards the relationship between the two variables. The best model for the regression was;

$$R = 57.2 + 19.9\beta - 1.24 \beta^2 \quad (7.7)$$

Equation (7.7) explains about 54% of the variation in R. Regression analysis revealed that the best model for predicting lateral error during return journeys was;

$$\delta y = 3.44 + 0.91\beta + 0.11R$$

(7.8)

The equations' R-sq was about 63%

There appears to be no trace of a linear relationship between arc radius and precession in the backward journey. This is based on the analysis which gave a correlation coefficient of 0.1 and explained variation of only 1%.

## 7.2 TEST RESULTS WITH VERSION 2 SDMR.

As was mentioned and listed earlier in this chapter, with Version 2 SDMR (the prototype having a design-error compensation mechanism) there were six main categories of test conducted. The outcome of those tests will be presented in this section. The tests with Version 2 SDMR reported here were those conducted at a drive speed of 40cm/s. The speed was chosen in order to be directly comparable with the Version 1 SDMR (prototype without design-error compensation mechanism).

The test runs for categories A and B covered the 5m test distance and the same five runs as with Version 1. With increase in the position error for other test categories, lack of space within the test area, and the consistency and repeatability in the trajectories, the tests were reduced to three runs with a test distance of 4m. The data recorded includes those at intervals of 1m.

#### 7.2.1 TEST RESULTS WITH THE SDMR OPERATING IN THE NORMAL STATE

##### (CATEGORY A).

Conducting tests in this category enables one to investigate the performance of the design and the prototype. It also identifies the likely source and cause of error that one witnesses. The result obtained from this category may then be compared with that of Version 1 and other test categories in order to know what factors are consistent irrespective of state, size and design modification, and those that are not.

The plots of the trajectories based on the readings for different SDMR posture are given in Figs. 7.14 to 7.25. The plot shows that during most of the journeys for the different postures the trajectories for both forward and backward journey cross each other. Fig. 7.15 shows that the tendency for crossing was present but did not happen before the SDMR reached its commanded travel distance. Another observation (see Figs. 7.16 to 7.21) was that the trajectories of the SDMR's forward and backward travels with the wheel drive gear on the left hand side of the wheel can be considered to be the reverse of that with wheel drive gear on the right side of the wheel.

The observations made in the paragraphs above have lead to two important conclusions which are;

- ▷ the effect of errors within the SDMR mechanism tends to reverse as when drive gear position reverses.
- ▷ the SDMR trajectories and position error for a given postures showed consistency and repeatability.

Fig. 7.14 Posture 1r-e: Forward and backward trajectories.

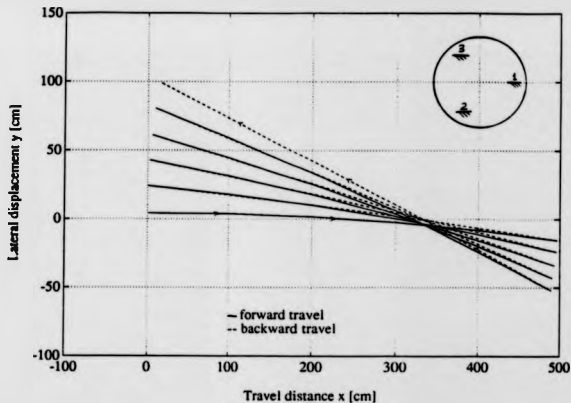


Fig. 7.15 Posture 1l-e: Forward and backward trajectories.

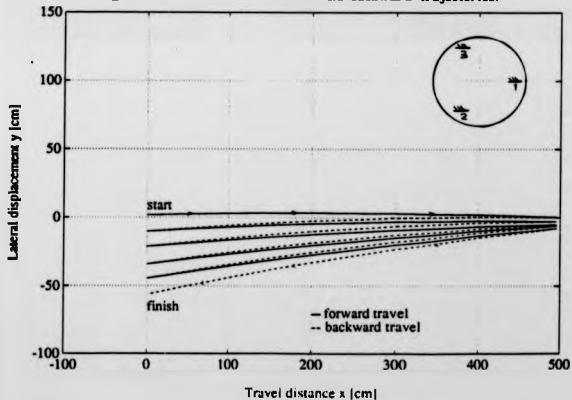


Fig. 7.16 Posture 2r-e: Forward and backward trajectories.

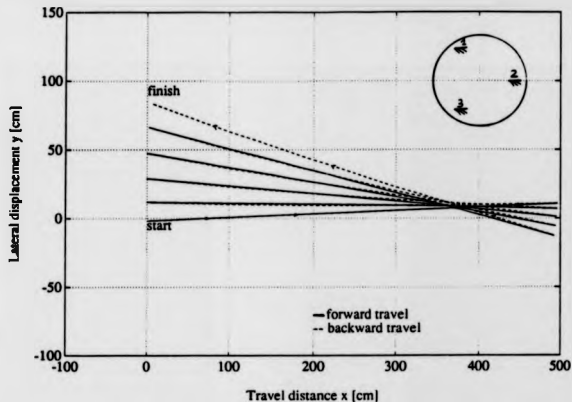


Fig. 7.17 Posture 2l-e: Forward and backward trajectories.

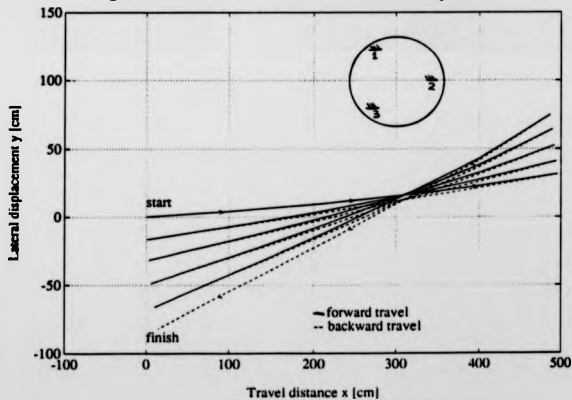


Fig. 7.18 Posture 3r-e: Forward and backward trajectories.

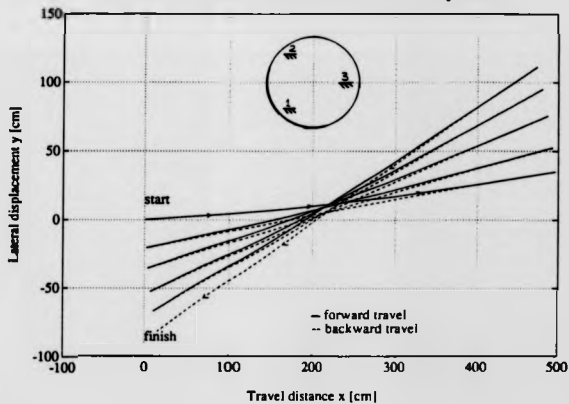


Fig. 7.19 Posture 3l-e: Forward and backward trajectories.

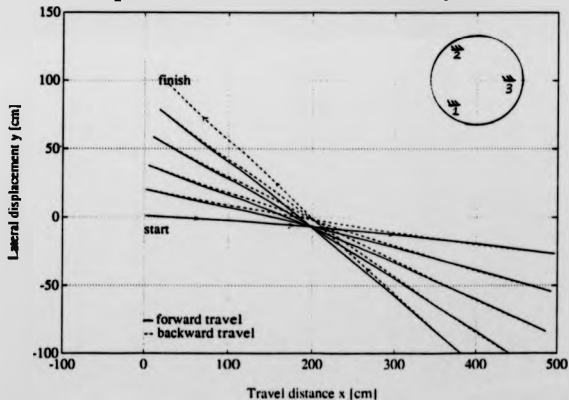




Fig. 7.20 Posture 13a-e: Forward and backward trajectories.

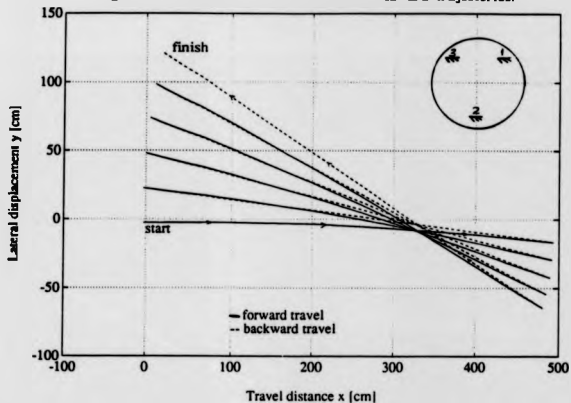


Fig. 7.21 Posture 13a-e: Forward and backward trajectories.

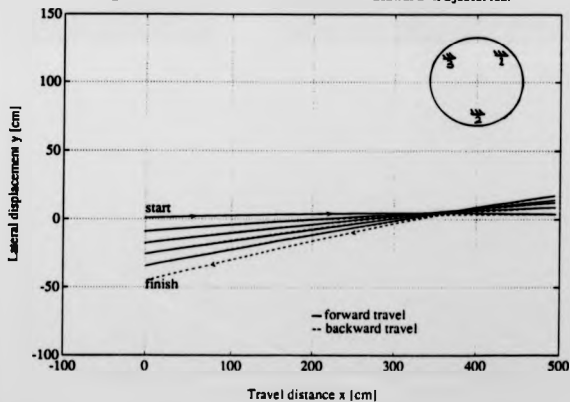


Fig. 7.22 Posture 2lsr-e: Forward and backward trajectories.

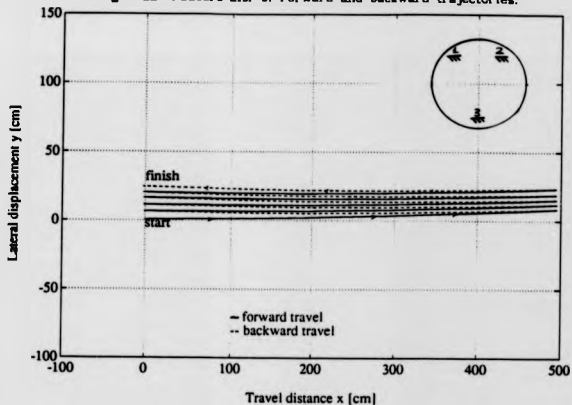


Fig. 7.23 Posture 2lsi-e: Forward and backward trajectories.

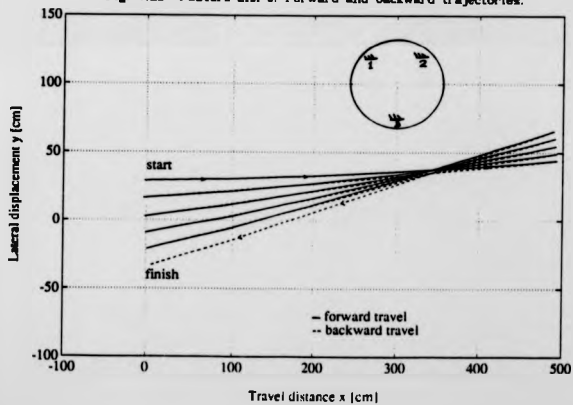


Fig. 7.24 Posture 32sr-e: Forward and backward trajectories.

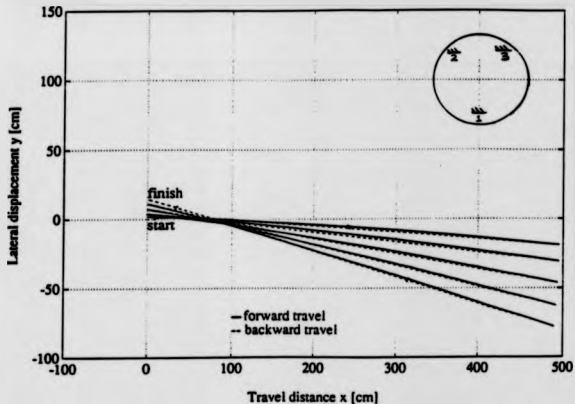
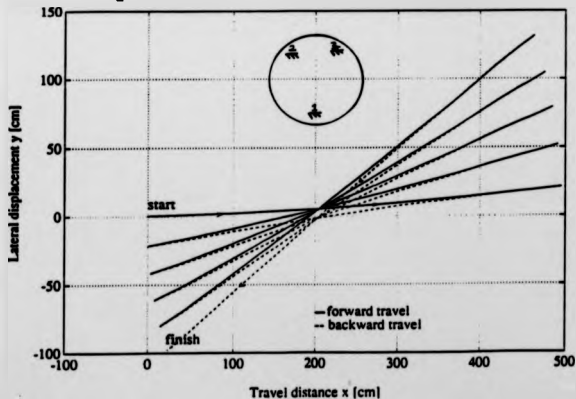


Fig. 7.25 Posture 32sl-e: Forward and backward trajectories.



#### 7.2.1.1 STATISTICAL ANALYSIS.

It can be seen from studying the raw data that no clear relationship is evident. For this reason further statistical analysis became necessary in order to draw any significant conclusion from the results. Hence analysis performed in section 7.1.2 is repeated here.

The SDMR postures and their respective precession ( $\beta$ ), lateral error ( $\delta y$ ), longitudinal error ( $\delta x$ ) and arc radius (R) are given in tables 7.4 and 7.5. Using the data in the tables, correlation between the variables were determined. For the forward travel, the correlation coefficients were;

	Precession ( $\beta$ )	Lateral error ( $\delta y$ )	Long. error ( $\delta x$ )
Lateral error	0.82		
Long. error	0.41	0.43	
Arc radius (R)	0.54	0.74	0.32

For the backward travels, the correlation coefficients were;

	Precession ( $\beta$ )	Lateral error ( $\delta y$ )	Long. error ( $\delta x$ )
Lateral error	0.29		
Long. error	-0.05	0.35	
Arc radius (R)	0.28	0.60	0.32

For the forward journey, the correlation coefficients indicates that there is strong linear association between precession and lateral error, and between arc radius and lateral error. The results are similar to that obtained with the Version 1 SDMR.

In the backward travel most of the significant linear association were lost except in the case of arc radius and lateral error. It can be inferred from the significance of the correlation that generally arc radius may be used as a useful basis for dealing with the position error in both forward and backward travels.

Regression analysis of the data in table 7.4 produced the equations given below as the most likely ones that can be used to predict lateral error and long. error, where the precession is known and the arc radius can be determined;

$$\delta y = 3.35 + 1.48\beta + 0.05R \quad (7.9)$$

$$\delta x = -4.88 - 0.30\beta - 0.04\beta^2 \quad (7.10)$$

Predicting arc radius from precession, the model with the highest statistical significance was;

$$R = 76.8 + 18.6\beta + 0.64\beta^2 \quad (7.11)$$

Equations (7.9) to (7.11) represent prediction models for forward travel. Equation (7.9) could explain up to about 80% of the variation in lateral error. For the longitudinal error it is the precession that had most influence, though it was not a linear relationship (equation 7.10). The non-linear relationship could explain only about 53% of the variation in longitudinal error. Equation (7.11) which shows that the best model for predicting arc radius from precession is a non-linear one, and could only explained 30% of the variation in arc radius.

Table 7-4: Mean values for precision, lateral error, longitudinal error and arc radius for the forward journey in different postures for Version 2 (HM in its Feet-1 test).

	SMM Postures									
	1r	1l	2r-g	2l-g	3r-g	3l-g	130r-g	130l-g	210r-g	210l-g
Precision (B)	-11.00	-9.00	-2.20	-4.00	1.50	-14.20	-9.00	-3.20	2.00	1.40
Lateral error (dr)	-24.54	9.19	-4.94	13.14	-1.54	-13.94	-13.94	-13.94	6.21	14.99
Longit. error (ds)	-5.54	-5.54	-2.07	-3.00	-5.11	-4.34	-5.11	-5.11	-4.09	-4.10
Arc radius (B)	-49.00	124.11	-102.00	103.54	102.51	-76.00	-61.20	62.04	100.00	113.41

Note: B is in (degrees), dr and ds in (cm), and B is in (s).

Table 7-5: Mean values for precision, lateral error, longitudinal error and arc radius for the backward journey in different postures for Version 2 (SMM in its Feet-1 test).

	SMM Postures									
	1r	1l	2r-g	2l-g	3r-g	3l-g	130r-g	130l-g	210r-g	210l-g
Precision (B)	0.00	7.20	0.00	4.40	3.50	9.20	7.90	4.00	-2.10	6.70
Lateral error (dr)	8.93	-15.32	10.23	9.09	-10.00	21.29	6.32	-15.65	-7.41	2.54
Longit. error (ds)	-0.44	-4.43	-4.62	-0.22	-7.99	-9.87	-4.10	-4.90	-3.45	-3.79
Arc radius (B)	-99.00	124.11	-102.00	103.54	102.51	-76.00	-61.20	62.04	100.00	113.41

Note: B is in (degrees), dr and ds in (cm), and B is in (s).

The prediction models for the backward travels are given as;  
for lateral error,

$$\delta y = 10.9 - 6.23\beta + 0.13R + 0.63\beta^2 \quad (7.12)$$

for longitudinal error,

$$\delta x = -4.43 - 0.67\beta + 0.01R + 0.06\beta^2 \quad (7.13)$$

for the arc radius,

$$R = -4.5 + 6.9\beta + 0.37\beta^2 \quad (7.14)$$

Equations (7.13) and (7.14) are statistically not significant as they could only explain about 20% and 8% of the variations in longitudinal error and arc radius. Equation (7.12) however was able to explain 78% of the variations in the lateral error that was occurring, with the arc radius playing a more prominent role.

For both forward and backward journey the statistical analysis conducted tends to show links between lateral error and precession or/and arc radius. Such links were evident with the Version 1 SDMR. However with Version 2, the model gave a better prediction based on the percentage of the variation which the equations were able to explain.

#### 7.2.2 TEST RESULTS IN WHICH THE SDMR WHEELS BARES UNEVEN LOAD (CATEGORY B).

This test was conducted in order to identify the influence of weight distribution to the overall performance and which aspect of the performance criteria was worst affected.

The location of the new centre of mass due to unbalanced wheel

loads is shown in Fig. 7.26. Load on wheel 1 was greater than that of wheel 3, with wheel 2 bearing the greatest load, at a ratio of about 16:14:20.

The plots of the trajectories from the results of the test are given in Figs. 7.27 to 7.38. When trajectory shapes which this test category exhibits during forward and backward travels are compared against those obtained in category A test (see Figs. 7.14 to 7.25), they were found to be similar in almost every aspect. There were marginal changes in the value of the position error. In some cases the errors in test category A were smaller than in test category B. In others the reverse was the case. Overall, the lateral error was higher when the load on the wheels was non-uniformly distributed.

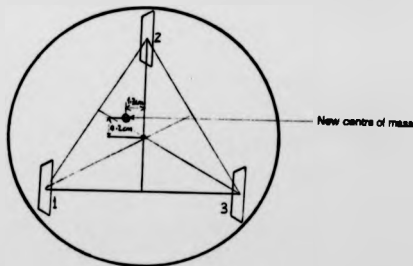


Fig. 7.26 Illustration of the location of the centre of mass.



Fig. 7.27 Posture Ir-u: Forward and backward trajectories.

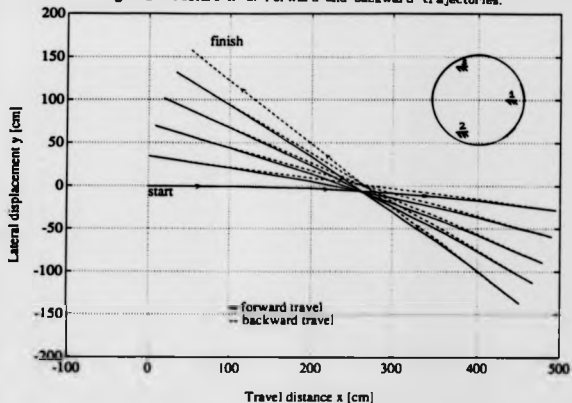


Fig. 7.28 Posture II-u: Forward and backward trajectories.

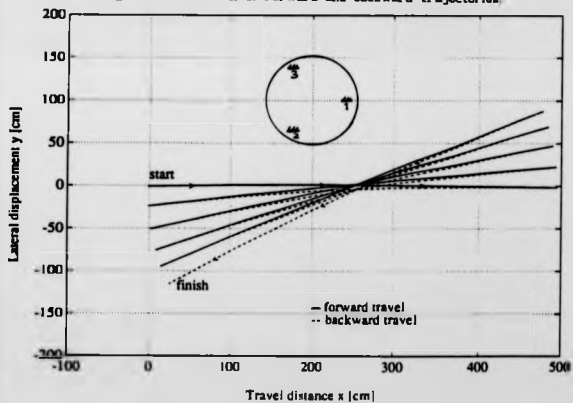


Fig. 7.29 Posture 2r-u: Forward and backward trajectories.

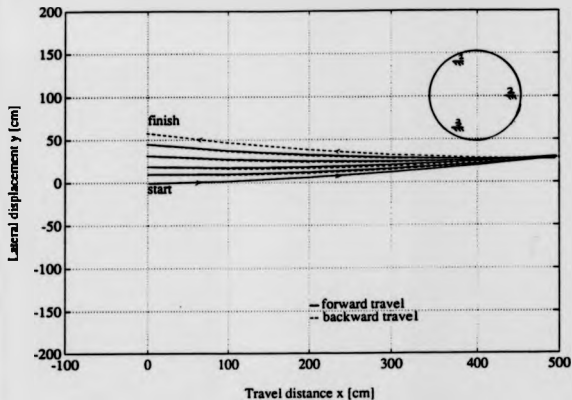


Fig. 7.30 Posture 2l-u: Forward and backward trajectories.

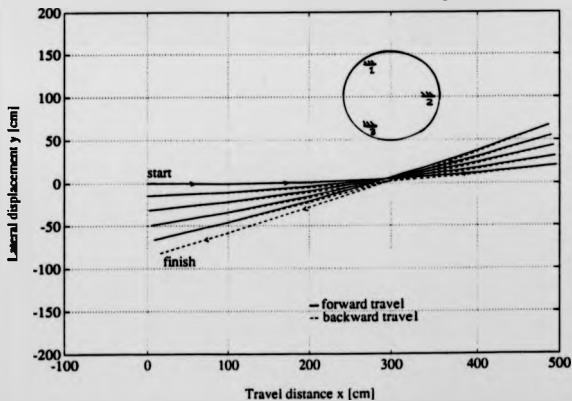


Fig. 7.31 Posture 3r-u: Forward and backward trajectories.

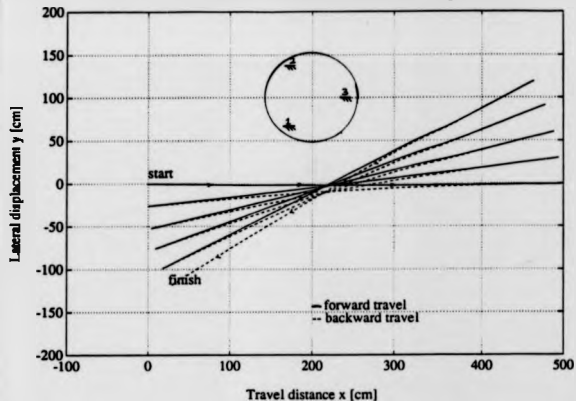


Fig. 7.32 Posture 3l-u: Forward and backward trajectories.

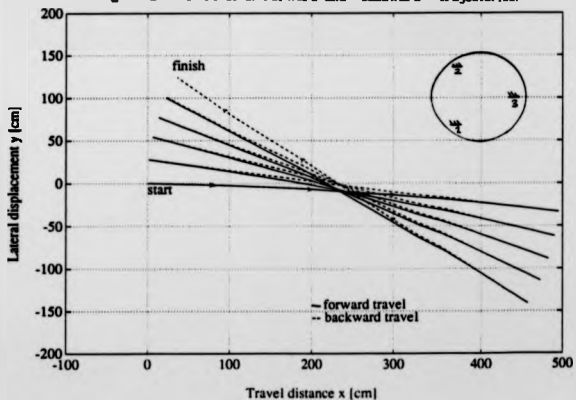


Fig. 7.33 Posture 13er-u: Forward and backward trajectories.

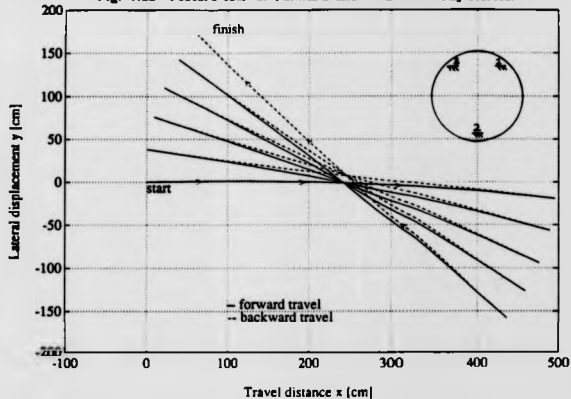


Fig. 7.34 Posture 13el-u: Forward and backward trajectories.

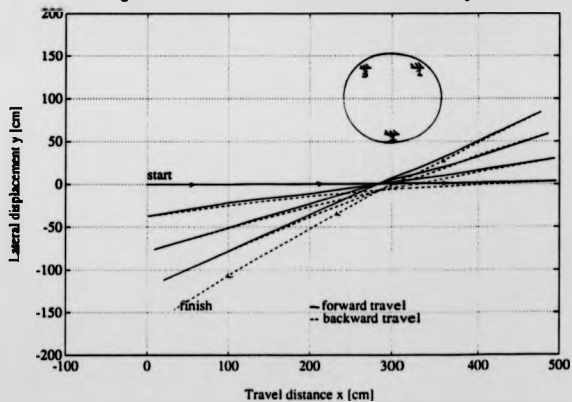


Fig. 7.35 Posture 21sr-u: Forward and backward trajectories.

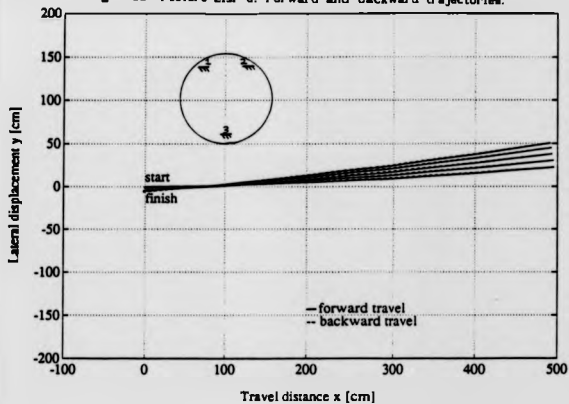


Fig. 7.36 Posture 21sl-u: Forward and backward trajectories.

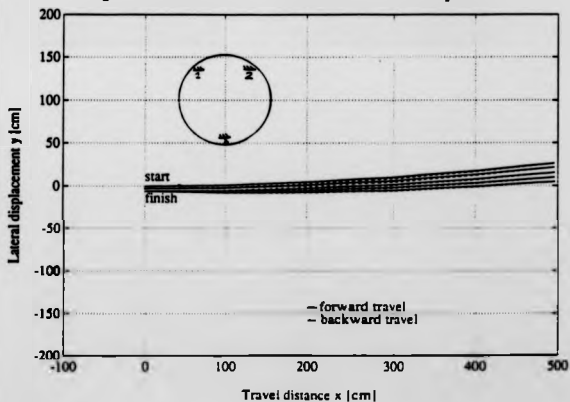


Fig. 7.37 Posture 32sr-u: Forward and backward trajectories.

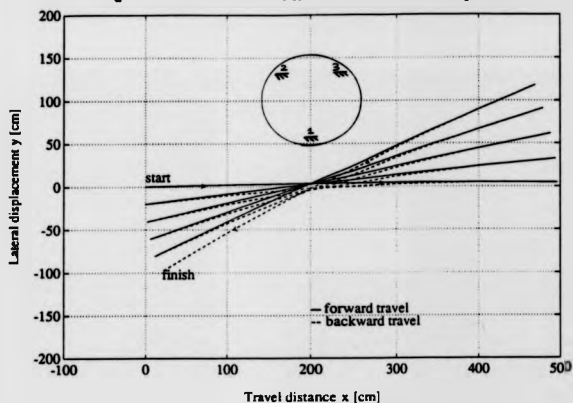
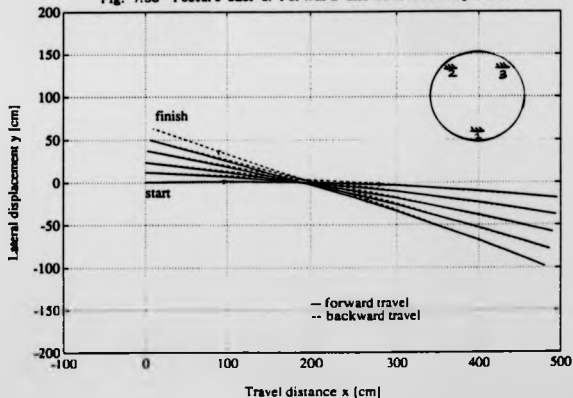


Fig. 7.38 Posture 32sl-u: Forward and backward trajectories.



Statistical analysis revealed that the sort of correlation that existed in test category A also existed in this test category. The main difference observed when this test results were compared with those of category A was an increase in error magnitude.

#### 7.2.3 TEST RESULTS WITH WHEEL NUMBERED 1 MISALIGNED (CATEGORY C)

This test was conducted to investigate the behaviour of the SDMR and the error that misalignment in one of the wheels might cause. Also to determine whether it is possible to identify specifically the contribution made by wheel misalignment to the overall performance. In view of the fact that wheel position and chassis orientation changes independently, such a test exposes the effects that misalignment has when it takes different wheel position with respect to chassis orientation.

In this test wheel numbered 1 was misaligned by  $5^\circ$  and it is illustrated in Fig. 7.39. In this test category and the remaining reported test categories, the test travel distance for each run was reduced to 4m, and three runs per test SDMR posture. The number of SDMR postures tested was reduced to six. The reason being that there were no significant information which the twelve test postures were revealing that six test postures could not reveal.

Plots of the trajectories of the test results are given in Figs 7.40 to 7.45. The trajectory plots revealed that when the wheel that was misaligned was leading the other two wheels, the SDMR trajectories for both posture 1r-mone and 1l-mone had the same

trajectory shape and the drift was of the same class (see Figs 7.40 and 7.41).

When the misaligned wheel was no longer leading the trajectories of the test posture with the wheel drive gear on the left side of the wheel tended to be a reversal of that when the wheel drive gear was on the right (see Figs. 7.42 to 7.45). When the trajectories of these posture were compared with those of the same posture in category A, it was discovered that shape of the trajectories and drifts were the opposite of each other. This indicates that the amount of misalignment introduced has reversed the resultant effect on the interactions within the mechanical system of the SDMR.

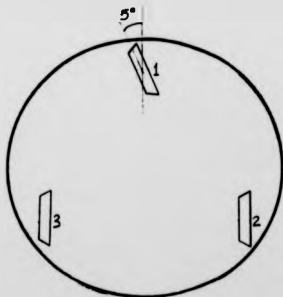


Fig. 7.39 Illustration of wheel 1 misaligned by 5°.



Fig. 7.40 Posture 1r-mone: Forward and backward trajectories.

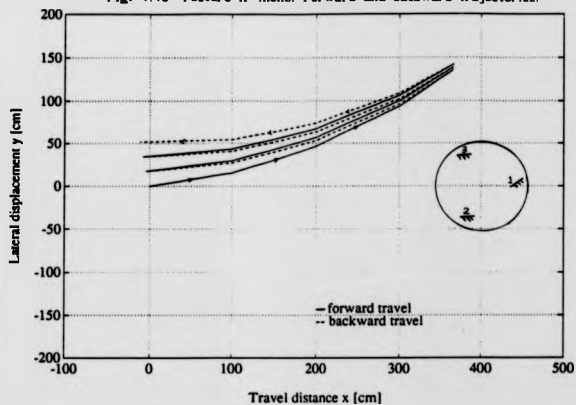


Fig. 7.41 Posture 1l-mone: Forward and backward trajectories.

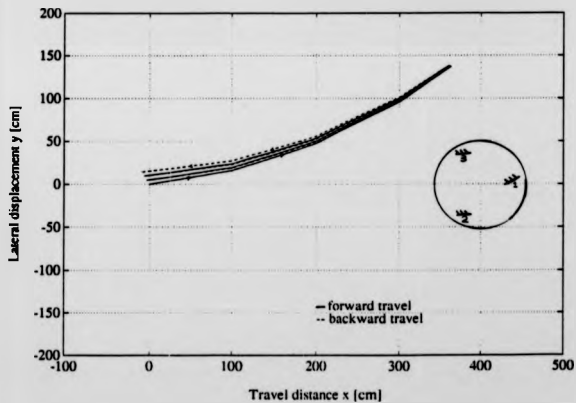


Fig. 7.42 Posture 2r-mone: Forward and backward trajectories.

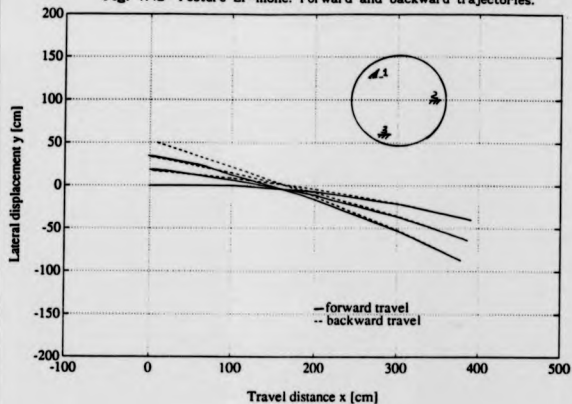


Fig. 7.43 Posture 2l-mone: Forward and backward trajectories.

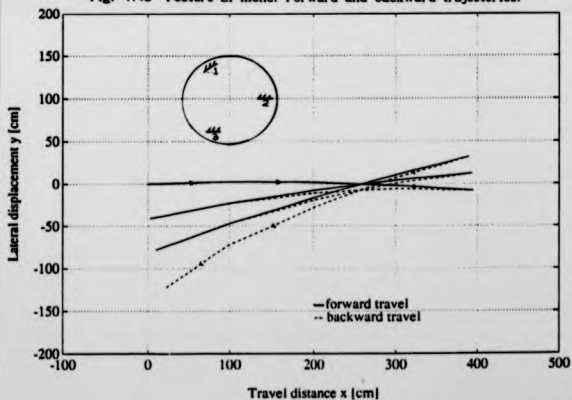


Fig. 7.44 Posture 3r-mone: Forward and backward trajectories.

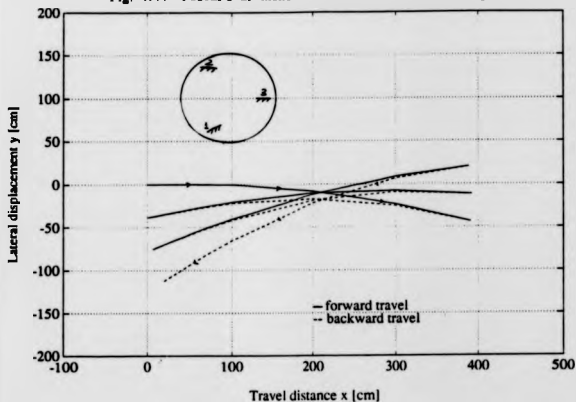
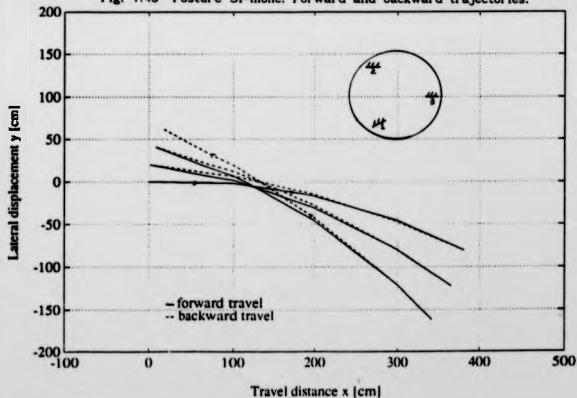


Fig. 7.45 Posture 3l-mone: Forward and backward trajectories.



The precessions recorded were very high, varying from  $+58^{\circ}$  to  $-59^{\circ}$ . The calculated results indicated that in most cases the mean lateral error was high with a value of up to 105.49cm, though small values of as low 8.07cm was obtained. Further analysis showed that there was positive correlation between precession and lateral error, and between arc radius and lateral error. There was no strong correlation between either longitudinal error and precession or arc radius.

#### 7.2.4 TEST RESULTS WITH TWO WHEELS MISALIGNED INWARDLY TOWARDS THE CENTRE OF MASS (CATEGORY D).

This test was conducted with the same objectives as that of category C. This was a case where wheels numbered 1 and 2 were misaligned by  $+4^{\circ}$  and  $-4^{\circ}$ , and it is illustrated in Fig. 7.46. Because all wheels of the SDMR are driven in unison the understanding of the influence that this sort of case will have is deemed necessary.

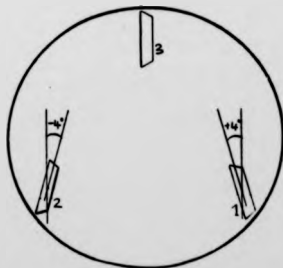


Fig. 7.46 Illustration of wheel 1 and 2 misaligned inwardly by  $+4^{\circ}$  and  $-4^{\circ}$ .

From the test data the trajectories for SDMR forward and backward journey for different posturas were plotted, and they are presented in Figs. 7.47 to 7.52. With the wheel which was not misaligned leading, the trajectories showed the characteristics which dominated that obtained from test category A. For example, posture 3l-min was a reflection of posture 3r-min, the trajectory shape and drift were similar. This was also the case in test category C (see Fig. 7.42 and 7.44). It must be noted that the size of the errors were significantly different as was expected.

The precessions of the SDMR were very high, up to  $-52^\circ$ . The results also revealed that the lateral error were very high, up to 1.5m for a 4m travel. This was however expected and it occurred when one of the misaligned wheels was leading. The precession when none of the misaligned wheels was leading dropped significantly to as low as  $0.5^\circ$ . This very result suggests that in posture 3r-min and 3l-min, the misaligned wheels were driving against each other and hence preventing the chassis from rotating significantly in any particular direction.

In both forward and backward journeys the data produced positive correlation for precession and lateral error. There was no such linear association between any of the following; arc radius and lateral error, precession and long. error, arc radius and long. error, and precession and arc radius.

Fig. 7.47 Posture 1r-min: Forward and backward trajectories.

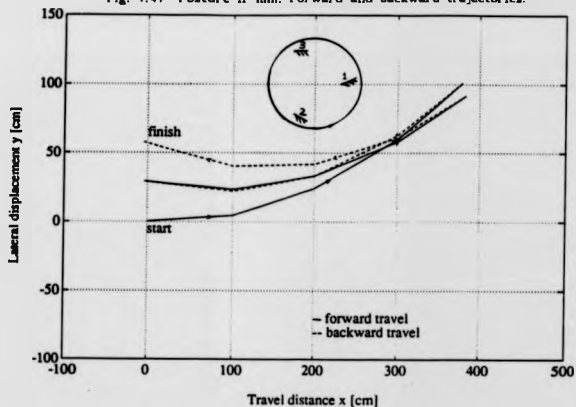


Fig. 7.48 Posture 1l-min: Forward and backward trajectories.

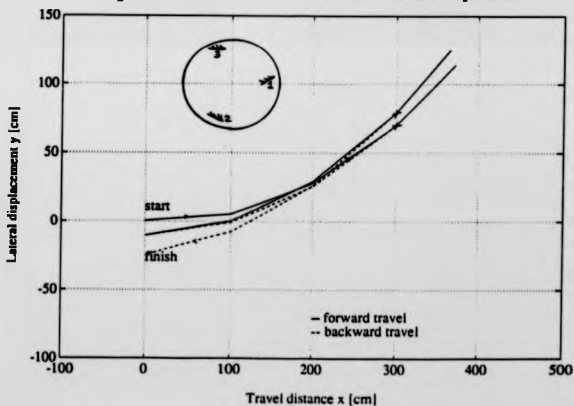


Fig. 7.49 Posture 2r-min: Forward and backward trajectories.

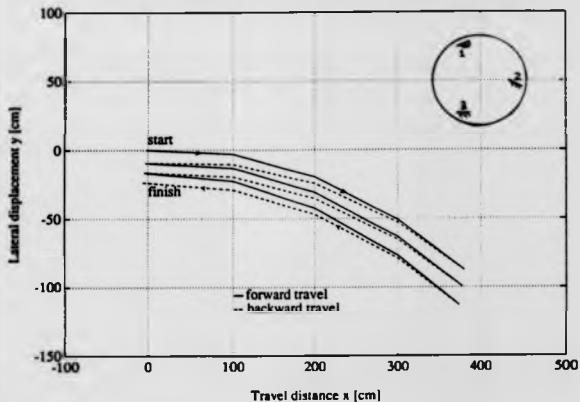


Fig. 7.50 Posture 2l-min: Forward and backward trajectories.

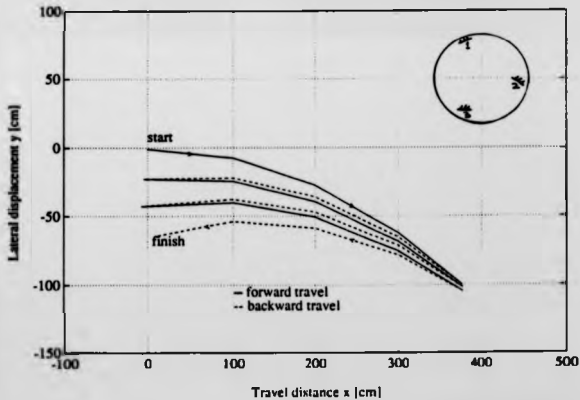


Fig. 7.51 Posture 3r-min: Forward and backward trajectories.

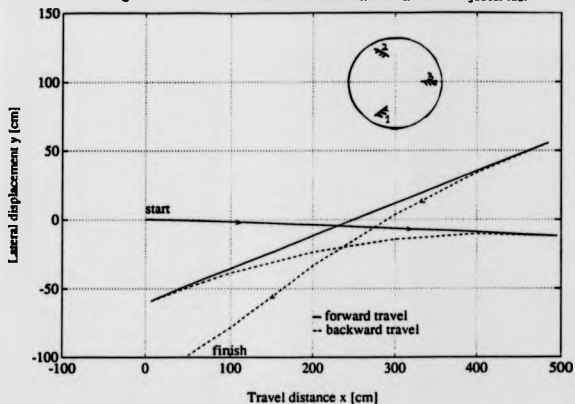
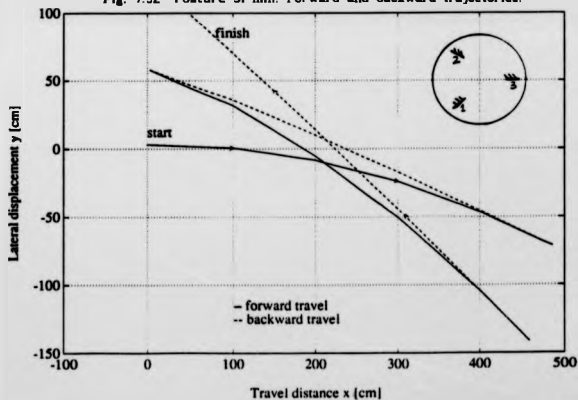


Fig. 7.52 Posture 3l-min: Forward and backward trajectories.





#### 7.2.5 TEST RESULTS WITH TWO WHEELS MISALIGNED OUTWARDLY FROM

##### THE CENTRE OF MASS (CATEGORY E).

This test shares the same objectives with that of category D. Here wheels numbered 1 and 3 were misaligned by  $+4^\circ$  and  $-4^\circ$ , as illustrated in Fig. 7.53.

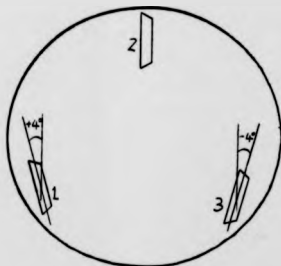


Fig. 7.53 Illustration of wheel 1 and 3 misaligned outwardly by  $+4^\circ$  and  $-4^\circ$ .

From the experimental test data the trajectories were plotted and they are shown in Figs. 7.54 to 7.59. The test results represented in Figs. 7.54 to 7.59 bears all the hallmarks of that obtained in category A. From the test results it was observed that when the wheel which was not misaligned was leading the SDMR precession, lateral error and longitudinal error dropped significantly when compared with those obtained in other postures. The results indicate that the SDMR made serious attempts to drive itself forward in the direction dictated by the

Fig. 7.54 Posture Ii-mout: Forward and backward trajectories.

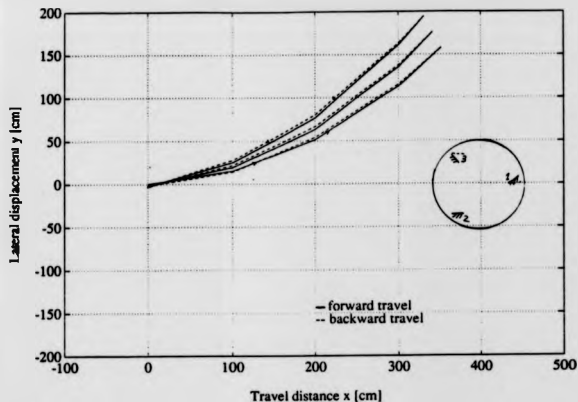


Fig. 7.55 Posture II-mout: Forward and backward trajectories.

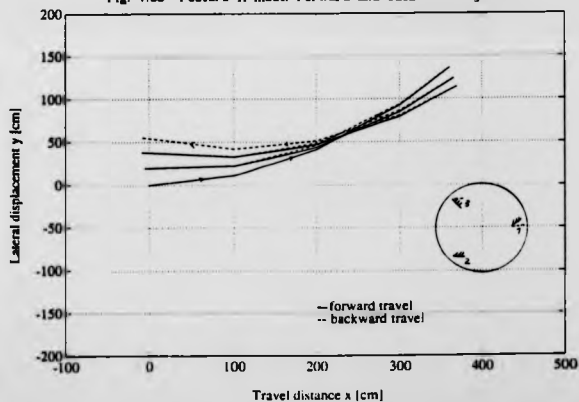


Fig. 7.56 Posture 2r-mout: Forward and backward trajectories.

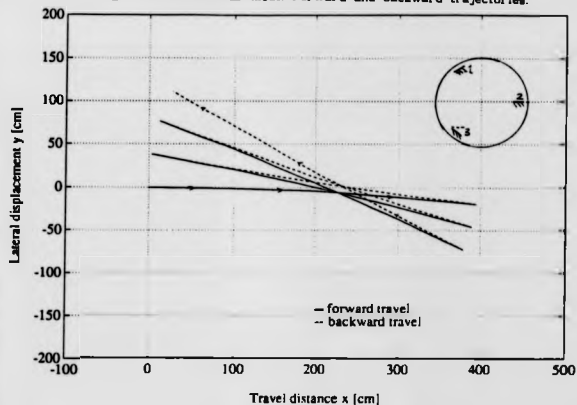


Fig. 7.57 Posture 2l-mout: Forward and backward trajectories.

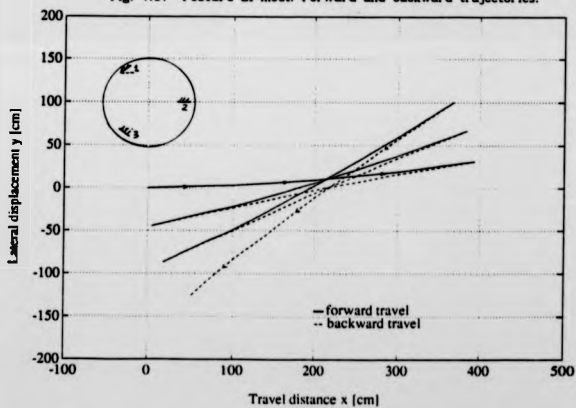


Fig. 7.58 Posture 3r-mout: Forward and backward trajectories.

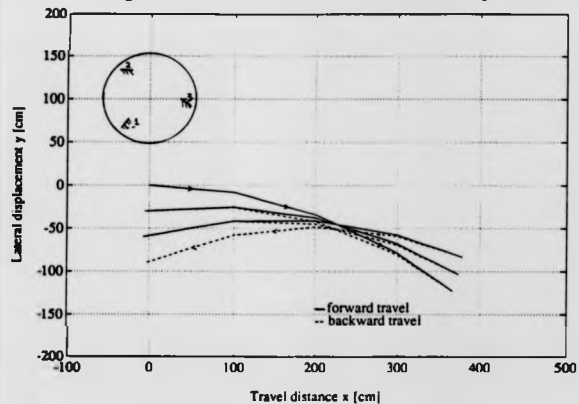
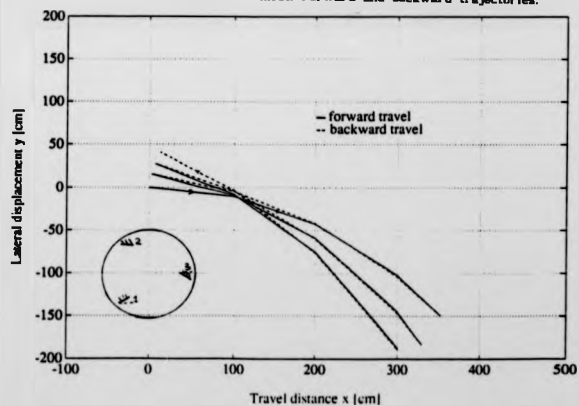


Fig. 7.59 Posture 3l-mout: Forward and backward trajectories.



non-misaligned wheel. This was the case in test category D. The sort of correlation that existed in test category D also existed in this test category.

7.2.6 TEST RESULTS WITH ONE WHEEL HAVING A SMALLER RADIUS  
(CATEGORY F).

This test category was undertaken to investigate the influence which different wheel radii have on the behaviour of the SDMR and whether from the test one can identify any distinct contribution such error source made. Here wheel number 1 had a radius of 9cm with the other two having an approximate radii of 10cm.

From the test results the trajectories were plotted and are presented in Figs. 7.60 and 7.65. The trajectories were similar to those in category A. The drift directions and the trajectories in many cases were similar. The trajectory reflectivity characteristics were evident. The position error-lateral error and longitudinal error, and precession were very much greater than those obtained in category A.

Statistical analysis indicated that there exists a strong positive relationship between precession and lateral error. The correlations obtained here were similar to those obtained in category A.

The results obtained in this test category were in line with those of two wheels misaligned. The significant increase in the magnitude of errors can be attributed to a continuous state of

Fig. 7.60 Posture Ir-rad: Forward and backward trajectories.

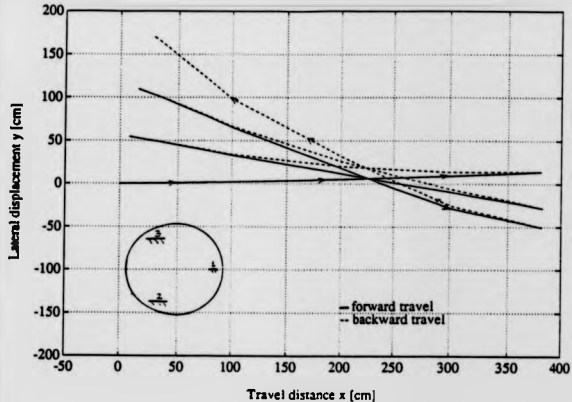


Fig. 7.61 Posture II-rad: Forward and backward trajectories.

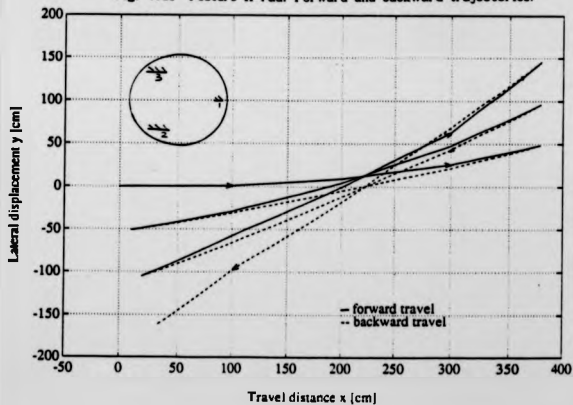


Fig. 7.62 Posture 2r-rad: Forward and backward trajectories.

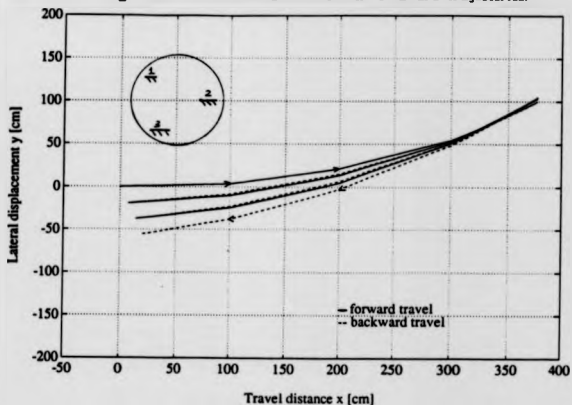


Fig. 7.63 Posture 2l-rad: Forward and backward trajectories.

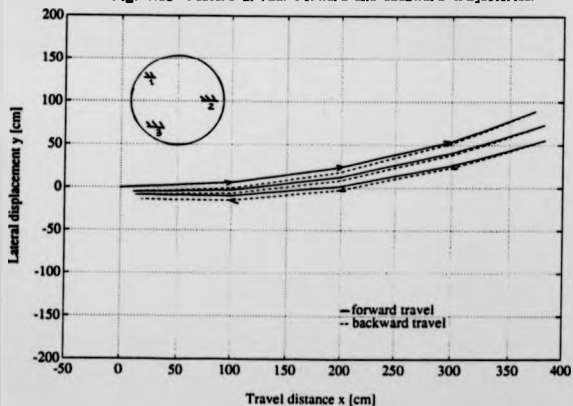


Fig. 7.64 Posture 3r-rad: Forward and backward trajectories.

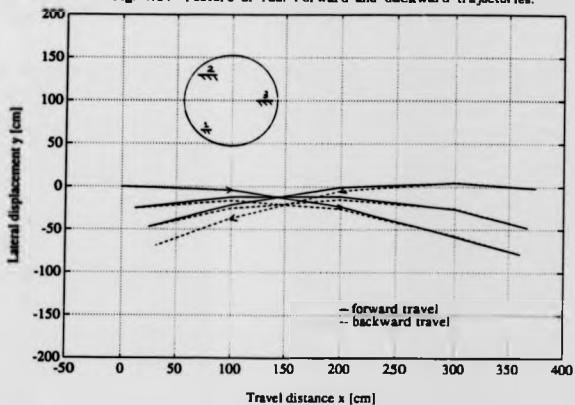
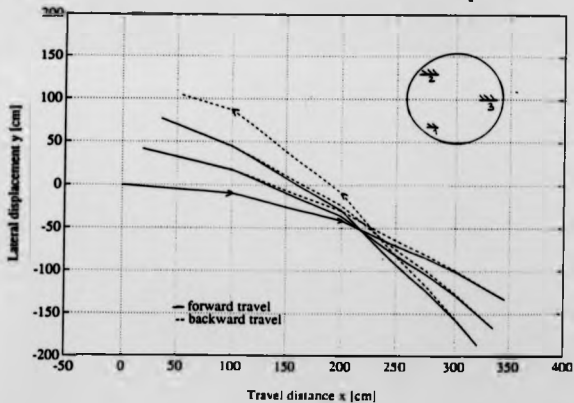


Fig. 7.65 Posture 3l-rad: Forward and backward trajectories.





wheel slippages during travel. This was seen as being caused by different wheel radii and the effect of all wheels being driven at the same speed. The increase in precession can be attributed to the wheels being driven along different paths resulting from their different surface speeds.

#### 7.2.7 COMBINED RESULTS.

Version 1 and Version 2 SDMR prototypes' precession, lateral error and arc radius were plotted against the SDMR postures (see Figs 7.66 to 7.71). Figs. 7.66 to 7.71 highlight the variation and influence different SDMR posture and Versions had on performance criteria.

The comparison of the results represented by the plots indicate that though there were similarities in behaviour, the outcome of performance is dependent on the form of interaction that occurs within the mechanical systems.

The combined results of the test conducted with Version 2 SDMR under different test conditions (categories A to F) are also presented. The plots are shown in Figs. 7.72 to 7.79. Test categories are represented with different line plots (see table 7.6 for line plot representation).

Fig. 7.66 SDMR lateral error for Version 1 & Version 2 Form-1 test:

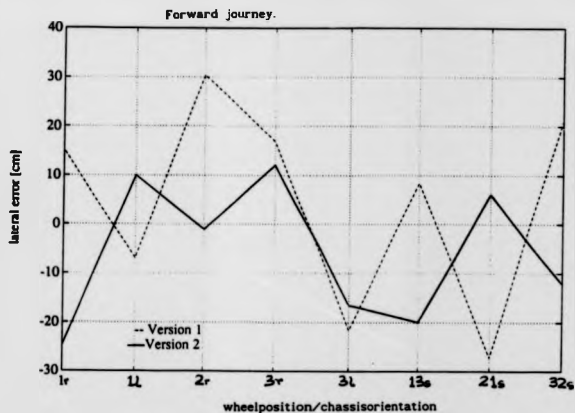


Fig. 7.67 SDMR lateral error for Version 1 & Version 2 normal state- Backward journey.

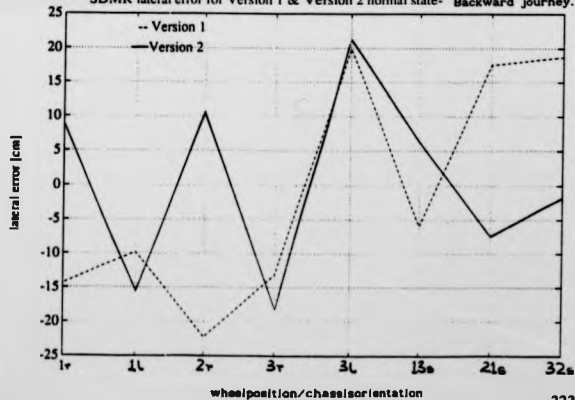


Fig. 7.68 SDMR arc radius for Version 1 & Version 2 normal state- forward journey.

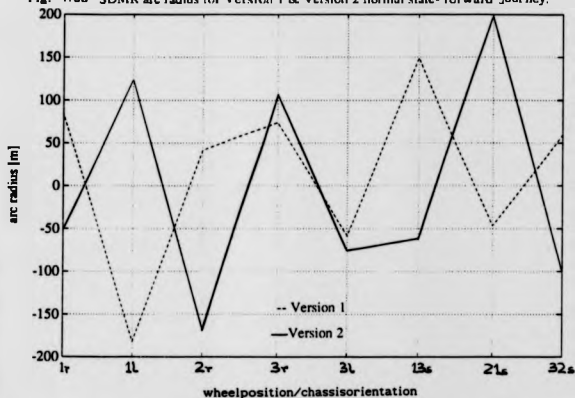


Fig. 7.69 SDMR arc radius for Version 1 & Version 2 normal state- backward journey.

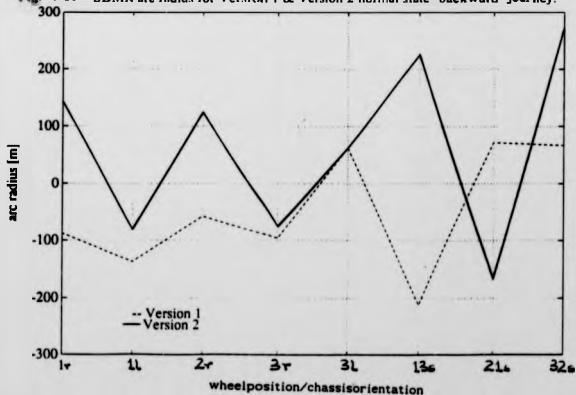


Fig. 7.70 SDMR precession for Version 1 & Version 2 normal state- forward Journey.

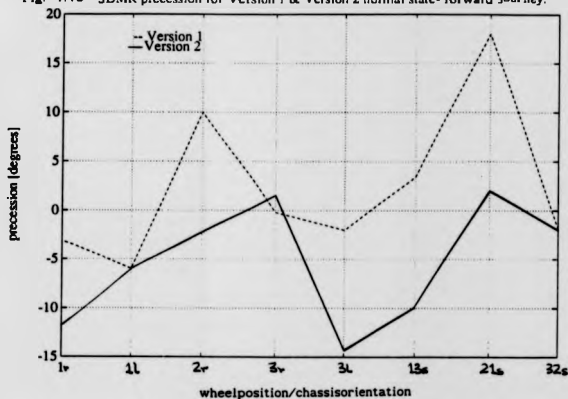


Fig. 7.71 SDMR precession for Version 1 & Version 2 normal state- backward Journey.

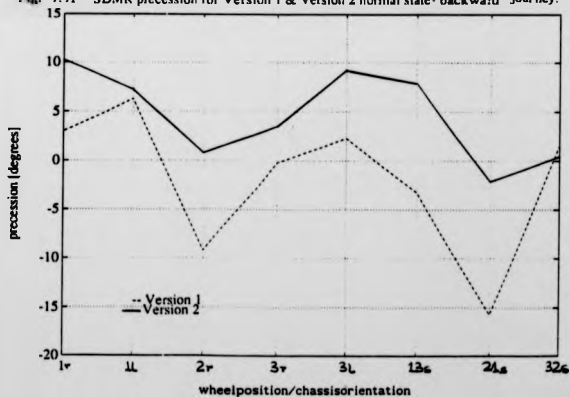


Table 7.6: Line type representation.

<u>Line type</u>	<u>Representation</u>
————	Test results for category A,
- - - -	Test results for category B,
————	Test results for category C,
- - - -	Test results for category D,
————	Test results for category E,
- - - -	Test results for category F.

Studying Figs. 7.72 to 7.79 it is evident that there are interactions between different test categories and SDMR postures. The plots also highlight the smaller error value that was obtained when the SDMR was operating in its normal state. Thus confirming the obvious assertion that improvement in construction of the SDMR will improve performance.

The different Version and difference state (categories A to E) results showed that lateral error, longitudinal error, precession and arc radius depends on the mechanical systems' errors, such as misalignment, different wheel radii and uneven load distribution.

Fig. 7.72 SDMR precession under different test condition\_ Forward Journey.

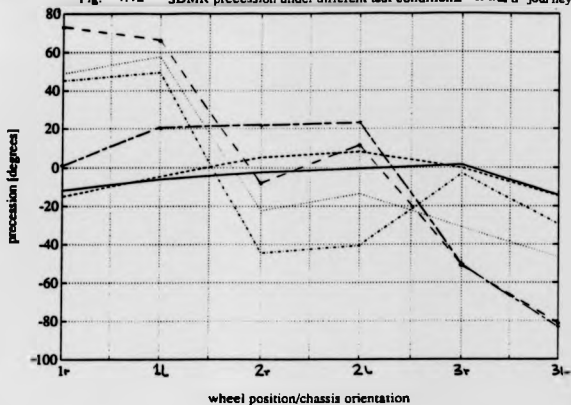


Fig. 7.73 SDMR lateral error under different test conditions \_ Forward Journey.

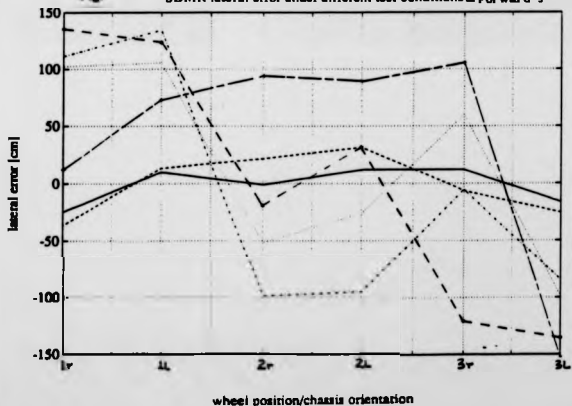


Fig. 7.74 SDMR longitudinal error under different test conditions - Forward journey.

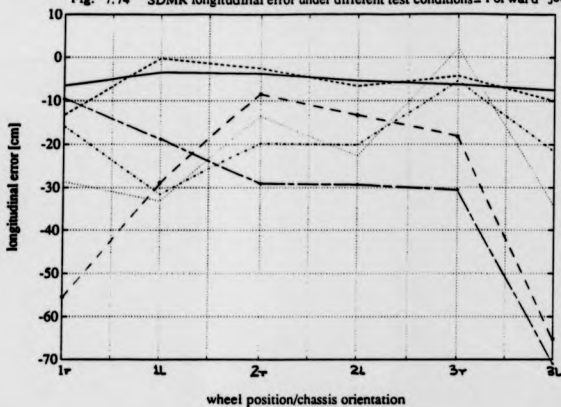


Fig. 7.75 SDMR path arc radius under different test conditions - Forward journey.

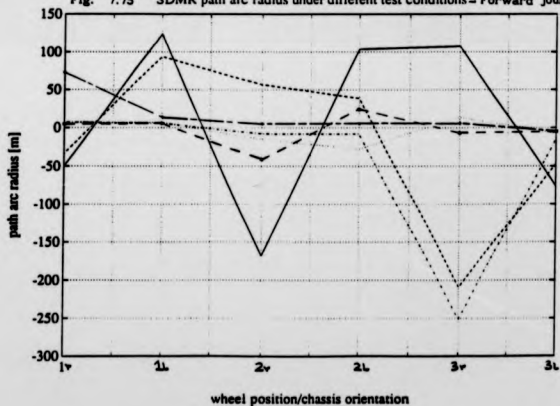


Fig. 7.76 SDMR precess under different test conditions - backward journey.

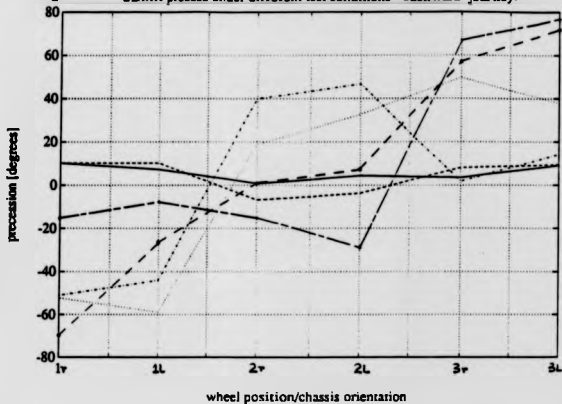


Fig. 7.77 SDMR lateral error under different test conditions - backward travel

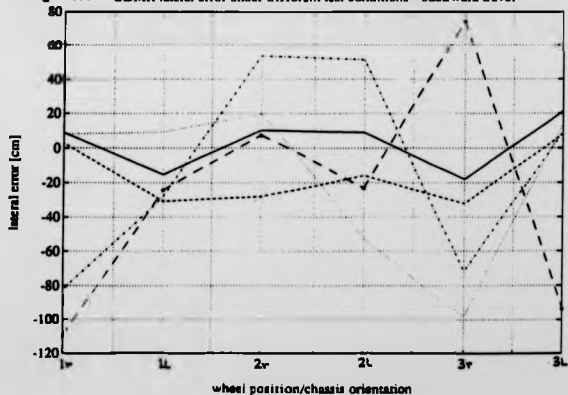




Fig. 7.78 SDMR long. error under different test conditions - Backward journey.

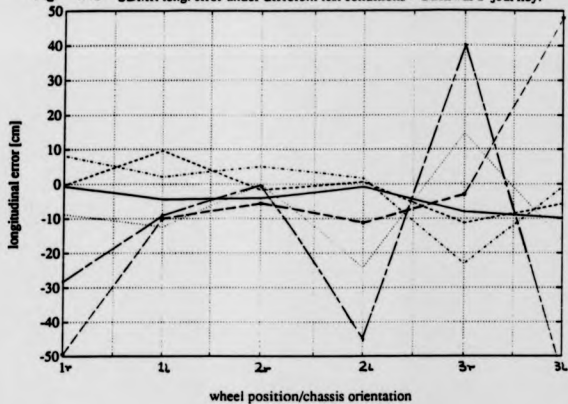
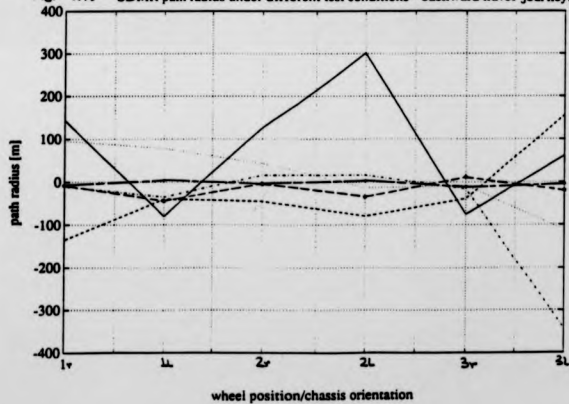


Fig. 7.79 SDMR path radius under different test conditions - backward travel journey.



#### 7.2.8 RESULTS SUMMARY.

The results of the different test categories permits the following inferences;

- what ever contributes to the mechanical systems' error, those which affect the alignment of the wheels tend to have a dominating influence on performance.

- the results suggest that the leading wheel during any travel tends to have marginally greater influence in the dictation of the trajectory shape and the drift that will occur.

- the test results obtained in the normal operating state (category A) can be said to be characterized by the effects of wheel misalignment. What tends to differ significantly between these test categories were the magnitude of precession and position error.

The overall outcome can be summarized as follows;

- (1) Errors change as SDMR posture changes.
- (2) The direction of the error generally reverses as the drive direction reverses.
- (3) The shape of the trajectories in relation to wheel drive gear positions indicates that the wheel drive gear position influences the trajectory.
- (4) The statistical analysis shows that position error can be predicted if the precession and arc radius are known. Hence to predict position error not only will the precession need to be monitored, the arc radius need to be determined also.
- (5) The statistical prediction model did not attach any particular importance to SDMR posture. But the difference in the

prediction model for forward and backward journey shows the significance of posture. Therefore an appropriate position error correction model that relies on precession or/and arc radius must take into account the SDMR posture.

(6) The Performance achievable is highly dependent on the quality of the construction of the SDMR mechanism. This was made more convincing when the steering transmission chains to the wheels of Version 1 SDMR were clamped to eliminate slack as shown pictorially in Fig. 7.80. The lateral error was reduced by 2% for 5m travel (initial error 4%), while the precession recording dropped to a zero mean from 3°. The trajectories improved as shown in plots of the different results for the same posture in Figs. 7.81 and 7.82.

(7) The results shows that the most important mechanical systems error to eliminate are those which influence the wheel heading, hence the quality of the steering subsystem is considered more crucial if improved performance of the SDMR is to be obtained.

(8) Since the test results in different test categories differ mainly in magnitude of position error, precession and arc radius, and not direction, it can be deduced that the SDMR behaviour and performance were highly dominated by the effects of wheel misalignment and slippages.



Fig. 7.80 Pictorial view of the steering transmission system clamped.

Fig. 7.81 Posture 1r: Forward and backward trajectories.

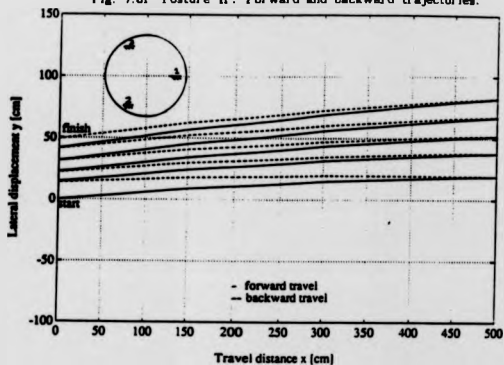
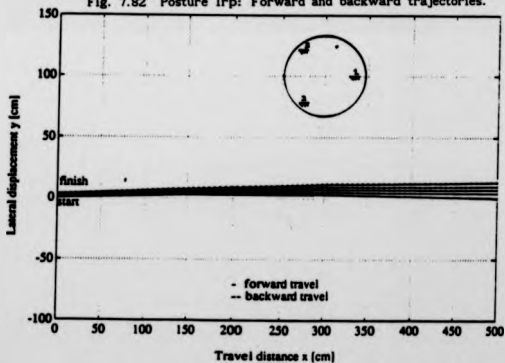


Fig. 7.82 Posture 1rp: Forward and backward trajectories.



## CHAPTER 2

### DISCUSSION OF RESULTS

The problems specific to a Synchro-Drive Mobile Robot (SDMR) that are highlighted by the experimental test are;

- (i) the errors present in the mechanical system of the SDMR vary with the direction of travel,
- (ii) the mechanical system errors fall completely outside the control loops of both the drive and steering subsystems when the wheels are driven by a single motor and steered by another single motor.

In dead-reckoning navigation [Tsumura'83] the information provided by the encoders attached to the shafts of the drive and steering motors are used to command the SDMR drive and steering mechanisms in order to keep the SDMR on its desired path at all times. This form of control which is most commonly used in wheeled mobile robots for short distance point to point control suffers from the fact the drive and steering mechanism may not follow the path the controller commands it to follow.

How to identify and handle the above issues is the concern of this work and they gave rise to the theoretical and experimental analysis reported in this thesis. This chapter concentrates on discussing the findings of the experimental tests. Different aspects of the theoretical findings have been dealt with in chapters 3, 4 and 5.

The experimental tests conducted (see chapter 6) were to identify the source, effect and extent of the problem. In this chapter they are discussed. Also considered here is a method of dealing with the effect of the problem.

Most other researchers [Crowley'89], [Wang'88] in trying to deal with the dead-reckoning problem have relied heavily on the information provided by sensors such as encoders. This method can be reliable where the encoders are attached to the wheels, and at the same time are able to provide information about the chassis orientation. Such a method can be applied successfully where chassis orientation and wheel heading are linked and interdependent. With a SDMR this method cannot be successful for two reasons, namely;

- ▷ The chassis orientation and wheel heading are independent, and this gives rise to different SDMR postures (see chapter 6 for some posture representation). A SDMR has a nominally fixed orientation.

- ▷ It is in practice very difficult to attach the encoders to the wheels and still be able to achieve the continuous  $360^\circ$  rotation necessary for unimpeded motion in any direction.

For the above reasons an alternative method not implemented before in any reported work has been proposed. The method relies on the information that the experimental test results provided. The experimental test results and the method of analysis have made it possible to estimate, in advance, the correction required

on the trajectory of the SDMR in order to get it to a given location knowing the current wheel heading with respect to chassis orientation (i.e. SDMR posture).

In most wheeled mobile robots dead-reckoning navigation is used as a relative navigation method [Jullier'83], [Hongo'85], [Holland'86] to cover for the mobile robot's operation in the interval between when absolute navigation (Appendix A, section A.2) is possible. How and when the absolute navigation method takes over control of the mobile robot depends to a greater extent on the accuracy of the dead-reckoning method. A good dead-reckoning navigation procedure will allow;

- (a) increase in accuracy of travel between the points where absolute navigation takes over,
- (b) the points to be further apart for the same precision, thus reducing the need for the absolute navigation system to compute a new position in a very short time interval.

The method proposed provides improved accuracy in the dead-reckoning position determination of a SDMR in recognition of its peculiar problems as regards the use of dead-reckoning navigation.

#### 8.1 RESULTS DISCUSSIONS.

The results of the experimental test runs were presented in chapter 7. In an ideal case, the lateral error, longitudinal error and precession should be zero, with the arc radius being infinity. This is however not realizable in practice because of deficiencies in the mechanical system. On the other hand the



magnitude of the errors which were observed seems high. It has to be borne in mind that no attempt was made to correct for the mechanical system error. But attempts were made to correct for the design-error which gave rise to Version 2 SDMR. However these results cannot be directly compared with those of any other SDMR because no similar results have ever been presented in the published literature.

Comparing the actual results with those reported by Hongo et al [Hongo'87] and Premi [Premi'85] the quality of performance is considered to be low. This level of performance which the prototypes gave can cause three major application problems;

- (1) An absolute navigation method such as the camera based technique (see Appendix A.2) when used to guide the SDMR will be required to intervene more frequently in the control of the SDMR. This is to prevent the trajectory executed and position error that does occur from getting out of range. Such a high demand on the operation of the absolute navigation system may not be easily met, especially if the SDMR's high manoeuvrability and rapid response to direction change is utilized.

- (2) The magnitude of its position error and precession may make it impossible for the SDMR to dock and orientate accurately at say a work station (see Figs. 8.1a and 8.1b).

- (3) There will be need for more space within the SDMR travel route in order that it can get from location A to say location B (see Fig.8.2). Thus it may not be possible for the SDMR to get to a desired location, without colliding with obstacles just off the planned path.

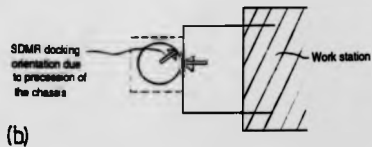
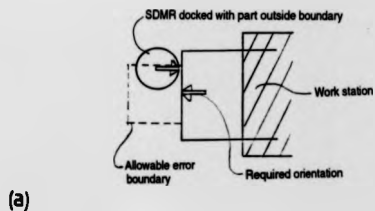


Fig. 8.1 Two of the possible SDMR docking errors.

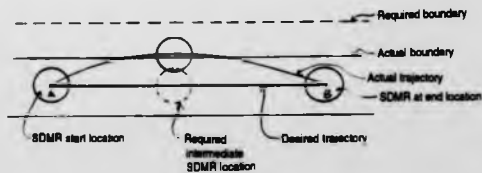


Fig. 8.2 SDMR space requirement.

The above three issues create the need for improvements to the performance that can be achieved by the SDMR.

It was evident from the test results that the drift in the SDMR increases gradually as the distance increases. SDMR drift is due to the errors that exists within the mechanism. These errors arise from sources which have been discussed in chapter 3. The errors originate from the power transmission system, the tyre, the wheel alignment, the nature of the floor surface, sensors used and computation technique. From experimental observation, those that have significant influence in the results presented are those originating from the transmission system, the tyre and the wheel alignment and these are seen as mechanical system errors.

The mechanical system errors are of two major forms, namely; wheel misalignment and wheel size difference. Wheel misalignment of the SDMR can be caused by; initial (static) misalignment, unequal play in the steering system due to slack, backlash, tolerances and dimensioning, and unequal forces producing different angular displacement. Wheels having different radii can arise due to; unequal static wheel size (unladen), variations in wheel size due to variable loading, the effect of different wheel radii can also be introduced by dynamic fluctuations in drive input due to slack, backlash, tolerances and dimensioning in drive transmission system.

The effect of wheel misalignment and different wheel radii are

precession of the chassis and wheel slippage. Wheel misalignment causes the three wheels not to maintain their parallelism. Parallelism is fundamentally important for proper behaviour of a SDMR in straight line motion, because the wheels are driven at equal speeds. Driving misaligned wheels at equal speeds causes chassis precession and wheel slip. In a situation where there is no wheel slippage, the lateral error ( $\delta y$ ) and arc radius ( $R$ ) should be directly related to precession ( $\beta$ ). The analysis of the result presented in chapter 7, shows that the use of precession as a independent variable for determining lateral error and arc radius cannot explain more than 40% of the variations in  $\delta y$  and 13% in  $R$ , for the Version 1 SDMR. For the Version 2, the values of 67% and 29% were obtained. It is clear that the behaviour of Version 2 SDMR is more predictable on the basis of precession alone than that of Version 1, and in both cases the unexplained variation must be caused by slip.

The effects of different wheel radii were that of precession and slippage. This is based on the evidence provided by the results of the different wheel radii test (test category F in chapter 7). SDMR precession and wheel slippage give rise to lateral drift.

The trajectory plots of the test results showed consistency for a given SDMR posture over several runs. The consistency implies that irrespective of posture, certain phenomenon that cause position error were present as long as the SDMR posture was maintained. When the posture changes the nature of the effects changed but the repeatability characteristic was still there.

Investigation revealed that the above phenomenon was caused by;

- (a) the mechanical system errors such as slack and backlash,
- (a) the torque developed about the wheel assembly z-axis which produces a steering effect and is hereby termed wheel 'torque-steer'.

Wheel torque-steer phenomenon can be explained using the approach used to analyze wheel forces/torque in chapter 3. In [Wong'78] it was shown that for small slip angle, cornering force is slightly behind the applied side force. The cornering force generates torque (or couple) (see chapter 3, section 3.1.2) which is called the self-aligning moment. In the same vein, drive power transmitted to the wheel through the bevel gear arrangement, develops a side force at the wheel centre. This side force in-turn gives rise to a lateral force which acts in the direction that opposes the side force. These two forces which are not collinear because of the effect of slip angle, load and tyre material that affects the line of action of the normal force, will produce a couple. The couple developed will have a twisting effect on the wheel. The sort of effect this couple has on a system was discovered to depend on the design. For a conventional mobile robot such a tricycle configuration the effect of such a couple may not be significant. This is because the amount of mass that should be accelerated to achieve any significant wheel angular displacement about the z-axis is high. With a Synchro-Drive Mobile Robot (SDMR), such a couple can have a significant influence because inertia involved during wheel angular displacement about the z-axis is very low (see Appendix

B). The couple acts to takes up any free-play in the system and the unwanted steering effect that results from this is called 'torque-steer'.

The direction in which the wheel torque-steers depends on the wheel drive gear position and the direction of drive torque applied to the wheel. The synchronized nature of the drive mechanism causes the wheel torque-steer to occur in the same direction in all three wheels. That is, all three wheels either steer to the right or all three steer to the left (see Figs. 8.3a and 8.3b).

The deficiency in the steering mechanism is collectively called wheel 'free-play' (see chapter 3 for further details). In the prototypes the free-play angles were significant and were up to 10° in some wheel positions. The amount by which the wheel torque-steer displaces the heading of individual wheel is determined by the available free-play. Free-play was found to be consistent in a given posture, but changes as the posture changes. It was also observed during the tests that the drive input displaced the wheels about the z-axis, thus giving it a heading different from intended heading. The rate at which free-play is taken-up depends on the drive acceleration. However from tests, difference in rate of take-up of free-play with different drive acceleration was not significant. The free-play and wheel 'torque-steer' were observed to be highly repeatable in a given posture.



Fig. 8.3a Wheel 'torque-steer' to the right.

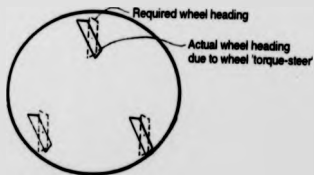


Fig. 8.3b Wheel 'torque-steer' to the left.

The wheel torque-steer that takes up the free-play angle helps explain why the SDMR in executing a drive command, heads off always in a new path both for forward and backward travels, and also repeating approximately the same position error and precession for several runs (see trajectory plots in chapter 7). The second contributory factor is the effect of precession itself. Precession changes the chassis orientation and hence the wheel heading frame of reference relative to the fixed global frame of reference.

The wheel torque-steer also helped to explain why the SDMR always executed a circular curved path when the demand was for a straight line. This is based on the fact that wheel torque-steer takes up the free-play in the steering system. Since the free-play angle of the three wheels were not the same, when the wheels are each subjected to torque-steer, each of the wheels takes up a different angle, thereby loosing the required wheel parallelism. With loss of parallelism, and due to the wheels equal drive speeds, there is a resultant force whose line of action is a function of the misalignment of the three wheels. The resultant force drives the SDMR through a path whose direction changes with distance along the path.

The error in the trajectory executed depends largely on three factors, which are; the resultant SDMR heading after wheel torque-steer, the precession angle and wheel slippage. To separate and obtain the individual effects of these factors was not possible. But what is certain is that if the boundary of the



control space is not exceeded, then SDMR precession and slip is related to the resultant SDMR heading angle, caused by the initial wheel misalignment and wheel torque-steer taking up the wheel free-play.

The occurrence of precession and slip lead inevitably to drift. Test results showed that precession, drift and position error change as SDMR posture changes. These occurred for the following reasons:

- ▷ The wheel torque-steer direction changes as the wheel drive gear position and drive input direction changes.
- ▷ The resultant direction of travel of the SDMR which is dependent on the wheel headings, changes as the SDMR posture changes.
- ▷ As the SDMR posture changes so does its wheelbase parameters (see chapter 3 and 4 on how the changes occur). Changes in the wheelbase parameters changes the value of any resultant force that affects the SDMR.

Since the drive torque attempts to displace the heading of the wheels during acceleration from rest, it implies that the state of the steering mechanism greatly affects the trajectory executed by the SDMR. If for instance the steering mechanism has minimal slack, backlash and tolerances, the effect of wheel torque-steer will be minimized because of lack of free-play angle. Hence an improved steering mechanism will allow for SDMR wheel adherence to the required heading, thereby giving improved performance in terms of reduced position error and precession angle. This will

be true if the initial wheel alignment is error-free and if the wheels are of equal wheel radii. The prototypes used to conduct the test had slack, backlash and tolerances which were considered to have a significant influence on the outcome of the SDMR performance.

The reasons for the different results can also be explained by the analysis of the arc radius of the path taken. The curvature  $r_c$  of the path is  $1/R$ , where  $R$  is the arc radius and from chapter 3, section 3.3.1,  $r_c$  was also determined as (see equations (3.8));

$$r_c = \frac{(t)}{(\lambda)} + \frac{v_R}{(\lambda)t} \quad (8.1)$$

where

$$(t) = \frac{F_1 + F_2 + F_3 - 3K}{m} \quad (8.2)$$

$$(\lambda) = \frac{0.29l(F_1 + F_3) - 0.58l(F_2) - M_c}{I} \quad (8.3)$$

$F_1$ ,  $F_2$ , and  $F_3$  are the wheels' tractive force,

$K$ , is the motion resistance on each wheel,

$M_c$ , is the moment of resistance to the chassis rotation about the centre of mass,

$m$ , is the mass of the SDMR,

$I$ , is mass moment of inertia,

$v_R$ , is the linear velocity of the centre of mass,

$l$ , is the horizontal distance between the first and the last wheel location.

Equation (8.1) implies that  $r_c$  changes as the forces on the wheels change. Because of differences in factors such as slack, backlash, etc. the forces on the wheels are not the same, hence  $r_c$  and invariably the trajectories will not be the same. Even if forces acting on the wheels are the same, with change in SDMR posture the value of the length parameters 0.291 and 0.581 changes. This change will give rise to change in value of  $r_c$ .

Therefore the results of the experimental test in terms of different value for different SDMR posture should be expected. Another finding of the curvature analysis is that even if the mechanism has minimal mechanical systems error, the changes in length parameters and posture is bound to cause execution of different trajectories. Only a totally error free system will not give different trajectories for the same specified path, but under different SDMR postures.

**8.2 MAIN DIFFERENCES BETWEEN SDMR CONFIGURATION AND CONVENTIONAL MOBILE ROBOT CONFIGURATION WHEN OPERATING IN AN ERROR STATE.**  
The main differences that the effects of mechanical systems error such as wheel misalignment have on the SDMR configuration and that of a conventional mobile robot configuration (for example the tricycle, having front wheel drive and steering system) are:

(1) With a conventional mobile robot, the position error which the mechanical inaccuracies of the sort displayed in the prototype will be very much greater than that obtained with the SDMR. The reasons for this can be shown using two diagrams

representing the two different designs (see Figs. 8.4 and 8.5). Considering Figs. 8.4 and 8.5, if wheels numbered 1 are misaligned by say angle  $\theta$ , the tendency is for the mobile robot to drive in the direction dictated by  $\theta$ . For the conventional mobile robot, because wheel 1 is driven it will attempt to drive the mobile robot in the direction  $\theta$ . And because wheels 2 and 3 are free to roll at any speed, they will therefore roll at different speeds, hence allowing wheel 1 to dictate completely the mobile robot heading, which will be directly related to angle  $\theta$ . Hence the magnitude of the position error will depend completely on that of the angle of misalignment.

With the SDMR configuration, the case is such that wheel 1 will attempt to drive the mobile robot through a path dictated by angle  $\theta$ . On the other hand, wheels 2 and 3 because they are driven at the same speed as wheel 1 will attempt to drive the mobile robot along a path with zero angle misalignment. The resulting effect is that wheels 2 and 3 will together oppose the drive direction of wheel 1. The tendency is for the SDMR position error to be reduced because of the 'correcting actions' of wheels 2 and 3 that attempt to take the SDMR along the required path. Hence the position error is not completely dependent on wheel 1 misalignment angle  $\theta$ .

It can therefore be said that a SDMR has a 'self-position-error' reduction mechanism. This characteristic on the other hand plays a part in making the resulting position error difficult to correct. This is because the position error is a result of

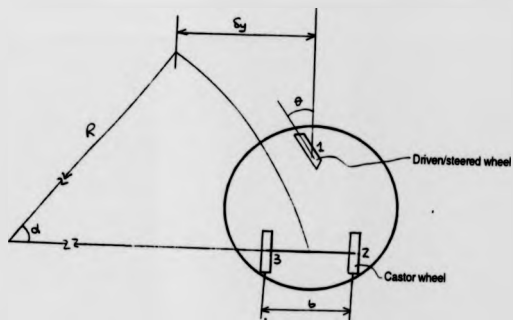
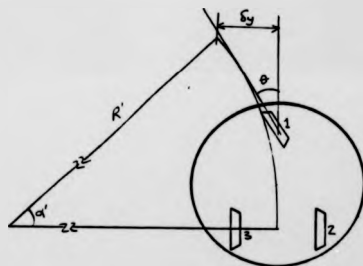


Fig. 8.4 Illustration of conventional mobile robot.



Note: All wheels driven and steered

Fig. 8.5 Illustration of SDMR.

opposing forces where precession and slip determines the dominant direction, therefore making it difficult to be accurately monitored.

(2) With the conventional configuration the misaligned wheel will cause the individual wheels to adjust their speeds. From measuring the displacement of the two undriven wheels (wheel 2 and 3), using encoders, the forward displacement, the arc radius and change in heading can be determined (see Appendix B, section B.4).

(3) The effect that any resultant force creates with the conventional mobile robot is independent of heading. For the SDMR, the resultant and its effect depend to a considerable extent on the heading. This is because conventional mobile robot chassis changes its orientation directly with change in heading. Therefore for any new heading, the relationship between chassis orientation and wheel heading remain the same. For the SDMR the chassis is nominally fixed irrespective of change in heading. Therefore for any new heading the relationship between chassis orientation and wheel heading changes. The consistency in behaviour of a conventional mobile robot makes its position error easier to predict, whereas for the SDMR this is less easy but can be done if sufficient information is obtained on the relationship between errors and the posture.

### 8.3 FORMULATION OF POSITION ERROR CORRECTION METHOD.

Very small values of free-play in the steering system of a SDMR may be expected to give a low magnitude of position error. This approach, though entirely possible, may give rise to an expensive SDMR which cannot be afforded in certain applications that would otherwise benefit from the flexibility which a SDMR provides. For such an application, a realistic solution might be a SDMR that uses components that may allow significant free-play angle together with an error compensation system.

This will allow high values of errors to occur within the steering system but the effect of these errors on the SDMR path can be kept within tolerable limits using error correction. The analysis in section 8.1 and chapters 3 and 4 shows that even with minimal mechanical systems error we are bound to obtain different results for different SDMR postures. To accommodate the results obtained from different SDMR postures, we need a position error correction method that takes into account the different postures. The method proposed is one that can achieve considerable error reduction in a SDMR with significant mechanical systems error and so make it capable of performing with a much higher level of accuracy than would otherwise be the case.

Due to its mechanical systems error the SDMR behaved as if there was steering input during path execution which gave rise to a circular path when the demand was for a straight path. The method proposed to correct for the position error which occurs is to introduce a correcting steering action that will counter that

which arises from the mechanical systems error.

The method relies heavily on the path arc radius. The experimental results shows that as SDMR posture (henceforth considered as angle  $\psi$ ) changes so too does the precession ( $\beta$ ), lateral error ( $\delta y$ ), longitudinal error ( $\delta x$ ) and arc radius ( $R$ ). The situation during path execution can be illustrated with the aid of Fig. 8.6. In Fig. 8.6 the intention is to drive the SDMR from point A with the posture  $\psi$ , to point B through a distance  $S$ . But the uncorrected outcome is that the SDMR translates from point A through a circular curved trajectory to point C. By so doing it precesses through an angle  $\beta$  and along an arc with radius  $R$ . The test results show that  $\beta$  and  $R$  varies non-linearly with  $\psi$  due to slip. For this reason the approach taken is to make use of a look-up table such as that given in tables 8.1 and 8.2.

Table 8.1 Look-up table for different SDMR test postures for the forward travel direction.

SDMR Postures												
	1r-o	1l-o	2r-o	2l-o	3r-o	3l-o	130r-o	130l-o	210r-o	210l-o	320r-o	320l-o
Arc radius (R)	143.41	-90.32	126.44	301.32	-75.23	62.01	225.00	-79.70	-166.96	-64.60	-50.52	274.06

Table 8.2 Look-up table for different SDMR test postures for the backward travel direction.

SDMR Postures												
	1r	1l	2r-o	2l-o	3r-o	3l-o	130r-o	130l-o	210r-o	210l-o	320r-o	320l-o
Arc radius (R)	-49.80	124.11	-167.80	103.54	107.51	-76.09	-61.30	167.04	190.60	113.41	90.19	-102.04



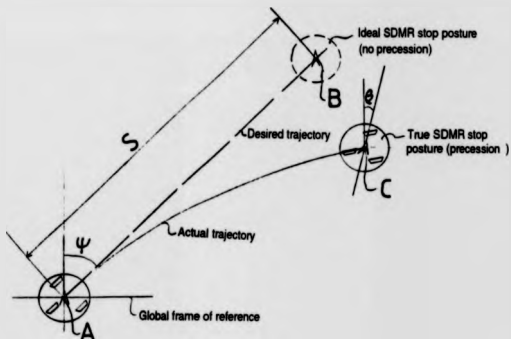


Fig. 8.6 Illustration of trajectory executed by the SDMR.

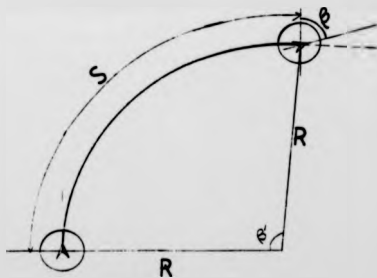


Fig. 8.7 Path parameters.

The test results analysis showed reasonable correlation between  $\beta$  and  $R$ . The correlation was not completely linear, hence what was experienced can be visualized with the aid of Fig. 8.7 above. The arc length  $S$  (distance traveled) is related to the arc radius  $R$  and angle  $\beta'$ , as  $S = \beta'R$  (see Fig. 8.7).  $\beta$  is not necessarily equal to  $\beta'$  because of factors such as slip therefore  $\beta$  is considered less reliable in trying to correct for the drift and position error. Other reasons for using arc radius are;

- In determining the values of  $R$  for the executed test trajectories, the measured x,y data of the curved path was used. Therefore arc radius  $R$  is more closely related to the path than precession angle  $\beta$ .
- Correlation determined in chapter 7, section 7.2.1 shows that arc radius  $R$  was significantly more associated with the lateral error in both forward and backward travels.

For a given posture  $\psi$ , the value of  $R$  can be obtained from the look-up table. Knowing the distance to be traveled, the actual angle  $\beta'$  can be determined as;

$$R = S/\beta' \quad (8.6)$$

$$\beta' = S/R \quad (8.7)$$

For a conventional mobile robot, the position error could be corrected just by steering the wheels through angle  $\beta'$  with an opposite sign. But for a SDMR this is not the case, because of constant wheel parallelism. Therefore to achieve position error correction the requirement is for a steering angle correction rate ( $\dot{\beta}'$ ). For the example illustrated by Figs. 8.6 and 8.7, the SDMR moves along an uncorrected path of arc radius say  $+R$ , so to

correct this we need to instruct the SDMR to actually steer with radius of  $-R$ .

Since;  $v = -R\omega$  (- because we want to correct for +)

where;  $v$ , is the drive speed (m/s) and

$\omega$ , is the steering rate (rad/s),

we have;  $\omega = -(v/R)$  (8.8)

substituting equation (8.6) in (8.8) gives,

$$\omega = -(v\beta'/S) \quad (8.9)$$

Equations (8.8) and (8.9) gives the steering rate required during path execution to enable the effect of the errors arising from say mechanical system deficiencies to be corrected. If there is a user demand for a steering input, the value obtained from either equation must be added to that steering input *irrespective* of the instructed path.

Equations (8.8) and (8.9) appears very simple but in fact the steering rate has to be constantly varied. This is because the value of  $\beta'$  is a function of posture angle  $\psi$  and even when the SDMR moves along a corrected straight line path, the chassis will precess. Consider the exaggerated case where it is necessary to correct an angle  $\beta'$  of  $90^\circ$ . Such a precession will take the SDMR from the posture shown in Fig. 8.8a to that of Fig. 8.8b, thus completely changing the SDMR posture  $\psi$ . Changing  $\psi$  means that the resulting path errors will also have changed. Therefore there is the need to change the error correction rate. As the error correction rate changes so does the radius  $R$ . Hence the radius achieved during error correction will be similar to that shown in Fig. 8.9.

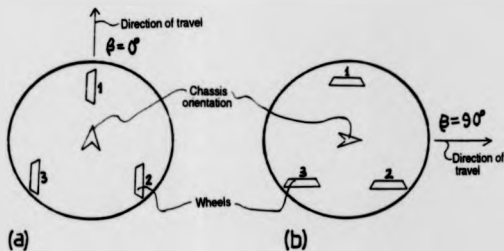


Fig. 8.8 Change in SDMR posture due to chassis precession.

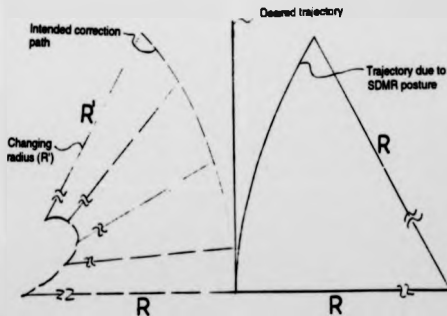


Fig. 8.9 Illustration of the required correction radii.

The method of position error correction proposed here has two main issues to contend with:

(1) There has to be a continuous steering input to the SDMR. This is because steering rate and not steering angle is used as the correcting factor.

(2) The chassis precession is not corrected by this method. The chassis precession cannot be corrected if the SDMR drive and steering systems are in permanent synchronization. Decoupling of one or two wheels is possible [Nakano'83] but this leads to a very complex design and introduces yet more possibilities for mechanical errors, therefore a more practical approach is to have an independent rotatable 'platform' (Fig. 8.10), which will achieve body rotation. Note, there is still a fixed chassis orientation. The body orientation can be varied by either linking it to the wheel heading or by steering it independent of the wheel heading, and correcting for precession where it becomes necessary.

Having developed a method of position error correction, it should be noted that it was not implemented in the prototypes SDMR. This is due to two major reasons:

(i) The path specification method in use at present allows for only straight line commands.

(ii) The control software also is so limited that it cannot handle two crucial aspects of the position error correction method, namely; the ability to utilize the look-up table and the capability to sustain continuous steering of the wheels.

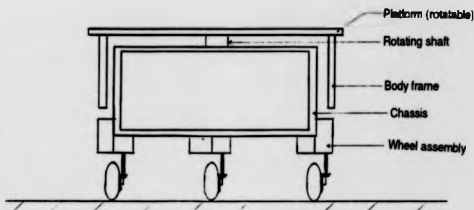


Fig. 8.10 Diagram showing SDMR chassis, body and platform.

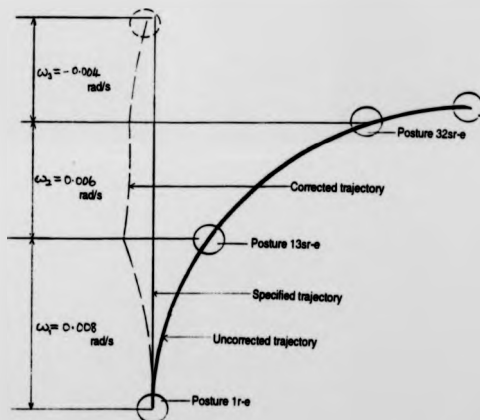


Fig. 8.11 Illustration of the changing steering rate and position error corrected trajectory.

Though the proposed position error correction method could not be implemented, the way it can operate in practice can be illustrated using the earlier example where the SDMR was assumed to have precessed by  $90^\circ$ . For a 5m travel distance and drive speed of 0.4m/s, the implementation could be thus:

$90^\circ$  precession will take the SDMR through say three of the postures whose test results were recorded, and these posture are; Posture 1r-e =  $0^\circ$ , Posture 13r-e =  $30^\circ$ , Posture 32r-e =  $90^\circ$ . The arc radius for these postures from the look-up table (see table 8.2) are;

Posture 1r-e = -49.88m

Posture 13r-e = -61.3m

Posture 32r-e = 90.19m

Substituting the values of the drive speed and arc radius in equation (8.8) gives the steering rate necessary to correct for position error that will arise (assuming that only three posture changes occur). The steering rate for the three known posture which the SDMR will go through will be,

for posture 1r-e = 0.008 rad/s

for posture 13r-e = 0.006 rad/s

for posture 32r-e = -0.004 rad/s

This shows that based on the test results, for the SDMR in executing the path with a precession of  $90^\circ$  will operate at three different steering rate. The regions of these steering rate and the nature of the corrected trajectory is illustrated in Fig. 8.11 above.

The above calculated results were simulated under the assumptions

that;

- there were three posture changes when the SDMR travels the 5m distance with  $90^\circ$  precession,
- posture 1r-e changed to posture 13r-e after 2m travel, and posture 13r-e changed to posture 32r-e after 4m travel and that posture 32r-e was maintained at the end of travel.

At a drive speed of 40 cm/s the plot of the simulated result is shown in Fig. 8.12. The plot shows that the lateral error after using the position error correction method was about -0.22m. Without the position error correction, a precession of  $90^\circ$  for a 5m travel will cause a lateral error of 3.12m. Therefore by applying the position error correction the lateral error has been reduced by a factor of 14. This is a significant improvement bearing in mind that the simulation assumed only three posture changes, which the tests conducted provided the required input correction values. It should however be borne in mind that a precession of  $90^\circ$  is a highly exaggerated one. The position error correction is continuous and not discrete, hence to further improve the accuracy of positioning more posture data is needed or the validity of linear interpolation between points may be investigated.



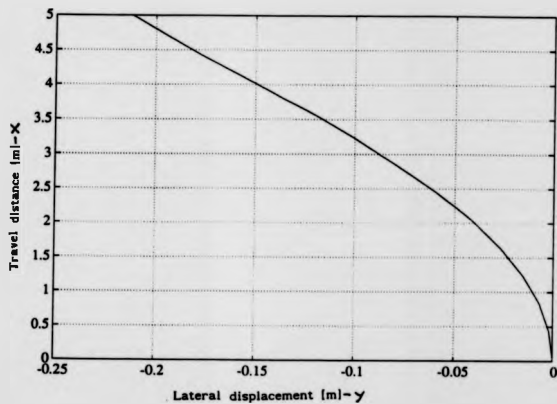


Fig. 8.12 Plot of the simulated corrected position error.

## CHAPTER 9

### CONCLUSIONS AND RECOMMENDATIONS FOR FURTHER WORK

In this final chapter, the study of mobile robots in general and that of Synchro-Drive Mobile Robot (SDMR) in particular are concluded. The chapter comprises of two sections; section 9.1 dealing with the issues covered by the study and the contributions made, and section 9.2 covers the areas that requires further investigation in the light of the research conducted.

#### 9.1 CONCLUSIONS.

Different configurations of wheeled mobile robots have been studied with particular attention to those capable of omnidirectional motion. Omnidirectional motion enables movement flexibility through high manoeuvrability. The investigation considered the benefits and limitation of individual designs. Analysis revealed that there exists three major ways in which a conventional wheel assembly can be configured in order to be capable of omnidirectional motion. The three ways were classified as (see Figs. 9.1, 9.2, and 9.3): wheel-offset from the steering axis of the wheel assembly, Type-1; differential gear coupled wheel set, Type-2; and wheel-set on the steering axis of the wheel assembly, Type-3. Also it was revealed through literature search that implementation of Type-3 wheel assembly had not previously been reported.

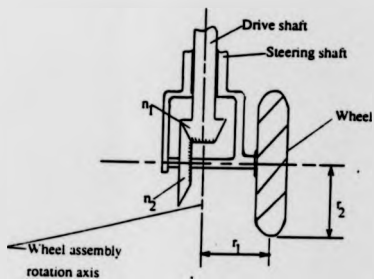


Fig. 9.1 Type-1 wheel assembly.

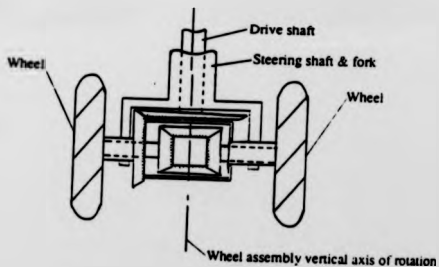


Fig. 9.2 Type-2 wheel assembly.

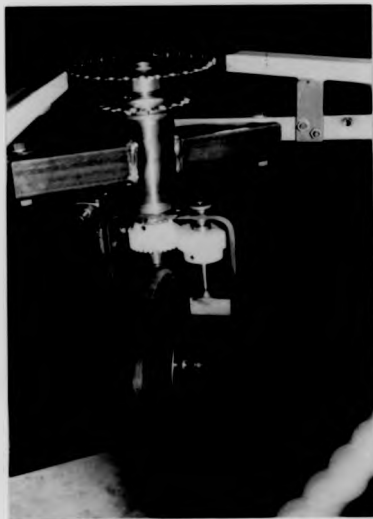


Fig. 9.3 Type-3 wheel assembly.

Comparative analysis of SDMR's shows that;

- ▷ The effect of tractive force on both Type-1 and Type-3 of SDMRs is the same, but that of lateral force and self-aligning torque gives different results.
- ▷ Type-3 has the tendency for more predictable handling behaviour. This is attributed to the nature of the relationship between the lateral force, free-play angle, self-aligning torque, the effect of load transfer during manoeuvres, and twisting moment.

Factors that influence SDMR performance were studied. The study gave an insight into the effects created by the interaction between wheel and floor surface and the impact that the mechanical systems error and change in heading has on the response of the SDMR to drive and steering commands. One such impact is the varying speed at which stability is retained. The SDMR trajectory when operating in a mechanical systems error state without a steering input command was analyzed. The analysis shows that a cornu spiral curve or a circular curve is possible. The test finding is that the prototype SDMRs trajectories were those of circular curve.

A kinematic model that determines the SDMR velocities and acceleration has been formulated. The method uses homogeneous transformation based on a matrix format. The kinematic model assisted in the design comparison and in establishing the boundaries of the control space for the SDMR. The model revealed the cause of steering induced error (design-error) which the

Type-3 SDMR possesses. The design-error if not corrected makes such a wheel assembly an infeasible design option for SDMRs. This is because such an error will override any other form of position error correction incorporated. The design-error was corrected through a unique arrangement that makes use of differential and worm gear units. This approach was taken based on the findings of the SDMR analysis of the kinematic model. The model shows that the cause of the design-error was the effect of coupling that exists between the drive and steering subsystems. Such coupling was shown to be eliminated from the Jacobian matrix by multiplying it with a differential matrix factor.

The boundaries of control space for the SDMR have been successfully established and they permit the knowledge of onset of slipping and overturning of the SDMR. For stable operation there is a need to know the limits of speed and acceleration that a SDMR can use, within the limits of the kinematic and dynamic constraints. If any of the constraints are violated there will be unstable operation of the SDMR. The importance of investigating the control space boundaries was enhanced by the finding that:

- (i) The boundaries are affected by the configuration and posture of the mobile robot. Hence different configurations and postures achieves stability at different acceleration levels.
- (ii) A SDMR can achieve high steering rate due to low inertia involved during turning. This feature makes SDMRs more vulnerable to slipping and overturning if attempts are made to change heading at high steering rate.

From the study of control space it can be concluded that;

- since the acceleration at which slip or overturning can occur is dependent on the SDMR posture, posture is therefore an important parameter to be considered in the mobile robot's control system.
- once slip sets in, the three wheels of the SDMR will experience it simultaneously. This is because for the three wheels to slip the required acceleration is less than that required for either one or two wheels to slip.

The sources of error that affects the performance of SDMR was explored through theoretical and experimental considerations. The experimental investigation revealed that the errors which originate from the power transmission system, tyre, wheel alignment, etc. are of two main types, namely; wheel misalignment and difference in wheel size. Their effects cause SDMR precession and slippage, contributing to trajectory error and final position errors.

The experimental tests performed under different test conditions and their subsequent analysis allows the following conclusions to be drawn:

(a) For a given posture and test conditions the errors observed were highly repeatable.

(b) For a different posture the SDMR displays different mechanical system errors which can produce a significantly different trajectory.

(c) For a different posture the SDMR displays different capability with regards to stability.

(d) Since the wheels may be steered in any direction with any chassis orientation, any errors associated with either direction or orientation will cause the SDMR to move with path errors which are functions of the two variables, orientation and wheel heading.

(e) Even if the SDMR is geometrically perfect such that the behaviour of wheels 1, 2 and 3 is identical in every way and they are indistinguishable, the SDMR can still experience forces which will tend to deviate it from its desired path.

(f) For several forward and backward journeys, the SDMR always take a new path because of the effect of wheel 'torque-steer' and precession. Wheel torque-steer is significant because of the low inertia involved in steering the wheel assemblies.

(g) The error in the steering subsystem is more significant in terms of its effect on accuracy than that in the drive subsystem.

(h) The all-wheel drive system performs the function of an error-reduction system. This feature on the other hand makes the remaining error much more difficult to correct, because it can not be accurately predicted.

(i) The implementation of a dead-reckoning navigation technique requires a consideration of the SDMR posture in order to correct position errors.

(j) It is very difficult to isolate and quantify the contributions made by individual error sources to the overall



error due the presence of unquantifiable slip.

(k) The evidence through statistical analysis is that there is correlation between precession and lateral error, and between arc radius and lateral error but they are non-linear. Also that arc radius and not precession is a better parameter to use in position error correction.

The results obtained from the test cannot generally be compared against any other experimental results by other researchers. The work in this case is unique, in the sense that it focuses on the mechanics of SDMR's and their contribution to overall performance. The results obtained from the tests were solely based on navigating the SDMR using dead-reckoning, while those of other researchers are obtained after an absolute navigation method has corrected for the cumulated error of the dead-reckoning [Prami'85], [Hongo'87], [Banta'87].

The dead-reckoning navigation employed, which calculates the SDMR's position and heading from the rotation of the drive and steering motors, provided a position accuracy with mean cumulative error of about 5% for 5m of straight line travel. It has to be recognized that this error limit was achieved at fairly low speed of 40cm/s, but test performed at 100cm/s indicated that error did not vary significantly with speed. The magnitude of the error is probably high for most mobile robot applications, and hence there is a need for position error correction that can be incorporated into the dead-reckoning algorithm to tackle the deterioration in positional accuracy. In view of these facts a

method which makes use of look-up tables determined from experimental results with consideration of the SDMR posture was developed. The method is believed to be a very useful technique in achieving improved performance of a SDMR using dead-reckoning navigation. It is not however considered that dead-reckoning will ever be adequate as a sole navigation system but highly desirable to relieve the requirements placed on an absolute navigation system.

The experimental results were encouraging in that the SDMR demonstrated its ability to follow a programmed path by dead-reckoning, though with significant position error. However the position error was highly consistent for a given posture and thus lends itself to compensation. Unfortunately the error correction technique could not be implemented because the current control system is not appropriate for a SDMR, since it cannot handle posture changes and continuous steering rate. However, how the method could operate in practice has been shown.

The contributions made by the research reported in this thesis can be categorized as:

- (1) Analysis of different designs of mobile robot capable of omnidirectional motion, with special attention to the designs based on synchro-drive mechanism.
- (2) Making a new Synchro-Drive Mobile Robot (SDMR) design possible by developing a unique arrangement based on a differential gear unit that compensates the error due to the wheel assembly design.

- (3) Formulation and application of kinematic modeling for SDMR's in order to evaluate different conventional wheel assemblies capable of omnidirectional motion.
- (4) Application of kinematic modeling for SDMR's in order to study the control system requirements and the establishment of the boundary of control space to ensure stability.
- (5) Development of a new method of position error correction for SDMR's in order to correct for mechanical systems error.
- (6) Identification of the behaviour of SDMR's and their characteristics, such as the effect of changing posture on accuracy and stability, and the all-wheel drive system serving as an error-reduction mechanism.

## 9.2 RECOMMENDATIONS FOR FURTHER WORK.

Prior to this study, the description of the SDMR's motion and performance [Nakano'83], [Holland'86] have neglected any consideration of effects such as; changing wheelbase parameters due to change in heading, independent chassis orientation and wheel heading, fixed chassis orientation, and slippage. The determination of SDMR performance and characteristics based on experimental tests have given an insight into the significance of such features. The theoretical and experimental considerations have given a better understanding of the operation and control of a SDMR. Changes such as change in heading have been shown to be capable of producing different performance which in certain situations may cause the SDMR to become unstable or change the sign of any positional error.

In view of these facts, using the experimental test results a position error correction method was formulated. A simple control strategy was shown not to be capable of giving a satisfactory performance because of the requirements to consider SDMR postures, look-up position error correction value, and determine whether it is operating within its boundaries of control space in order to avoid unstable operation. The need to consider these factors has introduced new challenges in the study of control systems for SDMR's. Therefore there is a need to investigate and develop a control scheme that will take into account dynamic variability of the limits within which the SDMR must operate. The new control system that will be developed will also permit detailed study of the implementation of the proposed position error correction method. It has to be recognized that the position error correction method proposed does not eliminate the position error completely, but rather a significant proportion of the error should be eliminated.

Having given a full theoretical evaluation of two types of design for SDMR; Type-1 and Type-3, from which it is believed that Type-3 has advantage over Type-1 (which is now commercially available) in terms of stability, there is a need for further practical comparison in order to highlight any further operational differences. Also because both designs suffer different forms of design-error (Type -1, suffers drive induced error, while Type-3, suffers steering induced error), there is need for further research that will establish the differences in

their performance.

The kinematic model of a SDMR has been developed, and this is seen as a significant step toward designing an appropriate control for SDMRs. There is the need to further the study by applying the kinematic model to formulate the dynamic model using vector matrix format. It is realized that the kinematic model is the foundation for the dynamic model. The kinematic determination of position, velocities and acceleration can be applied to calculate dynamic forces and torques produced by the mechanism themselves. Also the consideration of boundaries of control space can be taken into the dynamic domain, establishing limits based on frictional force considerations rather than acceleration. There is also further research necessary to evaluate the significance which boundaries of control space have on performance and the means by which the boundaries can be widened to further improve performance.

## APPENDIX A

### RESEARCH PUBLICATIONS.

This appendix documents the research publications which the author of this thesis was involved in. The research covered by the Mobile Robot's group of the Department of Engineering fall into two main categories, which are; mobile robot mechanics, and mobile robot navigation. My main interest is in the mechanics and application of wheeled mobile robots in Manufacturing and domestic environments.

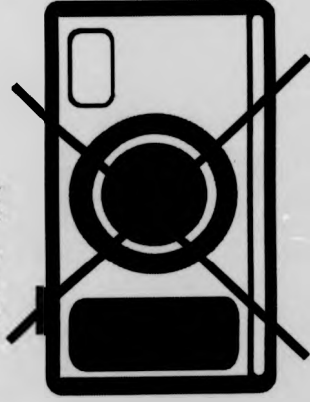
Though I have been involved in the publications of three technical papers those included in this Appendix are those relevant to the research work which this thesis covers. The Appendix are in two sections. Section A.1 covers the application areas where the type of wheeled mobile robot that I am interested in developing can be used. And also covered are the initial findings made at the earlier stage of this project and anticipated problems. I played a major role in writing the entire paper.

Section A.2 deals with the navigation aspect of the mobile robot. In this publication I was involved in the setting out the philosophy of the new 'absolute' navigation technique. My main contribution is in the Introduction, Vehicle design and on-board control.

The two publications now follows.

PUBLISHED PAPERS  
NOT FILMED FOR  
COPYRIGHT REASONS

part 6 part



## APPENDIX B

This appendix deals with two main issues in relation to the difference between SDMR and a conventional mobile robot. The issues covered are the analysis of the steering acceleration requirements, and the effect of mechanical system errors such as wheel misalignment.

### B.1 STEERING SYSTEM ACCELERATION REQUIREMENT.

The analysis presented here is to highlight the different acceleration requirement for steering a wheeled mobile robot. Three different designs, namely, Synchro-Drive configuration, Differential configuration and tricycle front wheel drive/steer configuration are considered.

High speed of travel and fast response to change in heading are influenced by the steering behaviour of the mobile robot. Steering system response can be considered as a representation of the ability of a steering system to respond to a change in angle. The parameters that can be used in evaluating a wheeled mobile robot's ability to a change in heading (steering input) are;

- (a) the inertia as seen by the motor shaft,
- (b) response time, and
- (c) acceleration/deceleration requirements for normal operation.

For a mobile robot, the determining factors in steering system response are:

- The motor and its inherent torque capability.
- Total system inertia.



The acceleration/decelerating evaluating parameter is used to determine the design that will give the fastest response with minimal inertia requirement for a given set of conditions.

For the sake of this analysis, a situation which assumes that the three mobile robots each based on the three designs given above (for details see chapter 2, section 2.1.3.2) are powered by electric motors of the same size and torque capabilities, and having the same overall mass.

The torque T required at the motor end is given by;

$$T = I \cdot \ddot{\omega}_m \quad (B.1)$$

where I, is the systems inertia and can be expressed as [Premi'85];

(1) For differential and tricycle mobile robot designs;

$$I = \left\{ J_1 G_1^2 + J_2 G_1^2 G_2^2 + \left[ (m_c + m_b) r_b^2 / 2 \right] G_1^2 G_2^2 \right\} \quad (B.2)$$

(2) For a Synchro-Drive Mobile robot (SDMR);

$$I = \left\{ J_1 G_1^2 + J_2 G_1^2 G_2^2 + \left( 3 m_s r_s^2 / 2 \right) G_1^2 G_2^2 \right\} \quad (B.3)$$

Equations (B.2) and (B.3) assumes that;

- ▷ the transmission chains are inextensible and of negligible mass,
- ▷ it ignores any rolling friction between the wheels and the floor surface, and
- it treats all the sprockets and gears as a disc component.

The symbols in the above equations represents:

$T$  : torque provided by the electric motor [Nm].

$J_1$  : moment of inertia of motor and sprocket [ $\text{kgm}^2$ ].

$J_2$  : moment of inertia of intermediate sprocket, spur gears and the drive wheel bevel gears [ $\text{kgm}^2$ ].

$G_1$  : gear ratio from motor sprocket to intermediate sprocket.

$G_2$  : gear ratio from intermediate sprocket to drive wheel sprocket.

$m_0$  : mass of the mobile robot's chassis + all parts fixed to it, such as motors [kg].

$m_w$  : mass of wheel assemblies [kg].

$m$  : ( $m_0 + m_w$ ) total mass of the mobile robot [kg].

$r_b$  : radius of the mobile robot's circular body [m].

$r_w$  : radius of the wheel assemblies [m].

$\omega_d$  : desired angular acceleration of the mobile robot [ $\text{rad./s}^2$ ].

$\omega_m = ?$  : angular acceleration of the motor shaft [ $\text{rad./s}^2$ ].

In as much as the three different designs may have the same overall mass, their steering response is influenced by two main factors, which are: the amount of inertia that should be overcome in achieving a change in heading, the systems gearing, hence gear ratio. These two factors affect the maximum turn rate that may be achieved before a given angle is reached.

The amount of inertia to overcome has a more significant influence on steering response than gear ratio, and this is shown

by a numerical example. For the sake of illustration a case which assumes that most of the parameters in equations (B.2) and (B.3) are known is given and are of the same values for the three different designs. That is taken;  $T = 0.7 \text{ Nm}$ ,  $J_1 = 4.5 \cdot 10^{-2} \text{ kgm}^2$ ,  $J_2 = 7.5 \cdot 10^{-2} \text{ kgm}^2$ ,  $G_1 = 1$ ,  $G_2 = 0.25$ ,  $m = 80 \text{ kg}$ ,  $m_c = 60 \text{ kg}$ ,  $m_s = 20 \text{ kg}$ ,  $r_s = 0.7 \text{ m}$ ,  $r_c = 0.35 \text{ m}$ ,  $\dot{\omega}_s = ?$

#### B.1.1 FOR A DIFFERENTIAL DESIGN.

In changing heading the mobile robot has to overcome its total rotational inertia, because of the need to re-orientate the mobile robot to its new heading. From equations B.1 and B.2,

$$T = I \cdot \dot{\omega}_s$$

$$\dot{\omega}_s = T/I$$

$$I = \left\{ J_1 G_1^2 + J_2 G_2^2 + \left[ (m_s + m_c) r_s^2 / 2 \right] G_1^2 G_2^2 \right\}$$

The torque considered here can be seen as being provided by a design making use of one electric motor, whereby the differential steering is achieved through a differential gearbox. Or it can be seen as being provided by two electric motors of equal capacity. That is each capable of providing a torque of  $0.7 \text{ Nm}$ .)

Substituting the values of the parameters in the above equations gives;

$$\begin{aligned} \dot{\omega}_s &= 0.7 / (4.5 \cdot 10^{-2} + (4.7 \cdot 10^{-2}) + (1.225)) \\ &= 0.55 \text{ rad./s}^2 \end{aligned}$$

### B.1.2 FOR A TRICYCLE DESIGN.

Also because of the need to re-orientate itself as in the differential design example, it has the same acceleration/deceleration value as that of the differential design, for the inertia calculation is based on the same parameters.

### B.1.3 FOR A SDMR DESIGN.

In calculating the angular acceleration, instead of using total mass  $m$ , a lower value,  $m_s$  is used. This is to account for its fixed orientation irrespective of change in heading, whereby only the wheel assemblies are steered. Therefore substituting the known values in equation B.1 and B.3 gives;

$$\dot{\omega}_s = T/I$$

$$I = \left[ J_1 G_1^2 + J_2 G_2^2 + \left( 3m_s r_s^2 / 2 \right) G_1^2 G_2^2 \right]$$

Substituting the values of the parameters in the above equations gives;  $\dot{\omega}_s = 0.7 / (4.5 \times 10^{-2}) + (4.7 \times 10^{-3}) + (0.23)$   
 $= 2.5 \text{ rad./s}^2$

From the numerical calculation, based on the set conditions, it can be seen that a SDMR has a faster response to directional change, when compared to the differential and tricycle designs. This implies that the steering torque has greater influence on mobile robot whose design is based on the synchro-drive mechanism.

### B.1 EFFECT OF MECHANICAL ERRORS.

Considering Figs. B.1 and B.2, if wheels numbered 1 are misaligned by say angle  $\theta$ , the tendency is for the mobile robot to drive in the direction dictated by  $\theta$ . For the conventional mobile robot, because wheel 1 is driven it will attempt to drive the mobile robot in the direction  $\theta$ . And because wheels 2 and 3 are free to roll at any speed, they will therefore roll at different speed, hence allowing wheel 1 to dictate completely the mobile robot heading, which will be directly related to angle  $\theta$ . Hence the magnitude of the position error will depend completely on that of the angle of misalignment.

With the conventional configuration the misaligned wheel will cause the individual wheels to adjust their speeds. From measuring the displacement of the two undriven wheels (wheel 2 and 3), using encoders, the forward displacement, the arc radius and change in heading can be determined as:

The arc length  $S$  is related to the angle  $\alpha$ , and the radius  $R$ , as  $S = \alpha R$ . The change in angle  $\Delta\alpha = (D_2 - D_3)/b$ , where  $D_2$  and  $D_3$  are displacements of wheel 2 and 3. The arc length of the mid-point between wheels 2 and 3 is given by;

$$\begin{aligned} D_2 + D_3 &= \Delta\alpha(R + b/2) + \Delta\alpha(R - b/2) \\ &= 2\Delta\alpha R = 2\Delta D \end{aligned}$$

Thus the forward displacement is given by;

$$\Delta D = (D_2 + D_3)/2 \quad (B.4)$$

and the change in heading is given by;

$$\Delta\alpha = (D_2 - D_3)/b \quad (B.5)$$

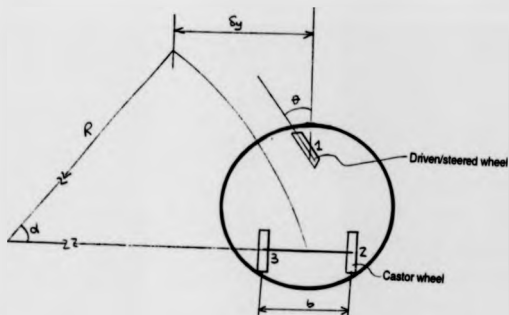
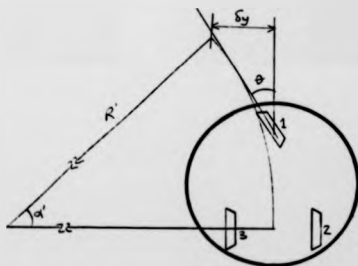


Fig. B.1 Conventional mobile robot with wheel misalignment error.



Note All wheels driven and steered

Fig. B.2 SDMR with wheel misalignment error.

Equations (B.4) and (B.5) shows that these variables can be directly determined in a conventional mobile robot, hence making the position error that occur possible to be determined and corrected. This direct approach is however not possible with the SDMR. This is because the three wheels are driven at the same speeds and they have equal influence. Thus each wheel will try to drive the SDMR through its own path. Hence there is the tendency to reduce any error that might occur. This phenomenon prevents any position determination method that relies of the displacement of the wheels or motor shafts from determining the value of the remaining position error as the SDMR position is not directly related to either.

The difference in performance between SDMR and conventional mobile robot such as that of the tricycle configuration when operating under mechanical systems error have been shown. Table B.1 is a summary of the main operational error differences,

Table B.1 Error differences between SDMR and Conventional mobile robot.

SDMR	Conventional
position error not known in dead-reckoning navig.	position error known in dead-reckoning navig.
smaller position error	large position error
variable mech. error	constant mech. error
error cumulative if precession is not known	error not cumulative

## APPENDIX C

### SYNCHRO-DRIVE MOBILE ROBOT (SDMR) SPECIFICATIONS.

In conducting the experimental tests two prototypes SDMR using the Type-3 wheel assembly design (i.e. wheel assembly with wheel set on the steering axis of the assembly) were used. The specifications for the two prototypes are stated in this Appendix (further details can be seen in chapter 5).

#### C.1 FIRST PROTOTYPE.

► Name:	Version 1 SDMR
► Primary Mission:	Factory automation
► Secondary Function:	Domestic and Medical applications
► Max. load carrying capacity:	200 kg
► SDMR unladen weight:	90 kg
► SDMR dimensions - chassis only:	1200 x 600mm (d x h)
► Transmission System:	Shaft and chain transmission.
► Max drive speed:	1 m/s
► Max drive speed on full load:	0.5 m/s
► Power Supply:	12V DC, 40 amp-hr sealed battery.
► Power Drive:	H-bridge circuit amplifier.
► Mobility characteristics:	Zero turning radius; 0-140 degree/sec. turn rate.
► Navigation Control:	Operates only in manual control.



- » Motion Controller: Hewlett-Packard, HTCL-1000 motion controller chip.
- » Features of Motion chip: Programmable digital filter, 8-bit parallel input/output port, Pulse width modulated (PWM) motor command port, Quadrature decoder for encoder signal, 24-bit position counter, 1-2 MHz clock operation.
- » PWM Signal: External frequency of clock/100 and the duty cycle is resolved into clock cycles.
- » Master Control Board: Intel 8088 processor in minimum mode running at a clock speed of 6MHz, with 32k of static RAM.
- » Master Board Operations: Computation of dead-reckoning algorithm, trajectory generation algorithm and path/trajectory control algorithm.
- » Position Feedback device: Optical shaft encoder with two channel output, resolution of 500 pulse per revolution.

## C.2 SECOND PROTOTYPE.

- ▷ Name: Version 2 SDMR
- ▷ Primary Mission: Factory automation
- ▷ Secondary Function: Domestic and Medical applications
- ▷ Max. load carrying capacity: 110 kg
- ▷ SDMR unladen weight: 50 kg
- ▷ SDMR dimensions - chassis only: 600 x 400mm (d x h)
- ▷ Transmission System: Shaft and chain transmission.
- ▷ Max drive speed: 2.5 m/s
- ▷ Max drive speed on full load: 1.5 m/s
- ▷ Power Supply: 12V DC, 40 amp-hr sealed battery.
- ▷ Power Drive: H-bridge circuit amplifier.
- ▷ Mobility characteristics: Zero turning radius; 0-180 degree/sec. turn rate; incorporates design-error correction mechanism.
- ▷ Navigation Control: Operates in either manual control or automatic mode via RF.
- ▷ Navigation Control: Operates only in manual control.
- ▷ Motion Controller: Hewlett-Packard, HTCL-1000 motion controller chip.
- ▷ Features of Motion chip: Programmable digital filter, 8-bit parallel input/output port, Pulse width modulated (PWM) motor command port, Quadrature decoder for encoder signal, 24-bit

position counter, 1-2 MHz clock operation.

- ▷ PWM Signal: External frequency of clock/100 and the duty cycle is resolved into clock cycles.
- ▷ Master Control Board: Intel 8088 processor in minimum mode running at a clock speed of 6MHz, with 32k of static RAM.
- ▷ Master Board Operations: Computation of dead-reckoning algorithm, trajectory generation algorithm and path/trajectory control algorithm.
- ▷ Position Feedback device: Optical shaft encoder with two channel output, resolution of 500 pulse per revolution.

# REFERENCES

- [Arai'81]; Arai, T., Nakano, E., Hashino, S. & Yamaba, K., "The Control and Application of 'Omni-Directional Vehicle (ODV)'", 8 Triennial World Congress of IFAC, Japan, Aug. 1981, pp. 1855-1860.
- [Autohelm]: Autohelm Personal Compass Instruction Manual.
- [Banta'87]; Banta, L.E.: Advanced Dead Reckoning Navigation For Mobile Robot, PhD Thesis, Georgia Institute of Technology, USA, Jan. 1987.
- [Barry'89]; Barry, S.: Omnidirectional Mobile Robot, Personal Communication, 1989.
- [Bekker'69]; Bekker, M.G.: Introduction to Terrain-Vehicle Systems, The University of Michigan Press, Ann Arbor MI, 1969.
- [Bundorf'68]; Bundorf, R.T., "The Influence of Vehicle Design Parameters on Characteristic Speed and Understeer", SAE Trans. vol. 76, 1968, pp. 548-560.
- [Carlisle'83]; Carlisle, B., "An Omni-directional Mobile Robot", Developments in Robotics, IFS Publ., 1983, pp. 79-87.
- [Chun'87] Chun, W., "Ground Vehicle Options", Proc. of SPIE - Mobile Robots II, Cambridge MA. Nov. 1987, pp. 188-194.
- [Collins'87]; Collins, T.J. and Kauzlarich, J.J., "Analysis of Parameters Related to the Directional Stability of Rear Caster Wheelchairs", RESNA 10th Annual conf., San Jose, California, 1987, pp. 507-509.
- [Crowley'85], Crowley, L.J. "Navigation for an Intelligent Mobile Robot", IEEE J. of Robotics and Automation, vol. RA-1, no. 1 March 1985, pp. 31-41.
- [Daniel'85]; Daniel, D.J., Krogh, B.H. and Friedman, M.B.,

- "Kinematics and Open-loop Control of an Ilonator-Based Mobile Robot Platform", IEEE Conf. on Robotics and Automation, St. Louis, Missouri, USA, Mar. 25-28, 1985, pp. 346-351.
- [Duggan'71] Duggan, T.V.: Power Transmission and Vibration Consideration in Design, Iliffe Book Ltd, London, 1971.
- [Flynn'88]; Flynn, M.A. and Brooks, R.A., "MIT Mobile Robots - What Next?", Proc. IEEE Int. conf. on Robotics and Automation, 24-29 April, 1988, Philadelphia, USA, pp. 611-617.
- [Fujie'85]; Fujie, M., Hosoda, Y., Iwamoto, T., Kamejima, K. & Nakano, Y., "Mobile Robot System with Transformable Crawler, Intelligent Guidance, and Flexible Manipulator", Proc. 3rd Int. symp. on Robotics Research, Oct. 7-11, 1985, Gouvieux, France, pp. 342-347.
- [Giralt'79]; Giralt, G. Sobek, R. and Chatila, R., "A Multi-Level Planning and Navigation System for a Mobile Robot; A First Approach to Hilare", Proc. IJCAI, Tokyo, Japan, Aug. 1979, pp. 335-338.
- [Greenwood'62] Greenwood, D.C.: Mechanical Power Transmission, McGraw Hill Book Co., New York, 1962.
- [Guttman'71]; Guttman, I.W. and Hunter, J.S.: Introductory Engineering Statistics, Wiley, 1971.
- [Helmers'83] Helmers, C., "Ein Heldenleben, (Or, A Hero's Life, With Apologies to R. Strauss)", Robotic Age, vol. 5, no. 2, Mar./April 1983, pp. 7-16.
- [Holland'86] Holland, J.M., "A Mobile Platform for Industrial Research", SME Technical paper MS 86-786, 1986, pp. 1-13.
- [Hongo'87] Hongo, T., Arakawa, H., Sugimoto, G., Tange, K. & Yamamoto, Y., "An Automatic Guidance System of a Self-Controlled Vehicle", IEEE Trans. on Ind. Elect., vol. IE- 34, no. 1, Feb. 1987, pp. 5-10.

- [Ilon'73] Ilon, B.E.: Directional Stable Self Propelled Vehicle, US Patent No. 3,746,112, July 1973.
- [Itô'87]; Itô, K.: Encyclopedic Dictionary of Mathematics, Mathematic Society of Japan, vol. II, MIT press, 1987.
- [Jonsson'85]; Jonsson, S., "New AGV with Revolutionary Movement", Proc. 3rd Int. conf. on AGVS, Oct. 15-17, 1985, Stockholm, Sweden, pp. 135-144.
- [Julliere'83]; Julliere, M., Marce, L. and Perrichot, H., "A Guidance System for a Vehicle which has to follow a Memorized Path", Proc. 2nd Int.conf. on AGVS & 16th IPA conf., Stuttgart, W. Germany, Jun. 7-9, 1983, pp. 211- 221.
- [Kumar'83]; Kumar, A. and Prakash, S. "Analysis of Mechanical Errors in Manipulators", Proc. 6th World Congress on Theory of Machines, Dec. 1983, New Delhi, India, pp. 960-963.
- [Kanayama'85]; Kanayama, Y. and Yuta, S., "Computer Architecture for Intelligent Robots", J. Robotic Systems, vol. 2, pt. 3, 1985, pp. 237-251.
- [Knasel'86] Knasel, T.M., "Mobile Robotics - State of the Art Review", Robotics, Jun. 1986, vol. 2, no. 2, pp. 149-155.
- [Lewis'73] Lewis, R.A. and Bejezy, A.K., "Planning Consideration for a Roving Robot with Arm", Proc. 3rd IJCAI, Stanford CA., USA, Aug. 1973, pp. 308-316.
- [Mariam'87]; Mariam, J.L. and Kraige, L.G.: Engineering Mechanics - Dynamics; vol. 2, John Wiley, 1987.
- [Moravec'83]; Moravec, H.P., "The Stanford Cart and CMU Rover", Proc. of the IEEE, Jul. 1983, vol. 71, no. 7, pp. 872- 884.
- [Muir'86]; Muir, P.F. and Neuman, C.P.: Kinematic Modeling of Wheeled Mobile Robots, Technical Report, CMU-RI-TR-86-12, Carnegie-Melon University, Pittsburgh, USA, June, 1986.
- [Muir'87]; Muir, P.F. and Neuman, C.P., "Kinematic Modeling for

- Feedback Control of An Omnidirectional Wheeled Robot", Proc '87, Int. conf. on Robotics and Automation, vol. 3, North Carolina, USA, Mar. 31 Apr. 3, 1987, pp. 1772- 1778.
- [Nakano'81]; Nakano, E., Arai, T., Yamaba, K. Hashino, S., Ono, T & Ozaki, S., "First Approach towards the Development of a Patient Care Robot", Proc. 11th ISIR, Tokyo, Japan, 1981, pp. 87-94.
- [Nakano'83]; Nakano, E. and Kaychi, N. "An Advanced Mechanism of the Omni-Directional Vehicle (ODV) and its Application to the working Wheelchair for the Disable", Proc. '83 ICAR, Tokyo, Sept. 12-13, 1983, pp. 277-284.
- [Nelson'89]; Nelson, W.L., "Continuous Steering-Function Control of Robot Carts", IEEE Trans. on Ind. Electronics, Aug. 1989, vol. IE-36, no. 3, pp. 330-337.
- [Nilsson'84]; Nilsson, N.J.: Shakey the Robot, Technical Note 323, Artificial Intelligent Centre, SRI Int., CA, USA, April 1984.
- [N-Nagy'86] N-Nagy, F. (editor): Advanced Robotics in Japan - Report of the Study Mission to Japan, ARASA, 1986.
- [Ponder'84]; Ponder, G. Dowling, K. and Blackwell, M.: A functional Vehicle for Autonomous Mobile Robot Research, CMU Technical Report No. CMU-RI-TR-84-28, 1984.
- [Premi'85]; Premi, S.K.: The Design of a Free-Ranging Automated Guided Vehicle (AGV) System, PhD Thesis, Imperial College of Science and Technology, University of London, UK, Apr. 1985.
- [Rose'89] Rose, W., "Powered Spheres - 'Walk' and 'Roll'", Eureka on Campus, Spring 1989, vol. 1. Germany, Jun. 7-9, 1989, pp. 195-209.
- [Segel'87]; Segel, L. "Theoretical Prediction and Experimental Substantiation of the Response of the Automobile to Steering

- Control", Proc. Inst. of Mech. Engineers, Automobile Division, 1956-1957.
- [Steed'60]; Stead, W.: Mechanics of Road Vehicle, Ilife, 1960.
- [Thring'83]; Thring, M.W.: Robots and Telechir, Ellis Horwood, Ltd, 1983.
- [Tsumura'83]; Tsumura, T., Fujiwara, N. and Hashimoto, M., "An Experimental System for Self-Contained Position and Heading Measurement of Ground Vehicle", Proc. Int. Conf. on Advanced Robotics, Tokyo, Japan, Sept. 12-13, 1983, pp. 269-276.
- [Tsumura'85]; Tsumura, T., Fujiwara, N. and Hashimoto, M., "New Method for Position and Heading Compensation of Ground Vehicle", Proc. Int. Conf. on Advanced Robotics, Tokyo, Japan, Sept. 9-10, 1985, pp. 429-436.
- [Van der Loos'86]; Van der Loos, H.F.M., Michalowski, S.J. and Leifer, L.J., "Design of an Omnidirectional Mobile Robot as a Manipulation Aid for the severely Disabled", Proc. 9th Ann. conf. on Rehab. Techn., Jun. 23-26, 1986, pp. 247- 248.
- [Wong'78]; Wong, J.Y.: Theory of Ground Vehicle, John Wiley, New York, 1978.
- [Wright'87]; Wright, D.D. and Watson, R.E., "Comparison of Mobility System Concept for a Mars Rover", Proc. of SPIE - Mobile Robot II, Cambridge, MA, vol. 852, Nov. 1987, pp. 180-187.
- [Wallace'85]; Wallace, et al., "First Results in Robot Road-Following", Proc. IJCAI, Los Angeles CA, USA, Aug. 1985, pp. 1089-1095.



THE BRITISH LIBRARY  
BRITISH THESIS SERVICE

PERFORMANCE EVALUATION AND DEVELOPMENT OF  
TITLE .. A SYNCHRO-DRIVE MOBILE ROBOT .....

CHARLES NNONYELUM J. NWUFOH,  
AUTHOR .....

DEGREE .....

AWARDING BODY University of Warwick  
DATE ..... (1992) .....

THESIS  
NUMBER .....

THIS THESIS HAS BEEN MICROFILMED EXACTLY AS RECEIVED

The quality of this reproduction is dependent upon the quality of the original thesis submitted for microfilming. Every effort has been made to ensure the highest quality of reproduction.

Some pages may have indistinct print, especially if the original papers were poorly produced or if the awarding body sent an inferior copy.

If pages are missing, please contact the awarding body which granted the degree.

Previously copyrighted materials (journal articles, published texts, etc.) are not filmed.

This copy of the thesis has been supplied on condition that anyone who consults it is understood to recognise that its copyright rests with its author and that no information derived from it may be published without the author's prior written consent.

Reproduction of this thesis, other than as permitted under the United Kingdom Copyright Designs and Patents Act 1988, or under specific agreement with the copyright holder, is prohibited.

1	2	3	4	5	6	REDUCTION X	21
CAMERA						I	
No. of pages							

D175040